INSTITUTO TECNOLÓGICO DE COSTA RICA

VICERRECTORÍA DE INVESTIGACIÓN Y EXTENSIÓN

DIRECCIÓN DE PROYECTOS

ESCUELA DE INGENIERÍA FORESTAL

INFORME FINAL DE PROYECTO DE INVESTIGACIÓN

Síntesis de madera magnética a base de nano partículas de hierro en especies forestales provenientes de plantaciones de rápido crecimiento en Costa Rica

Código: 14011044

(DOCUMENTO I)

INVESTIGADORES:
Ing. Alexander Berrocal J. Dr.
Ing. Roger Moya R. Dr.
M.Sc. Johana Gaitán Álvarez
Dra. Karla Jaimes Merazzo

Mayo, 2023

Índice general

1. Resumen

La madera magnética, material híbrido que combina las propiedades inherentes de la madera con las propiedades de nano partículas magnéticas, ha sido empleada en tableros de fibra y madera sólida, utilizando para su síntesis revestimientos e impregnaciones con fluidos magnéticos.

En el capítulo 1 la síntesis de nanopartículas de Fe_3O_4 en madera sólida de especies tropicales (*Pinus oocarpa*, *Vochysia ferruginea* y *Vochysia guatemalensis*), fue evaluada. *P*. *oocarpa* mostró los valores más bajos de porcentaje de ganancia de peso (WPG), la densidad disminuyó en relación a la madera no tratada, presentó menor contenido de cenizas y Fe_3O_4, mostró menor precipitación de nanopartículas de hierro, las señales asociadas a cambios en el componente madera (1153 cm^{-1}, 1739 cm^{-1}, 1601 cm^{-1}, 1505 cm^{-1}, 1462 cm^{-1}, 1419 cm^{-1} y 1251 cm^{-1}) no mostraron diferencias con la madera no tratada, presentó el menor diámetro de nanopartículas (aprox. 7,3 nm a 8,5 nm) y los parámetros de magnetización de saturación (Ms) fueron los más bajos. *V*. *guatemalensis* presentó un mejor comportamiento magnético, aunque se produjo mayor degradación de los componentes de la madera (mayor pérdida de densidad). Respecto a los diferentes tiempos de inmersión, las propiedades magnéticas no se vieron afectadas estadísticamente. Finalmente, los valores de magnetización de las especies estudiadas fueron inferiores a las nanopartículas de magnetita pura, porque las especies sólo retienen una cierta cantidad de estas nanopartículas (NP), y esto se refleja proporcionalmente en Ms.

En el capítulo 2 se abordó la síntesis in-situ de nanopartículas (NPs) de Fe_3O_4 en partículas de fibra de tres maderas tropicales (*P. oocarpa*, *V. guatemalensis*, y *V. ferruginea*). El contenido en NPs de Fe_3O_4 fue similar en las dos especies de Vochysia pero superior al de *P*. *oocarpa*. El contenido en cenizas era similar en las tres especies. Fue difícil demostrar la presencia de NPs de Fe_3O_4 en el espectro FT-IR. El diámetro de las nanopartículas variaba de 51 nm a 68 nm y los parámetros de magnetización de saturación eran bajos, pero estos valores eran superiores en *P*. *oocarpa*. El tablero magnético de partículas (MWPC) mostró que el uso de NPs disminuye la densidad de *P*. *oocarpa* pero aumenta la densidad de las especies de Vochysia. El hinchamiento y la absorción de humedad aumentaron en el MWPC-100 de *P*. *oocarpa* y *V*. *guatemalensis* pero disminuyeron en el compuesto de V. *ferruginea*. La adhesión interna disminuyó en el MWPC-100, pero no en la capa de MWPC. La dureza aumentó en la capa de MWPC en *P*. *oocarpa*, pero no en MWPC-100, esta propiedad aumentó en MWPC-100 y en la capa de MWPC fabricada con *V*. *ferruginea* y *V*. *guatemalensis*.

En el capítulo 3 se evaluó la síntesis de nanopartículas de Fe_3O_4 en chapas de madera de tres especies tropicales (*Gmelina arborea*, *V. ferruginea* y *P. oocarpa*). El método de impregnación sí afectó la síntesis de las nanopartículas, la impregnación a vacío-presión

fue la que presentó la mayor cantidad de Fe_3O_4 en las chapas. Al usar la impregnación vacío-presión se evidenció mayor señal de ferrita en los análisis SEM y XDR. En el análisis de propiedades magnéticas, fue claro que la curva de histéresis de la madera presentó un comportamiento ferromagnético en la síntesis por medio del método vacío-presión, mientras que por el método de inmersión el cambio fue de leve a nulo. También, se observó que *Vochysia ferruginea* fue la especie con mayor magnetización.

2. Abstract

Magnetic wood, hybrid material that combines the inherent properties of wood with the properties of magnetic nanoparticles, has been used in fiberboard and solid wood, using coatings and impregnations with magnetic fluids for its synthesis.

In chapter 1, the synthesis of Fe_3O_4 nanoparticles in solid wood of tropical species (*Pinus oocarpa*, *Vochysia ferruginea* and *Vochysia guatemalensis*) was evaluated. *P. oocarpa* showed the lowest values of weight gain percentage (WPG), density decreased in relation to untreated wood, besides presented lower ash and Fe_3O_4 content, showed lower precipitation of iron nanoparticles, signals associated with changes in the wood component (1153 cm^{-1}, 1739 cm^{-1}, 1601 cm^{-1}, 1505 cm^{-1}, 1462 cm^{-1}, 1419 cm^{-1} and 1251 cm^{-1}) showed no differences with untreated wood, besides presented the smallest diameter of nanoparticles (approx. 7.3 nm to 8.5 nm) and the saturation magnetization parameters (Ms) were the lowest. *V. guatemalensis* presented better magnetic behavior, although there was greater degradation of the wood components (greater loss of density). Regarding to the different immersion times, the magnetic properties were not statistically affected. Finally, the magnetization values of the species studied were lower than pure magnetite nanoparticles, because the species only retain a certain amount of these nanoparticles (NP), and this is reflected proportionally in Ms.

Chapter 2 addressed the in-situ synthesis of Fe_3O_4 nanoparticles (NPs) in fiber particles of three tropical woods (*P. oocarpa*, *V. guatemalensis* and *V. ferruginea*). The Fe_3O_4 NPs content was similar in the two Vochysia species but higher than in *P. oocarpa*. Ash content was similar in the three species. It was difficult to demonstrate the presence of Fe_3O_4 NPs in the FT-IR spectrum. The diameter of the nanoparticles varied from 51 nm to 68 nm and the saturation magnetization parameters were low, but these values were higher in P. oocarpa. Magnetic particle board (MWPC) showed that the use of NPs decreased the density of P. oocarpa but increased the density of Vochysia species. Swelling and moisture absorption increased in MWPC-100 of *P. oocarpa* and *V. guatemalensis* but decreased in the *V. ferruginea* composite. Internal adhesion decreased in MWPC-100, but not in the MWPC layer. Hardness increased in the MWPC layer in *P. oocarpa*, but not in MWPC-100, this property increased in MWPC-100 and in the MWPC layer made with V. *ferruginea* and *V. guatemalensis*.

Chapter 3 evaluated the synthesis of Fe_3O_4 nanoparticles in wood veneers of three tropical species (*Gmelina arborea*, *V. ferruginea* and *P. oocarpa*). The impregnation method did affect the synthesis of the nanoparticles, the vacuum-pressure method presented the highest amount of Fe_3O_4 in the veneers. When using vacuum-pressure method, a higher ferrite signal was evidenced in the SEM and XDR analysis. In the analysis of magnetic properties, it was clear that the hysteresis curve of the wood presented a ferromagnetic

behavior in the synthesis by means of the vacuum-pressure method, while by the immersion method the change in the curve was slight to null. Also, it was observed that *V*. *ferruginea* was the species with the highest magnetization level.

3. Introducción

La madera es un material con propiedades de polímero natural estructurado y ordenado, que posee excelentes características jerárquicas estructurales y físicas (Butta et al., 2015). Es un material utilizado en importantes aplicaciones ingenieriles como decoración de interiores, materiales de construcción y en la industria de muebles (Wang et al., 2019).

La estructura micro porosa de la madera permite combinar naturalmente compuestos inorgánicos y orgánicos (Wang et al., 2019) y además esta estructura porosa le permite introducir y almacenar sustancias que mejoran sus propiedades tales como resistencia a la biodegradación (Lykidis et al., 2016), propiedades reológicas (Ali & Javaid, 2017), propiedades mecánicas (Sohn et al., 2018), propiedades acústicas (Liu et al., 2017) y propiedades magnéticas.

La madera magnética es un compuesto que exhibe las propiedades ligeras inherentes de la madera con las propiedades magnéticas de nano partículas, logrando una adecuada armonía entre ambas (Dong et al., 2016). La madera magnética usualmente se ha usado en tableros de fibra de madera cargados de nanopartículas, revestimientos e impregnaciones con fluidos magnéticos (Merk et al., 2014).

Actualmente se conocen tres métodos típicos de fabricación de maderas magnéticas: impregnaciones, inmersiones en polvo y recubrimientos (Oka et al. 2007, 2009, Dong, Yan, Zhang, Zhang, y Li, 2016). Dentro de estos métodos, la impregnación de nanopartículas (NPs) basadas en ferrita como Fe_3O_4 (Gan, Gao, et al. 2017), $CoFe_2O_4$ (Gan et al. 2016) y MnFe2O4 (Wang et al. 2017), se encuentran entre los más importantes. Sin embargo, un método alternativo ha mostrado mejores resultados, este método consiste en el tratamiento de la madera con una mezcla de Fe^{3+} y Fe^{2+}, seguido de impregnación dentro de una solución de amoníaco, sintetizando in-situ Fe_3O_4 NPs con una reacción química de coprecipitación (Dong, et al., 2016; Lou et al., 2018; Mashkour & Ranjbar, 2018).

Buscando mejorar la síntesis de las partículas magnéticas de Fe_3O_4, en relación con el tamaño y permeabilidad en la madera, algunos grupos han impregnado la madera con soluciones de Fe^{3+} y Fe^{2+} bajo presión atmosférica, seguida de impregnaciones con soluciones de amoniaco (Gao et al., 2012). Estos métodos buscan sintetizar nano partículas de Fe_3O_4 a través de la reacción química de coprecipitación in situ en la madera, fabricando así la madera magnética.

Por su parte, otras personas investigadoras han trabajado en la mejora de los procesos de magnetizar la madera. Un caso exitoso es el elaborado por Dong et al. (2016), quienes introdujeron nanopartículas de hierro en la madera al vacío seguido por una impregnación atmosférica, obteniendo con éxito madera magnética y acortando enormemente el tiempo requerido para la impregnación de la solución precursora de hierro.

Debe ser considerado el hecho de que las especies empleadas para estos estudios han sido principalmente álamos, así como *Pinus radiata* y Norway spruce entre otras especies coníferas (Gan et al., 2017; Lou et al., 2018; Wang et al., 2019; Segmehl et al., 2018). Las cuales poseen un comportamiento muy diferente de impregnación, en comparación con las maderas tropicales que se encuentran el Costa Rica, dadas sus diferencias estructurales anatómicas.

Por otro lado, Costa Rica ha venido implementando programas de reforestación con maderas latifoliadas de rápido crecimiento utilizando una amplia variedad de especies para la producción de madera (Tenorio et al. 2016, Liu et al. 2018, Tenorio y Moya 2018), pero actualmente la incursión en mercados de alto valor con productos tecnológicamente desarrollados es aún limitada (Gaitán-Alvarez et al. 2020a, 2020b, Moya et al. 2020).

Las plantaciones forestales en regiones tropicales representan una gran oportunidad de producción aún con aspectos negativos como los anteriormente mencionados; sin embargo, es importante incrementar la calidad de la madera y el valor agregado de los productos mediante la implementación de tratamientos que minimicen los efectos negativos de la madera juvenil (Kojima, Yamamoto, Okumura, et al. 2009). De ahí la importancia de estudiar, evaluar y desarrollar tecnologías como la magnetización de la madera.

Tomando en consideración lo anterior, el objetivo de este estudio fue: optimizar el proceso de magnetización de madera en especies de rápido crecimiento de reforestación de Costa Rica.

Cinco especies provenientes de plantaciones forestales de rápido crecimiento en Costa Rica fueron utilizadas para evaluar la síntesis de madera magnética. Las especies seleccionadas fueron *Gmelina arborea (G.a), Tectona grandis (T.g), Vochysia ferruginea (V.f)* y *Vochysia guatemalensis (V.g)* y *Pinus oocarpa* (*P.o*). Para las pruebas en madera sólida se utilizó Pinus y las dos Vochysias, para los ensayos en tableros de partículas se utilizaron las mismas especies y para las pruebas en chapas de madera se sustituyó *V. guatemalensis* por *G. arborea*. Las pruebas preliminares en *T. grandis* no dieron resultados favorables al momento de intentar magnetizar la madera.

Para madera sólida, los resultados mostraron que la especie *P. oocarpa* presentó los valores más bajos de ganancia de peso, la densidad disminuyó en relación con la madera no tratada, presentó menor contenido de cenizas y Fe_3O_4, se evidenció menor precipitación de nanopartículas de hierro, las señales asociadas a cambios en el componente madera (1153 cm^{-1}, 1739 cm^{-1}, 1601 cm^{-1}, 1505 cm^{-1}, 1462 cm^{-1}, 1419 cm^{-1} y 1251 cm^{-1}) no mostraron diferencias con la madera no tratada, presentó el menor diámetro de nanopartículas (aprox. 7,3 nm a 8,5 nm) y los parámetros de magnetización de saturación (Ms) fueron los más bajos. Por el contrario, la especie que presentó un mejor comportamiento magnético fue *V. guatemalensis*, pero con el inconveniente de que se produjo una mayor degradación de los

componentes de la madera, por lo que hay una mayor pérdida de densidad. En relación con los diferentes tiempos de inmersión, las propiedades magnéticas no se vieron afectadas estadísticamente. Finalmente, los valores de magnetización de las especies estudiadas son inferiores a las nanopartículas de magnetita pura, ya que las especies sólo tienen una cierta cantidad de estas nanopartículas (NPs), y esto se refleja proporcionalmente en la magnetización de saturación.

Con respecto los tableros de partículas los resultados mostraron que el contenido en NPs de Fe_3O_4 era similar en las dos especies de Vochysia pero superior al de *P*. *oocarpa*. El contenido en cenizas era similar en las tres especies. Fue difícil demostrar la presencia de NPs de Fe_3O_4 en el espectro FT-IR. El diámetro de las nanopartículas variaba de 51 a 68 nm y los parámetros de magnetización de saturación eran bajos, pero estos valores eran superiores en *P*. *oocarpa*. Los tableros de partículas de madera magnética (MWPC) mostraron que el uso de NPs disminuye la densidad de *P*. *oocarpa,* pero aumenta la densidad en las especies de Vochysia. El hinchamiento y la absorción de humedad aumentaron en el MWPC-100 de *P*. *oocarpa* y *V*. *guatemalensis*, sin embargo, disminuyeron en el tablero de V. *ferruginea*. La adhesión interna disminuyó en el MWPC-100, pero no en la capa de MWPC. La dureza aumentó en la capa de MWPC en *P*. *oocarpa*, pero no en MWPC-100, y esta propiedad aumentó en MWPC-100 y en la capa de MWPC fabricadas con *V*. *ferruginea* y *V*. *guatemalensis*.

Finalmente, para las chapas de madera los resultados mostraron que el método de impregnación sí tuvo efecto en la síntesis de las nanopartículas, en este caso la impregnación con el método vacío-presión fue la que presentó la mayor cantidad de Fe_3O_4 en las chapas. De la misma forma, al usar la impregnación vacío-presión se evidenció mayor señal de ferrita en los análisis SEM y XDR. Mientras que, en el análisis de propiedades magnéticas fue claro que la curva de histéresis de la madera presentó un comportamiento ferromagnético en la síntesis por medio del método vacío-presión, mientras que por el método de inmersión el cambio fue de leve a nulo. A su vez también, se observó que la especie que logró mayor grado de magnetización fue *V. ferruginea.*

Logros y recomendaciones

Con relación a los principales logros obtenidos en este proyecto se pueden mencionar:

1. Al menos tres artículos científicos, uno de los cuales ya fue publicado (Revista Materials), otro fue sometido (Revista Wood and Fiber Science), el tercero está en edición para ser traducido y sometido a una revista de corriente principal.

2. Demostrar que a pesar de que los resultados obtenidos no fueron del todo satisfactorios en cuanto al uso de madera magnética para desarrollar productos ingenieriles de alto valor con madera sólida, tableros de partículas y tableros de chapa, si se pudo demostrar que es factible combinar madera con nanopartículas magnéticas y ácido poliláctico, que tendría importantes aplicaciones en el desarrollo de filamentos para impresión en 3D.

A partir de los resultados generados surgen algunas interrogantes que deberían ser abordadas a través de estudios posteriores en la misma línea:

a) Profundizar el estudio de materiales compuestos que incorporen la madera, para desarrollar productos novedosos tales como PLA con nanopartículas magnéticas para usos en impresoras 3D.

b) Ampliar el estudio de madera magnética en especies de mayor permeabilidad y capacidad de impregnación, por ejemplo, *Ochroma pyramidale* y especies de bosque secundario, lo que les permitiría dar mayor valor agregado a especies tropicales emergentes.

c) Valorar la aplicación de otras técnicas de impregnación de partículas magnéticas como por ejemplo recubrimientos con nanopartículas, que permitan una mayor proporción de magnetita de la que se logra con los métodos de inmersión y presión, debido al tipo de madera con que se está trabajando y sus propiedades de permeabilidad.

Finalmente, con respecto a los beneficios inmediatos y futuros de los resultados obtenidos se debe destacar:

a) Un incremento en el acervo de información relevante de plantaciones de rápido crecimiento en diferentes zonas del país, con posibilidad de ser utilizada a nivel regional en materia de magnetismo en maderas tropicales.

b) Haber generado experiencia práctica en el proceso de magnetismo de la madera, esta información se considera relevante para determinar posibles usos futuros de estas maderas y obtener productos de un mayor valor agregado.

c) Contar con una base científica adecuada para futuros proyectos relacionados con los temas abordados en el proyecto especialmente la combinación de madera con otros materiales para desarrollar biomateriales con aplicaciones novedosas, de tal forma que se incremente la información de propiedades de las maderas tropicales provenientes de plantaciones de rápido crecimiento.

d) Un aporte significativo la productividad académica de la Escuela de Ingeniería Forestal y del Instituto Tecnológico de Costa Rica, a través de al menos cinco publicaciones en índices superiores (Scopus y Web of Science).

4. Artículo 1: Tropical magnetic wood properties prepared in situ from iron oxide nanoparticles of three species growing in fast growth plantation

materials

MDPI

Article

In Situ Synthesis of Fe_3O_4 Nanoparticles and Wood Composite Properties of Three Tropical Species

Roger Moya [1,*], Johanna Gaitán-Álvarez [1], Alexander Berrocal [1] and Karla J. Merazzo [2]

[1] Instituto Tecnológico de Costa Rica, Escuela de Ingeniería Forestal, Apartado, Cartago 159-7050, Costa Rica; jgaitan@itcr.ac.cr (J.G.-Á.); aberrocal@itcr.ac.cr (A.B.)
[2] BCMaterials, Basque Center for Materials, Applications and Nanostructures, UPV/EHU Science Park, 48940 Leioa, Spain; karlamerazzo@gmail.com
* Correspondence: rmoya@itcr.ac.cr

Abstract: Magnetic wood is a composite material that achieves harmony between both woody and magnetic functions through the active addition of magnetic characteristics to the wood itself. In addition to showing magnetic characteristics, magnetic wood offers low specific gravity, humidity control and acoustic absorption ability. It has potential for broad applications in the fields of electromagnetic wave absorption, electromagnetic interference shielding, furniture, etc. This work reports on the synthesis of Fe_3O_4 nanoparticles (NPs) in wood from three tropical species (*Pinus oocarpa*, *Vochysia ferruginea* and *Vochysia guatemalensis*) using a solution of iron (III) hexahydrate and iron (II) chloride tetrahydrate with a molar ratio of 1.6:1 at a concentration of 1.2 mol/L ferric chlorate under 700 kPa pressure for 2 h. Afterward, the wood samples were impregnated with an ammonia solution with three different immersion times. The treated wood (wood composites) was evaluated for the weight gain percentage (WPG), density, ash content and Fe_3O_4 content by the Fourier transform infrared spectroscopy (FTIR) spectrum, X-ray diffraction (XRD) and vibrating sample magnetometry (VSM). The results show that the species *P. oocarpa* had the lowest values of WPG, and its density decreased in relation to the untreated wood, with lower ash and Fe_3O_4 NP content. The XRD and some FTIR signals associated with changes in the wood component showed small differences from the untreated wood. Fe_3O_4 NPs presented nanoparticles with the smallest diameter of (approx. 7.3 to 8.5 nm), and its saturation magnetization (M_s) parameters were the lowest. On the other hand, *V. guatemalensis* was the species with the best Ms values, but the wood composite had the lowest density. In relation to the different immersion times, the magnetic properties were not statistically affected. Finally, the magnetization values of the studied species were lower than those of the pure Fe_3O_4 nanoparticles, since the species only have a certain amount of these nanoparticles (NPs), and this was reflected proportionally in the magnetization of saturation.

Keywords: wood composites; magnetic properties; tropical wood; wood modification

Citation: Moya, R.; Gaitán-Álvarez, J.; Berrocal, A.; Merazzo, K.J. In Situ Synthesis of Fe_3O_4 Nanoparticles and Wood Composite Properties of Three Tropical Species. *Materials* **2022**, *15*, 3394. https://doi.org/10.3390/ma15093394

Academic Editor: Christian Müller

Received: 22 March 2022
Accepted: 2 May 2022
Published: 9 May 2022

1. Introduction

Metal–organic frameworks (MOFs) have been considered to be ideal precursor candidates for microwave absorption materials (MAMs) because of their tunable structure, high porosity and large specific surface area [1,2]. Very recently, the incorporation of organic and inorganic components within the wood matrix structure has been studied with the objective of improving its properties, including biodegradation resistance and rheological, mechanical, acoustic and magnetic properties [3]. The treatment used to magnetize wood combines the properties of the matrix (wood) with the properties of the magnetic nanoparticles (NP) [4–8]. This new composite can be applied in different ways, such as for electromagnetic shielding, indoor electromagnetic wave absorbers and heating plates, and in heavy metal absorption [9–11].

Three typical methods of magnetic wood fabrication are currently known: impregnation, powder immersion and coating [9,11,12]. Among these methods, impregnation

with ferrite-based NPs such as Fe_3O_4 [12], $CoFe_2O_4$ [13] and $MnFe_2O_4$ [14] is the most important. However, an alternative method has shown better results, which consists of treating wood with a mixture of Fe^{3+} and Fe^{2+}, followed by impregnation in an ammonia solution, synthesizing in situ Fe_3O_4 NP through a coprecipitation chemical reaction [15–17].

Wood prepared by this technique exhibits new properties or enhanced responses, such as high thermal performance, electromagnetic wave absorption, magnetic attraction, improved texture, easy processing and increased dimensional stability [18,19]. In fact, the process of magnetizing the wood positively transfers the magnetic properties of the fillers (the magnetic NPs) to the new composite [20]. Therefore, magnetic treatment is a promising way to endow wood with new functions and expand the applications of wood, especially the fast-growing wood species utilized in reforestation programs [11].

Some studies have demonstrated that several methods can be applied to magnetize wood. For example, Dong et al. [11] used poplar wood from trees in fast-growing plantations and concluded that this type of treatment allows the conversion of this species to multifunctional wood with high performance that could be applied where wood-based materials with high dimensional stability are required. Wang et al. [14,21] synthesized $FeNi_3$ NPs in *Pinus radiata* wood and determined that the in situ method provides soft, light and inexpensive magnetic wood composites with high industrial utility. Moreover, Gan et al. [22] used *Populus cathayana* wood and found that, despite this being a low-density species, the incorporation of Fe_3O_4 NPs within delignified wood provides a potential strategy to develop wood-based materials for magnetic applications.

Costa Rica has been implementing reforestation programs with fast-growing hardwoods, using a wide variety of species for wood production [23–25]. However, currently, the incursion into high-value markets with technologically developed products is still limited [26–28]. In these reforestation programs, species are harvested at early ages, which makes them juvenile wood [29] with negative properties such as low density, short fibers and the presence of growth stress [30].

Plantation forest trees in tropical regions represent a great production opportunity even with the aforementioned negative aspects; nevertheless, it is important to increase the quality of the wood and the added value of the products by implementing treatments that minimize the negative effects of juvenile wood [30]. Hence, studying, evaluating and developing technologies such as magnetized wood are important.

Besides the presence of juvenile wood in young trees, tropical hardwoods present a hierarchically and chemically more complex structure than softwoods [31–33]. These (hardwoods) are composed of fiber cells (35–70% of all cells) with the special function of providing mechanical support, while fluid is conducted through the vessels (between 6% and 55% of the total wood cells), which are enlarged cells with thin walls and large pore spaces.

The structural differences between softwoods and hardwoods depends on the flow of liquids within the wood, both during tree growth [34] and during the industrial harvesting process, which involves the flow of liquids inward (absorption) and outward (desorption) [35]. This makes the mechanisms of liquid flow in hardwood more complex, as more anatomical elements are involved. Treatments involving liquid flow or the introduction of NPs inside the wood matrix, especially in hardwood species, become challenging, and the wood treatments involving these species should be properly studied [26,27,36].

Given this context, the present work aimed to synthesize magnetic wood in three fast-growing species from Costa Rica, namely, *Pinus oocarpa*, *Vochysia ferruginea* and *Vochysia guatemalensis*, by in situ impregnation with $FeCl_3 \cdot 6H_2O$, $FeCl_2 \cdot 4H_2O$ and ammonia. The study evaluated the degree of synthesis of iron NP within the wood in terms of the weight gain percentage (WGP), wood density and Fe^{+3} absorption and by emission scanning electron microscopy (SEM), Fourier transform infrared spectroscopy (FTIR), X-ray diffraction (XRD) and vibrating sample magnetometry (VSM). An understanding of this wood-improving treatment of tropical species has potential for broad applications in the fields of electromagnetic wave absorption, electromagnetic interference shielding, furniture, etc.

2. Materials and Methods

2.1. Materials

The reagents used were iron (III) hexahydrate ($FeCl_3 \cdot 6H_2O$) $\geq$ 98% trademark purity Sigma-Aldrich (St. Louis, MO, USA); iron (II) chloride tetrahydrate ($FeCl_2 \cdot 4H_2O$) $\geq$ 98% trademark purity Sigma-Aldrich (St. Louis, MO, USA); ammonium hydroxide solution at 30% purity of the commercial brand LABQUIMAR (San Jose, Costa Rica); absolute ethyl alcohol of the trademark J.T. Baker (Madrid, Spain); and toluene of the trademark J.T. Baker (Madrid, Spain), all distributed by Industrial Casjim Costa Rica.

Sapwood from *Pinus oocarpa*, *Vochysia ferruginea* and *Vochysia guatemalensis* wood from fast-growing forest plantations in Costa Rica was used, which has been studied and showed good liquid permeability [26] and has also been tested due to its adequate absorption of different substances in the treatments toward the improvement of its properties [26,27,36]. It is important to clarify that in this article, the magnetic permeability was not investigated; therefore, the permeability indicated in the article refers only to liquid permeability. Twenty selected sapwood boards were dried in a moisture content (MC) between 12–15%, from which samples of 6 cm long $\times$ 3 cm wide and 2 cm thick were prepared.

2.2. In Situ Precipitation of Iron Oxide Nanoparticles within Wood

Samples preparation: The in situ preparation of iron oxide NPs in 20 sapwood samples was performed according to the procedure applied by Dong et al. [11] in which 15 samples were selected for impregnation, and 5 sapwood samples were left untreated. All samples were oven-dried at 0% MC. In this condition, the samples were placed in a 3 L capacity reactor, where a vacuum of -70 kPa was applied for 20 min. After the vacuum treatment, the sapwood samples still inside the reactor were exposed to distilled water circulating at room temperature (approximately 22 °C) to eliminate the soluble extractives in water; the process was ended when the water became clear. Afterwards, the samples were dried again to 0% MC. Next, in the same reactor, they were washed in an ethanol/toluene solution (1:2, v/v) with constant stirring at room temperature for 24 h in order to remove the extractives. Finally, the sapwood samples were dried to 0% MC.

In situ precipitation: The 15 extractive-free sapwood samples were then placed back in the reactor with a solution of iron (III) hexahydrate and iron (II) chloride tetrahydrate with a molar ratio of 1.6:1 at a concentration of 1.2 mol/L ferric chloride, which corresponded to 200 g/L of iron (III) hexahydrate and 90 g/L of iron (II) chloride tetrahydrate. To prepare the solution, both solutions were mechanically mixed. For this, the samples were first placed in the reactor under a vacuum of -70 kPa for 30 min, then the solution with the iron mixture was introduced at a pressure of 700 kPa for 2 h. After this time, the 15 treated sapwood samples were removed from the reactor and divided into 3 groups of 5 samples each. Each group was tested for three different immersion times in ammonia: 12, 24 and 48 h. After the corresponding times, the specimens were washed in deionized water until reaching a neutral pH.

Evaluation of the magnetizing process: The magnetic material was evaluated by the weight gain percentage (WGP), absorption and density of the samples. WGP was determined from the weights of the dry samples before and after in situ precipitation, following Equation (1). The absorption of the solution was obtained by Equation (2) from the weights of the dry samples before and after in situ precipitation. The density of the samples was obtained from the weights and dimensions of the dry samples before in situ precipitation (Equation (3)).

$$\text{Weight gain percentage (WGP)} = \frac{\text{Weight}_{\text{after in situ precipitation}}\ (\text{g}) - \text{Weight}_{\text{before in situs precipitation}}(\text{g})}{\text{Weight}_{\text{before in situ precipitation}}\ (\text{g})} \times 100 \quad (1)$$

$$\text{Solution absortion}\left(\frac{\text{L}}{\text{m}^3}\right) = \frac{(\text{Weigth}_{\text{after in situ precipitation}}(\text{g}) - \text{Weigth}_{\text{before in situ precipitation (g)}}}{\text{Volume of sample (cm}^3)} \times \frac{(100\ \text{cm})^3}{1\ \text{m}^3} \times \frac{1\ \text{L}}{1000\ \text{g}} \quad (2)$$

$$\text{Density}\left(\frac{\text{g}}{\text{cm}^3}\right) = \frac{\text{Weigth}_{\text{before sample preparation}}(\text{g})}{\text{Volume}_{\text{before sample preparation (cm}^3)}} \quad (3)$$

at room temperature using a MicroSense EZ7 (Milpitas, California, United States) vibrating sample magnetometer (VSM) in an external magnetic field of −20 to 20 kOe in steps of 2 Oe and 10 Oe at a low magnetic field and in steps of 100 and 500 Oe at higher fields and a time averaging of 100 ms. The saturation of magnetization (M_s), coercivity (H_c) and remanence (M_r) was extracted from the hysteresis loops. The experimental percentage of the magnetic material was obtained, which was calculated by a comparison with the M_s (emu/gram) of the composites with the pure Fe_3O_4. To evaluate the stability of the magnetic properties in an acidic environment, acid resistance tests were performed by immersing the samples in a 4% hydrochloric acid solution for 7 days. The magnetic properties were then evaluated by VSM. The dimensions of the samples for the magnetic tests were 3 × 3 × 7 (longitudinal) mm^3, and three samples were tested for each treatment and species.

2.4. Statistical Analysis

First, the normality and homogeneity of the data and the elimination of outliers in the variables evaluated were checked. A descriptive analysis was performed to determine the average, standard deviation and coefficient of variation for each variable measured. An analysis of variance (ANOVA) was applied with a statistical significance level of $p < 0.05$ to determine the effect of immersion time in ammonia (the independent variable) on the properties evaluated (the response variables). Tukey's test was used to determine the statistical significance of the differences in the averages of the variables.

3. Results and Discussion

3.1. Weight Gain Percentage, Absorption and Density of Magnetic Wood an Ash and Ferron Content

The values of WGP, absorption and the density of magnetic wood are presented in Table 1. WGP varied from 1.48% to 3.53% for *P. oocarpa*, from 4.21% to 6.49% for *V. ferruginea* and from 4.11% to 6.36% for *V. guatemalensis*. The absorption values were between 5.52 and 17.78 L/m^3, and the density values varied from 0.20 to 0.57 g/cm^3.

Table 1. Weight gain percentage, absorption and density of untreated wood and magnetic wood with three different immersion times in ammonia in three tropical wood species from fast-growth plantations in Costa Rica.

Species	Treatment (h)	Weight Gain (%)	Absorption (L/m^3)	Density (g/cm^3)
Pinus oocarpa	Untreated	-	-	0.57 (2.00)
	12	3.53 (55.48) ^{A}	9.78 (11.70) ^{A}	0.36 (4.35) ^{A}
	24	2.10 (16.21) ^{AB}	7.63 (13.44) ^{B}	0.37 (4.29) ^{A}
	48	1.48 (28.36) ^{B}	5.52 (23.30) ^{C}	0.38 (3.98) ^{A}
Vochysia ferruginea	Untreated	-	-	0.38 (3.40)
	12	6.49 (13.32) ^{A}	12.70 (9.48) ^{A}	0.20 (3.82) ^{A}
	24	6.09 (8.96) ^{A}	12.00 (9.22) ^{A}	0.20 (2.40) ^{A}
	48	4.21 (35.20) ^{B}	8.30 (34.05) ^{B}	0.20 (2.05) ^{A}
Vochysia guatemalensis	Untreated	-	-	0.37 (3.01)
	12	5.38 (15.50) ^{A}	14.15 (10.00) ^{A}	0.27 (7.59) ^{A}
	24	6.36 (48.96) ^{A}	17.78 (45.12) ^{A}	0.29 (4.10) ^{A}
	48	4.11 (15.06) ^{A}	11.07 (10.13) ^{A}	0.28 (5.61) ^{A}

Note: Numbers in parentheses mean coefficient of variation, and different letters in average mean significant differences between treatment at 95% in each species.

For the magnetic wood of *Pinus oocarpa*, treatment for 12 h had the highest values of WGP, but these were similar to that of 24 h, while the sample treated for 48 h presented the lowest values of WGP (Table 1). Regarding the absorption, the sample treated for 12 h had the highest value, followed by the 24 h treatment, while the 48 h treatment presented the lowest values (Table 1). In *Vochysia ferruginea*, the highest WGP and absorption values

The percentage of ash and the Fe_3O_4 NPs content formed in the treated samples were also determined. For each species and each different immersion time in ammonia and from the untreated wood, three samples were taken and ground to a size of 420 µm to 250 µm (40 and 60 mesh, respectively), and the ash percentage was determined according to ASTM-D1102-84 [37]. Once the ash content had been obtained, the ground samples were used to determine the Fe_3O_4 NPs content in the samples by the procedure of metal determination by direct aspiration in an atomic absorption spectrometer (AAnalyst 800, MA, USA), following ASTM D6357-19 standard [38]. Once the iron value of the tested sample had been obtained, the amount of Fe_3O_4 in the wood was calculated by Equation (4).

$$Fe_3O_4\left(\frac{mg}{kg\ wood}\right) = \frac{\text{Ash content}_{sample}(\%)}{100} \times \frac{Fe_3O_4\ \text{content}_{\ sample}(mg)}{1_{\ ash}(g)} \times \frac{1000_{\ ash}\ (g)}{1_{\ ash}(kg)} \quad (4)$$

with the ash and Fe_3O_4 NP contents evaluated as described above.

2.3. Experimental Techniques

Fourier transform infrared spectroscopy (FTIR): Three samples from each species and each different immersion time in ammonia and from one untreated wood sample were ground to a size of 420 µm to 250 µm (40 and 60 mesh, respectively). The ground material was dried to 0% MC. The samples were scanned by FTIR using a Nicolet 380 FTIR spectrometer (Thermo Scientific, Mundelein, IL, USA) with a single reflecting cell (equipped with a diamond crystal). The equipment was set up to take readings by accumulating 32 scans with a resolution of 1 cm^{-1}, with background correction before each measurement. The FTIR spectra obtained were processed with Spotlight 1.5.1, HyperView 3.2 and Spectrum 6.2.0 software developed by Perkin Elmer. Inc (Waltham, MA, USA).

Field emission scanning electron microscopy: Samples with dimensions of 5 mm wide × 5 mm thick × 10 mm long from of each species and immersion time and from the untreated wood were prepared, cutting two of their corners in the form of a truncated pyramid. On the top surface of the sample, a cut was made using an American Optical Corp model 860 microtome (Búfalo, NY, USA), providing a smooth surface with a little roughness to increase the quality of the microphotography. Scanning electron microscopy (SEM) was performed with a tabletop microscope (TM 3000, Tokyo, Japan without a gold or carbon film covering the sample, using a working distance (WD) of 3.8 to 5.8 mm at 7.5 kV voltage and 400× magnification. The formation of Fe_3O_4 NPs and the part of the anatomical elements where the iron was deposited were observed.

X-ray diffraction (XRD): XRD was performed on samples from each species studied and each immersion time in ammonia and from untreated wood, using a PANanalytical Empyrcan Series 2 diffractometer, Madrid, Spain (Cu–Kα, 6°–40° 20) in conjunction with PANalytical High Score Plus software (version 5.1, Madrid, Spain). Sawdust from the treated and untreated samples was used and placed on a neoprene rectangle on a glass plate for measurement. The parameters of the apparatus were set as follows: Cu–Ka radiation with a graphite monochromator, a voltage of 40 kV, an electric current of 40 mA and a 2 h scan range from 5° to 55° with a scanning speed of 2°/min. The average diameter of the crystalline Fe_3O_4 NPs in the magnetic wood was evaluated on the basis of its XRD pattern using the Scherrer equation (Equation (5) [39], which provides a lower bound on the coherent scattering domain size, referred to as the crystallite size. The values for the equation were obtain using PANalytical High Score Plus software for the peak at 30°.

$$D = \frac{K\lambda}{(\beta \cos\theta)} \quad (5)$$

where D is the diameter of the Fe_3O_4 NPs, λ is the X-ray diffraction wavelength (0.15418 nm), K is the Scherrer constant (0.89), β is the peak full width at half maximum (FWHM) and θ is the Bragg diffraction angle.

Vibrating sample magnetometry (VSM): The magnetic hysteresis loops (magnetization versus applied magnetic field) of wood samples of the different treatments were determined

were observed in the 12 h and 24 h treatments, and the treatment for 48 h showed the lowest values (Table 1). In *Vochysia guatemalensis*, no differences were observed among the treatments. In relation to density in the three tropical species, all magnetizing treatments decreased the wood density, for which the highest decrease occurred in *P. oocarpa* and the lowest in *V. guatemalensis* (Table 1).

As expected, ash content and Fe_3O_4 NP content were higher under all magnetization treatments in the three species than in the untreated wood. The ash content in *P. oocarpa*, *V. ferruginea* and *V. guatemalensis* varied between 0.15% and 4.11%, between 1.47% and 10.40% and between 2.51% and 7.85%, respectively. The highest percentage was observed in the 12 h and 24 h treatments, and the lowest values were in the 48 h treatment (Figure 1a). The Fe_3O_4 content varied from 0.07 to 817.19 mg/kg for *P. oocarpa*, from 0.70 to 4298.45 mg/kg for *V. ferruginea* and from 0.65 to 1907.7 mg/kg for *V. guatemalensis* (Figure 1b).

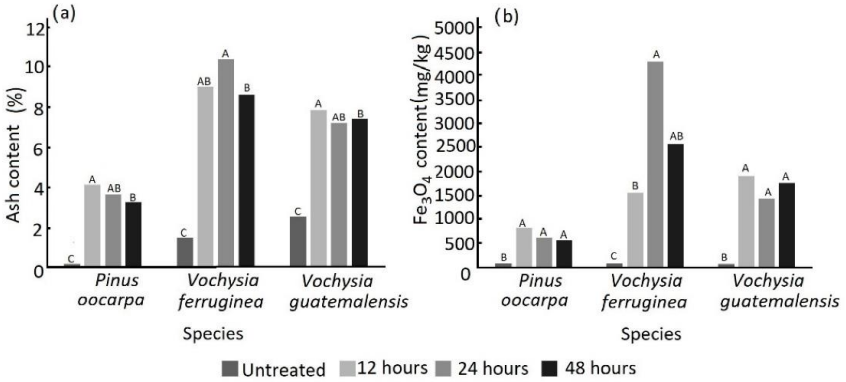

Figure 1. Ash (**a**) and Fe_3O_4 NPs (nanoparticles) (**b**) content of untreated wood and magnetic wood with three different immersion times in ammonia in three tropical wood species from fast-growth plantations in Costa Rica. Note: Letters mean significant differences between treatment at 95% in each species.

It was observed that in *P. oocarpa*, the Fe_3O_4 content was highest under the 12 h treatment at 817.19 mg/kg; however, no statistically significant differences were found among the three immersion times (Figure 1b). In *Vochysia ferruginea*, a statistically significant difference was observed among the different treatments: the highest content of Fe_3O_4 NPs was observed for 24 h of magnetization at 4298.45 mg/kg (Figure 1b). In *Vochysia guatemalensis*, the magnetization process increased the Fe_3O_4 NP content for all three immersion times, and the highest value was observed for the 12 h magnetization treatment at 1907.12 mg/kg (Figure 1b).

The WGP values were lower than those obtained by Dong et al. [11] for fast-growing poplar wood (*Populus tomentosa*) using the same Fe_3O_4 precipitation method. These authors reported an average of 27.93%, while the present study obtained values lower than 6.09% (Table 1). Meanwhile, Gao et al. [40] obtained a very wide range of WGP in fir wood samples from 5.8 to 78%; the lower limit of this range is congruent with the WGP values of the two *Vochysia* species, but *P. oocarpa* presented lower WGP values (Table 1). Likewise, the values found here are congruent with those reported by Hamaya et al. [41], who did not indicate the species used for impregnation with the iron NP but reported a WGP lower than 4.6%, a percentage slightly lower than those found in the two *Vochysia* species and similar to the percentages of *P. oocarpa* (Table 1).

Another important factor with respect to WGP and the solution absorption values is that there was a tendency for these values to decrease with an increase in the immersion time in ammonia in *P. oocarpa* and *V. ferruginea*, while the opposite occurred in *V. guatemalensis* (Table 1). This behavior may be attributed to the fact that the alkaline condition of the ammonia solution leads to partial degradation of lignin and hemicellulose [16,18,40,42,43],

which accentuates the degradation of these polymers with an increasing immersion time of the wood in ammonia. This results in less precipitation of Fe_3O_4 NPs.

The effect of the immersion time in ammonium was confirmed by observing the values of the ash and Fe_3O_4 NP content. Although there was a significant increase in these parameters through the treatment for producing Fe_3O_4 NPs in situ, these decreased for the 48 h immersion time in *P. oocarpa* and *V. ferruginea* (Figure 1). Again, the degradation of lignin and hemicellulose that occurs when using prolonged immersion times [16,18,40,42,43] leads to reduced precipitation of Fe_3O_4 NPs, decreasing the amount of these (Figure 1a) and the amount of inorganic material (ash content) present in the wood after the thermal degradation process had been applied to determine ash content [41]. The increase in the amount of ash in these species agreed with studies carried out by other authors on other species [16,18,40,42,43], and they attributed the increase in inorganic material in the wood to the in situ deposition of iron.

The absorption and retention of Fe_3O_4 NPs varied among the different tropical hardwood species. Such variability is attributed to the wood's permeability or the fluid flow in the wood [42], which can vary depending on the anatomical elements comprising them. In hardwood species, the liquid flow occurs mainly in the longitudinal direction through the lumina of the vessels, which are connected at the end to another vessel through the perforation plates [42]. Radial flow occurs through the radial parenchyma, which is fed by radiovascular punctuations. The liquid then flows transversally through the lumen of the ray cells, passing to other ray cells through the pits at the ends or the lateral pits of other rays [42]. Radial flow is favored when the rays comprise more than three series in width [42]. These variations that occur in these anatomical elements produce variations in the absorption (Table 1) and retention of Fe_3O_4 NPs (Figure 2a).

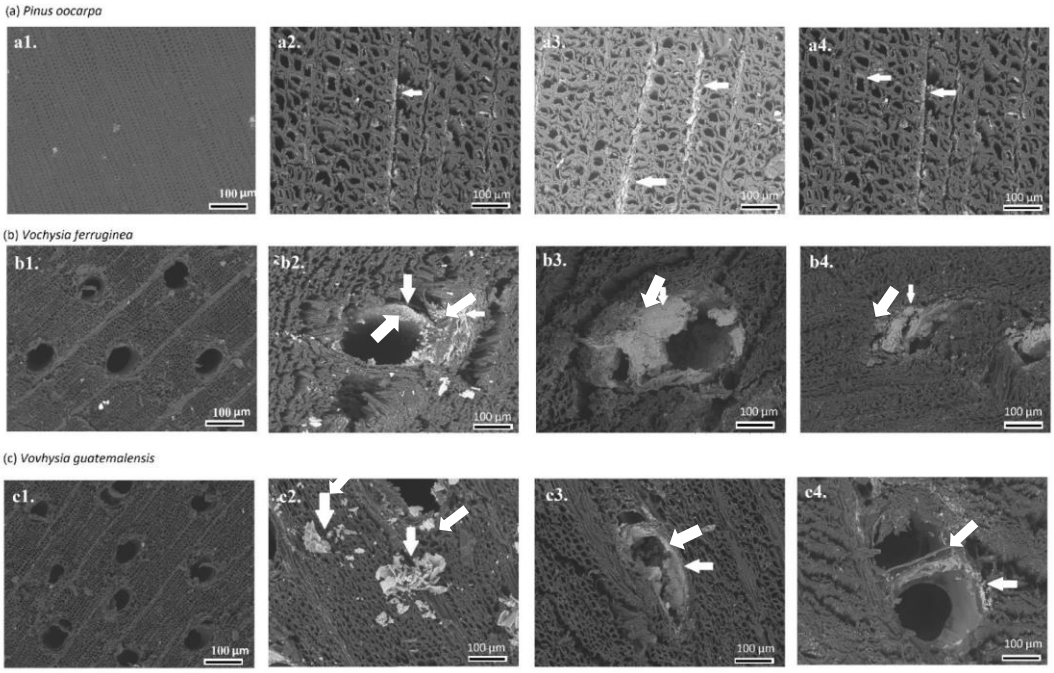

Figure 2. Scanning electron microscope (SEM) images showing Fe_3O_4 NPs formation of magnetic wood with three different immersion times in ammonium (1: untreated, 2: 12 h, 3: 24 h; 4: 48 h) in three tropical wood species (**a–c**) from fast-growth plantations in Costa Rica. Note: The white arrow indicates the formation of Fe_3O_4 NPs in the rays, fibers or vessels.

The major effect on wood after the magnetizing process was the decrease in wood density (Table 1), with the possible consequence of degradation in other wood properties due to its relationship with mechanical properties [43]. This decrease is attributed to the fact that during the deposition of the Fe_3O_4 NPs, the NPs attach to the inner surface of the lumen of the fiber [16], then the dissolution of lignin and hemicellulose occurs during the ammonia immersion process [44], and components with a low molecular weight are removed from the wood [41].

The decreases in density in *P. oocarpa* resulting from the Fe_3O_4 NP deposition method disagrees with the results for other wood magnetizing methods, such as the one developed by Oka et al. [9,18], who treated wood with Mn–Zn ferrite powder and a polyvinyl acetate resin emulsion mixed in water to create the magnetic coating material. According to Liu et al. [22], alkaline immersion makes the method more invasive in the structural components of the wood compared with other methods that do not use it.

3.2. SEM Observation

The SEM images showed deposits of iron NPs in different anatomical elements of the magnetic wood (Figure 2a–c) and the untreated samples of each species (Figure 2(a1,b1,c1)). In *P. oocarpa*, during the magnetizing process, the iron was deposited principally in the rays and, in a smaller amount, in the fibers (Figure 2(a2–a4)). In *V. ferruginea* (Figure 2(b2–b4)) and *V. guatemalensis* (Figure 2(c2,c3)), we can observe the iron deposits in the walls of the vessels and a smaller amount in the fibers. In addition, no wood collapse was observed due to the treatment, as occurred in *Populus* species [16] and *Fagus sylvatica* [45].

The process of Fe_3O_4 NPs deposition has been extensively detailed in different studies; however, most of them have concentrated on softwood species, such as *Pinus sylvestris* [41] and *Picea abies* [46]. Studies that have described research into the formation of Fe_3O_4 NPs in softwood species, which is more extensive, have focused on the location of Fe_3O_4 NPs within the fibers [11,17,18,47–50], leaving a void in the knowledge about the formation of NPs in other wood structures, such as vessels and rays; therefore, the present study aimed to cover this neglected element.

By observing the specific location of Fe_3O_4 NPs in each of the species, it was found that although *P. oocarpa* is a softwood species, the deposition of NPs mostly happened in the fibers [41,46], which was not expected, since it has been observed that in this species, deposition occurs mainly in the rays. This species has a number of resin canals in the axial and radial directions in the wood structure (over 10%), where the resin is deposited in the ducts themselves or in adjacent cells [47], thus preventing an adequate flow of liquid during the process of magnetizing the wood [48]. This situation means that the greatest amount of Fe_3O_4 NPs is likely to form in the rays and a little amount in the lumens of the fiber.

Fe_3O_4 NP formation occurs mainly in the lumina of the vessels, followed by the radial and axial parenchyma and, to a lesser extent, in the fibers (Figure 2). This pattern of in situ deposition in the different anatomical elements is attributed to the fluid transport mechanisms within the hierarchical structure [49]. The flow within hardwood happens within one of the anatomical components, the vessels [42]; therefore, greater in situ formation of Fe_3O_4 NPs inside this component was expected. After the vessels, the rays are the next anatomical elements in terms of the flow inside the wood, particularly for radial conduction [27]. Therefore, the formation of Fe_3O_4 NPs in these anatomical elements is to be expected. In the case of fibers in hardwood species, these constitute anatomical elements of trees used for structural support, not to transport liquid [42]; therefore, little in situ formation of Fe_3O_4 NPs is expected in the fibers (Figure 2c).

3.3. XRD Spectrum

The crystalline structures of untreated and treated specimens were characterized by XRD (Figure 3a–c). Untreated wood of the three species showed the typical diffraction angles at 2θ of cellulose [50] at 15.8°, 22.2° and 34.6°, corresponding to (101), (102) and (040),

respectively (Figure 3a–c). The patterns of the iron composites showed that the two peaks of cellulose (at 15.8° and 22.2°) were slightly weaker in the treated specimens and that the peak at 34.6° was covered by other peaks at 35° for all three species (Figure 3a–c). According to Dong et al. [11], these changes indicate that part of the crystalline structure of the wood was damaged, confirming that the ammonia treatment affects the wood's structure.

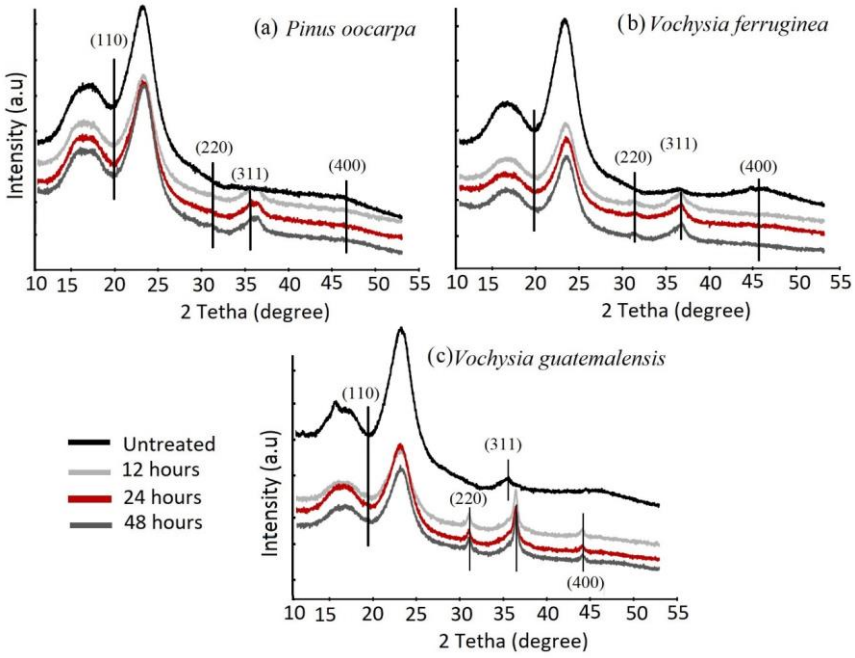

Figure 3. X-ray diffraction (XRD) in untreated wood and magnetic wood of three tropical wood species from fast-growth plantations in Costa Rica: (**a**) *Pinus oocarpa*, (**b**) *Vochysia ferruginea* and (**c**) *Vochysia guatemalensis*.

In addition to these changes, magnetized wood presented diffraction peaks at 2θ: 30°, 35° and 44°, which corresponded to the (220), (311) and (400) planes of Fe_3O4, respectively (JCPDS number 19-0629) (Figure 3a,b), indicating a cubic phase with the space of $Fd\bar{3}m$ [51]. Although no differences were found among the different immersion times in ammonia, there were differences among species. In the case of the three treatments tested in *P. oocarpa*, the weakest diffraction peaks were found at 30° (220), 34° (311) and 44° (400); in fact, the peaks at 30° (220) and 34° (311) were almost null (Figure 3a). In *V. ferruginea*, the strongest peaks were located at 30° and 35°, especially under the 12 h and 24 h treatments (Figure 3b). In *V. guatemalensis*, the strongest diffraction peaks were found at 30°, 35° and 44°, especially under the 48 h treatment (Figure 3c). These differences in the patterns and the determination of particle size using the Scherrer equation (Equation (5)) [38] showed that the dimensions of the deposited Fe_3O_4 NPs were different in each of the species: the largest size was obtained in *V. ferruginea*, followed by *V. guatemalensis*, and the smallest was found in *P. oocarpa* (Table 2). The particle sizes in *P. oocarpa* agreed with the values found by Mashkour and Ranjbar [17]; the values for the *Vochysia* species were slightly larger than those reported by Lou et al. [16] and Gao et al. [40]. However, XRD showed inorganic particles, and we suggest that these were Fe_3O_4. This result must be considered with care because Fe_2O_3 presents a similar spectrum to Fe_3O_4, and the latter particle can be oxidized to Fe_2O_3 during storage. However, the author tried to avoid this forming during the research, and the magnetic test showed magnetic characteristics.

Table 2. Particle size of Fe_3O_4 NPs in the magnetic wood with three different immersion times in ammonia in three tropical wood species from fast-growth plantations in Costa Rica.

Treatment (h)	Nanoparticle Size (nm)		
	Pinus oocarpa	*Vochysia ferruginea*	*Vochysia guatemalensis*
12	7.27 (3.13) ^{B}	19.23 (1.98) ^{A}	12.58 (1.78) ^{A}
24	7.84 (2.15) ^{AB}	18.19 (2.45) ^{AB}	12.74 (2.51) ^{A}
48	8.49 (2.78) ^{A}	17.88 (1.96) ^{B}	12.58 (2.65) ^{A}

Note: Numbers in parentheses mean coefficient of variation, and letters mean significant differences between treatment at 95% in each species.

The smallest NPs were found in *P. oocarpa*; the largest NPs were in *V. ferruginea*, and an intermediate size was found in *V. guatemalensis*. The time of immersion in ammonia also affected the size of the particles in the different species. The largest NPs were observed for the 48 h magnetizing process, followed by the 24 h and 12 h treatments in *P. oocarpa*. In the case of *V. ferruginea*, the largest NPs were found for the 12 h treatment, but no differences among the treatments were found in *V. guatemalensis* (Table 2). Regarding previous results about the size of NPs, *P. oocarpa* and *V. guatemalensis* presented particle sizes smaller than the values reported by Gao et al. [40], Dong et al. [11,16], Li et al. [24], and Garskaite et al. [44], but the NP size in *V. guatemalensis* was similar to the results of those studies.

3.4. FTIR Spectrum

FTIR was used to track the changes in the chemical composition of the untreated and treated specimens. Although in Figure 4 the range from 1950 to 3500 cm^{-1} is not presented, this region presents the absorption bands assigned to the O–H stretching vibration of hydroxyl groups (3340 cm^{-1}), and the bands at 2901 corresponded to asymmetric -CH_3 [12]. No differences were observed between the untreated and treated samples in this region. The range from 650 to 1950 cm^{-1} in the FTIR spectra showed the changes in the structures of cellulose (an alteration in the peak at 1153 cm^{-1}), hemicellulose (a change in the peak at 1739 cm^{-1}) and lignin (modification of the peaks at 1601, 1505, 1462, 1419 and 1251 cm^{-1}).

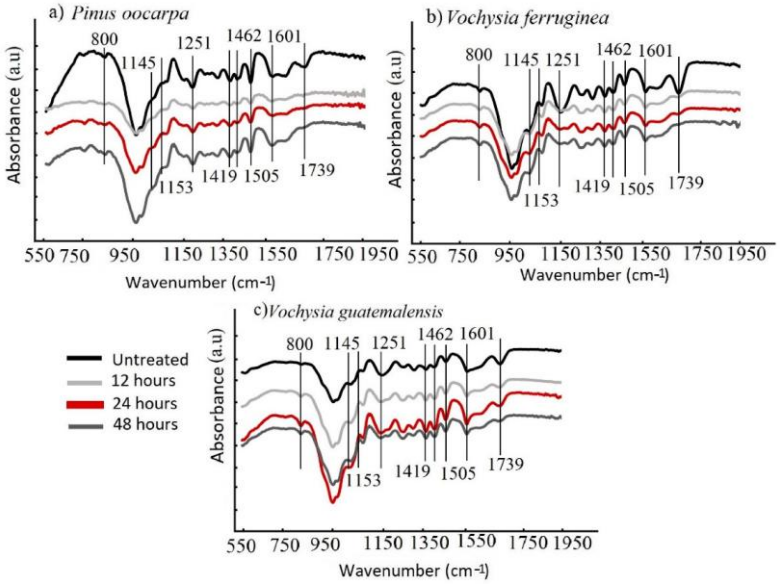

Figure 4. Fourier transform infrared spectroscopy (FTIR) spectrum of untreated and magnetic wood with three times of three tropical wood species (**a**–**c**) from fast-growth plantations in Costa Rica: (**a**) *Pinus oocarpa*, (**b**) *Vochysia ferruginea* and (**c**) *Vochysia guatemalensis*.

The main vibrations, where the greatest changes in the wood occurred, were identified at the peaks at 1251 cm^{-1}, which is related to the C–O stretching vibration; 1505 cm^{-1} for the cell wall components of lignin; 1601 cm^{-1} for the cell wall components of cellulose; 1739 cm^{-1}, assigned to C=O stretching in nonconjugated ketones and ester groups; 2901 cm^{-1}, corresponding to asymmetric CH_3; and 3340 cm^{-1}, the absorption band assigned to the O–H stretching vibration of hydroxyl groups [11,13,22,38]. The weakened signal at 1739 cm^{-1} belonged to the C=O stretching vibration absorption peak of hemicellulose [52], which tended to be decreased by the magnetizing process in all three species. This weakening was in agreement with the studies presented by Gao et al. [40], Dong et al. [11,16], Gan et al. [13,14], Liu et al. [24], Wang, et al. [21], Yuan et al. [40] and Garskaite et al. [44]; in these studies, the weakening was attributed to hemicellulose degradation.

The modification of the structure of cellulose was not affected: the 1145 cm^{-1} signal indicating the stretching vibration of C–O in the glucose of cellulose [39] was similar in untreated and treated wood. Meanwhile, major weakening of the lignin signal occurred at 1601 cm^{-1} (C=C aromatic skeletal vibrations [41]) and 1251 cm^{-1} (the ester linkage of carboxylic groups of the ferulic and p-coumaric acids of lignin [53]) in all three wood species; although other signs of lignin at 1505 cm^{-1}, 1462 cm^{-1} and 1419 cm^{-1} did not suffer any modification.

It was seen that in *P. oocarpa*, the signal at 1739 cm^{-1} tended to decrease after the magnetizing process (Figure 4a). In *V. ferruginea*, the greatest changes in the signal intensities occurred at 1251, 1739 and 2240 cm^{-1}, where the signals were weaker compared with those in the untreated samples (Figure 4b). In *V. guatemalensis*, the signals at 1251 and 1739 cm^{-1} tended to decrease after the magnetizing process, and the signal at 1601cm^{-1} increased, especially under the treatment for 48 h (Figure 4c).

According to the FTIR spectra, cellulose and hemicellulose were less affected in *V. guatemalensis*, confirming that this species was less affected by the ammonia treatment during the magnetization process. However, the lignin was moderately affected, which proves that the wood density was less affected compared with the other two species (Table 1).

The formation of Fe_3O_4 in the bands below 800 cm^{-1} and the bands around 561 and 667 cm^{-1} made it difficult to demonstrate the formation of Fe_3O_4 because there were overlaps with other signals; therefore, other techniques that measure the wavelength between 650 and 450 cm^{-1} are needed [51,54]. Despite the signal overlapping at 800 cm^{-1}, it was possible to observe that this peak corresponded to tetrahedral sites of the crystal lattice, and this was a result of the oxidation of Fe^{2+} and Fe^{3+} [41], which increased mainly in the wood of *V. ferruginea* and *V. guatemalensis* (Figure 4b,c). In the wood of *P. oocarpa*, there was little evidence of a peak (Figure 4a), thus confirming the low measured Fe_3O_4 NP content (Figure 1a) and the poor treatment observed through SEM photographs (Figure 2a) compared with the other two wood species.

3.5. Magnetic Properties of Wood

Figure 5a–c show the hysteresis curves of the untreated wood and magnetic wood. The representative magnetic properties (H_c, M_r and M_s) were extracted from the hysteresis loops, while the percentage of magnetic NPs present in the samples was calculated from the saturation magnetization of the pure Fe_3O_4 NPs for which the value was 15.37 emu/g. As a side note, it is well known that NPs show a lower M_s compared with the M_s of their bulk materials [55]; in this case, the bulk Fe_3O_4 had an Ms of 93 emu/g [56].

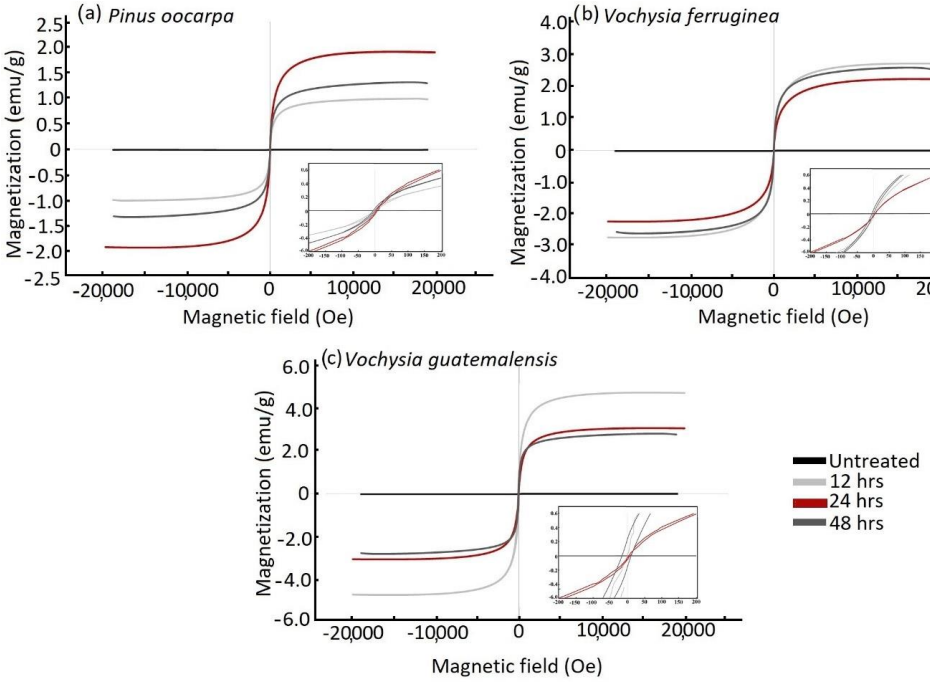

Figure 5. Magnetic hysteresis curves of untreated wood and magnetic wood with three different immersion times in ammonia in three tropical wood species from fast-growth plantations in Costa Rica: (**a**) *Pinus oocarpa*, (**b**) *Vochysia ferruginea* and (**c**) *Vochysia guatemalensis*.

In the case of the untreated wood, the hysteresis loops showed diamagnetic behavior with a negligible M_s (Figure 5), which is the expected behavior of wood. On the other hand, the treated wood (i.e., magnetic wood) of all specimens exhibited a clear hysteresis loop corresponding to ferromagnetic behavior (Figure 6). However, large differences among species were found. For example, the saturation of magnetization was the lowest (from 1.0 to 2.5 emu) in *P. oocarpa* (Figure 5a) and the highest in *V. guatemalensis* (Figure 5c), and *V. ferruginea* had intermediate values (Figure 5b). These results indicate that the species *P. oocarpa* was less magnetized and *V. guatemalensis* was the most magnetized. The variation in the saturation of magnetization of the analyzed species was produced by the variation in the precipitation of the Fe_3O_4 NPs, which corresponded to the different amounts of this compound that every species maintained (Figures 1a and 2a); this difference in the amount is related to the variation in WGP (Table 1). It has previously been indicated that such variability is attributed to the wood's permeability or the fluid flow in the wood [42], which varies depending on the anatomical elements of the wood.

An important aspect regarding the values of H_c, M_r and M_s of the species in this work is that they presented lower values compared with those of previous studies [11,40,47]. Although previous studies have used other methods of precipitating the NPs of Fe_3O_4, these low values may be associated with the low aptitude for the flow of liquid substances in the studied species. However, this result is congruent with other wood modification treatments in these tropical species, such as mineralization, acetylation and furfurylation, which have also shown low saturation magnetization values due to the low permeability of the liquids in the wood [27,36]. In this case, we related the differences in the magnetic properties in this work compared with other studies to the immersion times in ammonia.

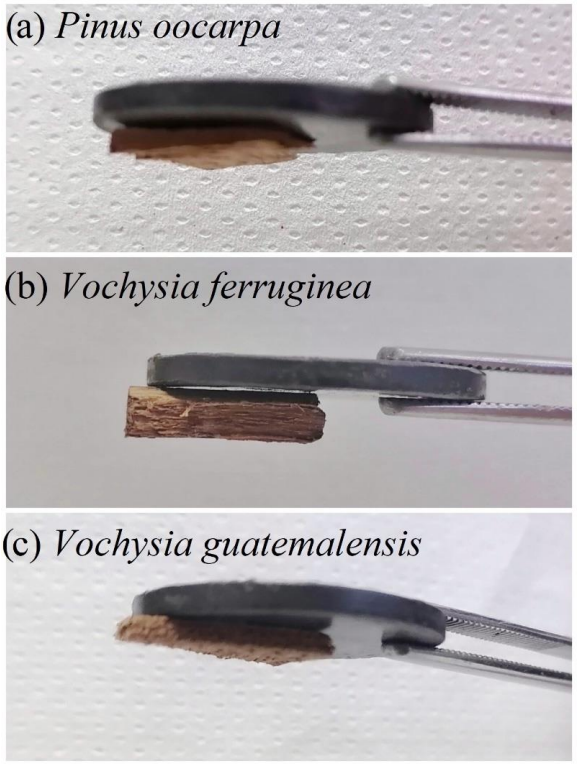

Figure 6. Magnetic wood samples from fast-growth plantations in Costa Rica. The figure shows a permanent magnet attracting the wood as a way to show the magnetic behavior of the samples.

The major difference related to the M_s among the species and different treatment time. It is worth mentioning that this difference is not great and it lies in the differences of the corresponding experimental percentage of the Fe_3O_4 NPs present in the wood, as explained before, which, in some cases, increased by one order of magnitude. For example, *Pinus oocarpa* under the 24 h treatment had the highest M_s (Figure 5a), but still showed no statistical difference from the 12 h and 48 h treatments (Table 3). In the case of *Vochysia ferruginea*, the M_s values presented a linearly inverse behavior: the M_s decreased with an increase in immersion time. Regarding the values of H_c, samples treated for 12 h and 48 h showed a similar hysteretic behavior between each other (i.e., similar values of H_c); even so, these values were higher than that of the 48 h treatment (Figure 5b). In *Vochysia guatemalensis*, the treatment with the highest M_s was observed in the sample subjected to 12 h of the magnetizing process (Figure 5c), but there was no significant difference in the other samples with different treatment times (Table 3). According to these results, the different immersion times in ammonia had no effect on the magnetic properties of the wood, a result that disagrees with the study by Lou et al. [16], which found that the M_s increased with immersion time, which was attributed to the increase in the attachment of Fe_3O_4 generated in situ to the surface of the wood fibers.

Table 3. The coercivity (H_c), retentivity (M_r), saturation magnetization (M_s) and the experimental percentage of magnetic wood with three different immersion times in ammonia in three tropical wood species from fast-growth plantations in Costa Rica.

Species	Treatment (h)	M_s (emu/g)	H_c (Oe)	M_r (emu/g)	Experimental Percentage (%)
Pinus oocarta	12	1.05 ^{B}	4.39 ^{A}	0.01 ^{B}	6.83 ^{B}
	24	1.83 ^{B}	3.87 ^{A}	0.01 ^{B}	11.88 ^{B}
	48	1.10 ^{B}	3.76 ^{A}	0.02 ^{B}	7.16 ^{B}
Vochysia ferruginea	12	2.98 ^{B}	2.45 ^{A}	0.12 ^{B}	19.40 ^{B}
	24	2.34 ^{B}	0.73 ^{A}	0.00 ^{B}	15.22 ^{B}
	48	2.21 ^{B}	2.34 ^{A}	0.02 ^{B}	9.56 ^{B}
Vochysia guatamalensis	12	3.74 ^{B}	11.87 ^{A}	0.17 ^{A}	24.35 ^{B}
	24	3.05 ^{B}	7.08 ^{A}	0.12 ^{A}	19.87 ^{B}
	48	3.29 ^{B}	17.73 ^{A}	0.25 ^{A}	21.38 ^{B}

Note: Letters mean significant differences between treatment at 95% in each species.

If we compare these M_s values with the Fe_3O_4 NP content (WGP in Tables 1 and 3), the lowest value of Ms in *P. oocarpa* agrees with the lowest NP content, although the M_s values of *V. guatemalensis* and *V. ferruginea* are not exactly aligned with the measured NP content. Within each species, *V. ferruginea* had a linear increase in M_s with an increase in NP content, as both decreased with treatment time, while in the other two species, there was no such linear relationship. This nonlinear behavior or incongruence among the species might be because there is little inhomogeneity in the dispersion of the nanoparticle content among the samples [57], resulting in small differences in the magnetic values.

In general, the values of H_c and M_r were very low (Table 3), which indicates the low magnetic properties of the wood [11]. There is also no linear tendency between the treatment time and these values (M_r and H_c). One crucial consideration worth mentioning in the analysis of these values is the NP diameter found by XRD (Table 2). The mechanism by which the NPs alters the magnetization depends on their dimensions, as a maximum H_c can be found for the diameter at which a change between multidomain and monodomain behavior occurs, which, in the case of Fe_3O_4, is around 128 nm [58–61]. Without going much further into this analysis, since it is outside the scope of this work, a low H_c was expected, since the size of the NPs in the magnetic wood was much lower than this value (corresponding to a monodomain switching). On the other hand, superparamagnetism in Fe_3O_4 NPs is expected below 20 nm in diameter, for which almost no hysteresis ($H_c \approx 0$) and lower remanence and saturation magnetization can be obtained. Since the NPs in this work had approximately these dimensions, this might contribute to these lower values. This point is under further study.

Regarding the process, previously, Gan et al. [12] indicated that the alkaline immersion is more invasive of the structural components of the wood than other magnetizing methods, so in the case of these species, the immersion time did not significantly alter the magnetic properties of the wood composites, although the immersion itself might affect the adhesion of the magnetic nanoparticles in the samples.

4. Conclusions

The synthesis of Fe_3O_4 NPs in three tropical species (*Pinus oocarpa*, *Vochysia ferruginea* and *Vochysia guatemalensis*) by in situ impregnation with Fe^{3+} and Fe^{2+} and immersion in ammonia for three different times showed different Fe_3O_4 nanoparticle and wood composite properties. The lowest precipitation occurred in *P. oocarpa*, resulting in lower M_s; on the contrary, the species with the highest M_s was *V. guatemalensis*. In spite of the small effect on the magnetic properties, the change in wood characteristics was evident, such as a decrease in density and changes in the XDR and FTIR spectra, which are associated with changes in the cellulose, lignin and hemicellulose of the wood present in the wood

composites. Contrary to other treatments in other species, the ammonia immersion time had no effect on the magnetic properties or changes in the wood structure.

Author Contributions: Conceptualization, R.M. and J.G.-Á.; methodology, R.M. and J.G.-Á.; software, R.M. and K.J.M.; validation, R.M.; formal analysis, R.M. and K.J.M.; investigation, R.M., J.G.-Á. and A.B.; resources, A.B.; data curation, R.M, A.B. and K.J.M.; writing—original draft preparation, R.M. and J.G.-Á.; writing—review and editing, R.M. and J.G.-Á.; visualization; supervision, R.M. and A.B.; project administration, A.B.; funding acquisition, A.B. All authors have read and agreed to the published version of the manuscript.

Funding: This research received no external funding.

Institutional Review Board Statement: Not applicable.

Informed Consent Statement: Not applicable.

Acknowledgments: The authors wish to thank Vicerrectoría de Investigación y Extensión of the Instituto Tecnológico de Costa Rica (ITCR, Cartago, Costa Rica) for the project financial support.

Conflicts of Interest: The authors declare no conflict of interest.

References

1. Zhang, M.; Han, C.; Cao, W.-Q.; Cao, M.-S.; Yang, H.-J.; Yuan, J. A Nano-Micro engineering nanofiber for electromagnetic absorber, green shielding and sensor. *Nano-Micro Lett.* **2021**, *13*, 27. [CrossRef] [PubMed]
2. Ren, S.; Yu, H.; Wang, L.; Huang, Z.; Lin, T.; Huang, Y.; Yang, J.; Hong, Y.; Liu, J. State of the art and prospects in metal-organic framework-derived microwave absorption materials. *Nano-Micro Lett.* **2022**, *14*, 68. [CrossRef]
3. Wang, L.; Li, N.; Zhao, T.; Li, B.; Ji, Y. Magnetic properties of $FeNi_3$ nanoparticle modified *Pinus radiata* wood nanocomposites. *Polymers* **2019**, *11*, 421. [CrossRef] [PubMed]
4. Pineda, X.; Quintana, G.C.; Herrera, A.P.; Sánchez, J.H. Preparation and characterization of magnetic cellulose fibers modified with cobalt ferrite nanoparticles. *Mater. Chem. Phys.* **2021**, *259*, 122778. [CrossRef]
5. Lykidis, C.; Bak, M.; Mantanis, G.; Németh, R. Biological resistance of pine wood treated with nano-sized zinc oxide and zinc borate against brown-rot fungi. *Eur. J. Wood Wood Prod.* **2016**, *74*, 909–911. [CrossRef]
6. Ali, M.Z.; Javaid, A. Mechanical and rheological characterization of efficient and economical structural wood-plastic composite of wood and PVC. *J. Chem. Soc. Pak.* **2017**, *39*, 183–189.
7. Liu, J.; Declercq, N.F. Acoustic Wood anomaly in transmitted diffraction field. *J. Appl. Phys.* **2017**, *121*, 114902. [CrossRef]
8. Sohn, J.; Cha, S. Effect of Chemical modification on mechanical properties of wood-plastic composite injection-molded parts. *Polymers* **2018**, *10*, 1391. [CrossRef]
9. Oka, H.; Kataoka, Y.; Osada, H.; Aruga, Y.; Izumida, F. Experimental study on electromagnetic wave absorbing control of coating-type magnetic wood using a grooving process. *J. Magn. Magn. Mater.* **2007**, *310*, e1028–e1029. [CrossRef]
10. Oka, H.; Uchidate, S.; Sekino, N.; Namizaki, Y.; Kubota, K.; Osada, H.; Dawson, F.P.; Lavers, J.D. Electromagnetic wave absorption characteristics of half carbonized powder-type magnetic wood. *IEEE Trans. Magn.* **2011**, *47*, 3078–3080. [CrossRef]
11. Dong, Y.; Yan, Y.; Zhang, Y.; Zhang, S.; Li, J. Combined treatment for conversion of fast-growing poplar wood to magnetic wood with high dimensional stability. *Wood Sci. Technol.* **2016**, *50*, 503–517. [CrossRef]
12. Oka, H.; Tanaka, K.; Osada, H.; Kubota, K.; Dawson, F.P. Study of electromagnetic wave absorption characteristics and component parameters of laminated-type magnetic wood with stainless steel and ferrite powder for use as building materials. *J. Appl. Phys.* **2009**, *105*, 07E701. [CrossRef]
13. Gan, W.; Gao, L.; Xiao, S.; Zhang, W.; Zhan, X.; Li, J. Transparent magnetic wood composites based on immobilizing Fe_3O_4 nanoparticles into a delignified wood template. *J. Mater. Sci.* **2017**, *52*, 3321–3329. [CrossRef]
14. Gan, W.; Gao, L.; Liu, Y.; Zhan, X.; Li, J. The Magnetic, Mechanical, Thermal Properties and Uv Resistance of $COFe_2O_4/SiO_2$-Coated Film on Wood. *J. Wood Chem. Technol.* **2016**, *36*, 94–104. [CrossRef]
15. Wang, H.; Yao, Q.; Wang, C.; Ma, Z.; Sun, Q.; Fan, B.; Jin, C.; Chen, Y. Hydrothermal synthesis of nanooctahedra mnfe2o4 onto the wood surface with soft magnetism, fire resistance and electromagnetic wave absorption. *Nanomaterials* **2017**, *7*, 118. [CrossRef]
16. Dong, Y.; Yan, Y.; Wang, K.; Li, J.; Zhang, S.; Xia, C.; Shi, S.Q.; Cai, L. Improvement of water resistance, dimensional stability, and mechanical properties of poplar wood by rosin impregnation. *Eur. J. Wood Wood Prod.* **2016**, *74*, 177–184. [CrossRef]
17. Lou, Z.; Han, H.; Zhou, M.; Han, J.; Cai, J.; Huang, C.; Zou, J.; Zhou, X.; Zhou, H.; Sun, Z. Synthesis of magnetic wood with excellent and tunable electromagnetic wave-absorbing properties by a facile vacuum/pressure impregnation method. *ACS Sustain. Chem. Eng.* **2018**, *6*, 1000–1008. [CrossRef]
18. Mashkour, M.; Ranjbar, Y. Superparamagnetic Fe_3O_4@ wood flour/polypropylene nanocomposites: Physical and mechanical properties. *Ind. Crops Prod.* **2018**, *111*, 47–54. [CrossRef]

19. Oka, H.; Terui, M.; Osada, H.; Sekino, N.; Namizaki, Y.; Oka, H.; Dawson, F.P. Electromagnetic wave absorption characteristics adjustment method of recycled powder-type magnetic wood for use as a building Material. *IEEE Trans. Magn.* **2012**, *48*, 3498–3500. [CrossRef]
20. Trey, S.; Olsson, R.T.; Ström, V.; Berglund, L.; Johansson, M. Controlled deposition of magnetic particles within the 3-D template of wood: Making use of the natural hierarchical structure of wood. *RSC Adv.* **2014**, *4*, 35678–35685. [CrossRef]
21. Wang, Y.; Moo, Y.X.; Chen, C.; Gunawan, P.; Xu, R. Fast precipitation of uniform $CaCO_3$ nanospheres and their transformation to hollow hydroxyapatite nanospheres. *J. Colloid Interface Sci.* **2010**, *352*, 393–400. [CrossRef] [PubMed]
22. Gan, W.; Liu, Y.; Gao, L.; Zhan, X. Magnetic property, thermal stability, UV-resistance, and moisture absorption behavior of magnetic wood composites. *Polym. Compos.* **2017**, *38*, 1646–1654. [CrossRef]
23. Tenorio, C.; Moya, R.; Salas, C.; Berrocal, A. Evaluation of wood properties from six native species of forest plantations in Costa Rica. *Bosque (Valdivia)* **2016**, *37*, 71–84. [CrossRef]
24. Liu, C.L.C.; Kuchma, O.; Krutovsky, K.V. Mixed-species versus monocultures in plantation forestry: Development, benefits, ecosystem services and perspectives for the future. *Glob. Ecol. Conserv.* **2018**, *15*, e00419. [CrossRef]
25. Tenorio, C.; Moya, R. Evaluation of wood properties of four ages of *Cedrela odorata* trees growing in agroforestry systems with Theobroma cacao in Costa Rica. *Agrofor. Syst.* **2018**, *93*, 973–988. [CrossRef]
26. Moya, R.; Gaitan-Alvarez, J.; Berrocal, A.; Araya, F. Effect of $CaCO_3$ in the wood properties of tropical hardwood species from fast-grown plantation in Costa Rica. *BioResources* **2020**, *15*, 4802–4822. [CrossRef]
27. Gaitán-Álvarez, J.; Moya, R.; Berrocal, A.; Araya, F. In-situ mineralization of calcium carbonate of tropical hardwood species from fast-grown plantations in Costa Rica. *Fresenius Environ. Bull.* **2020**, *29*, 9184–9194.
28. Gaitán-Alvarez, J.; Moya, R.; Mantanis, G.I.; Berrocal, A. Furfurylation of tropical wood species with and without silver nanoparticles: Part I: Analysis with confocal laser scanning microscopy and FTIR spectroscopy. *Wood Mater. Sci. Eng.* **2021**, 1–10. [CrossRef]
29. Adebawo, F.G.; Naithani, V.; Sadeghifar, H.; Tilotta, D.; Lucia, L.A.; Jameel, H.; Ogunsanwo, O.Y. Morphological and interfacial properties of chemically-modified tropical hardwood. *RSC Adv.* **2016**, *6*, 6571–6576. [CrossRef]
30. Kojima, M.; Yamamoto, H.; Marsoem, S.N.; Okuyama, T.; Yoshida, M.; Nakai, T.; Yamashita, S.; Saegusa, K.; Matsune, K.; Nakamura, K.; et al. Effects of the lateral growth rate on wood quality of Gmelina arborea from 3.5-, 7- and 12-year-old plantations. *Ann. For. Sci.* **2009**, *66*, 507. [CrossRef]
31. Musah, M.; Wang, X.Ñ.; Dickinson, Y.; Ross, R.J.; Rudnicki, M.; Xie, X. Durability of the adhesive bond in cross-laminated northern hardwoods and softwoods. *Constr. Build. Mater.* **2021**, *307*, 124267. [CrossRef]
32. Pandey, K.K. A study of chemical structure of soft and hardwood and wood polymers by FTIR spectroscopy. *J. Appl. Polym. Sci.* **1999**, *71*, 1969–1975. [CrossRef]
33. Gibson, L.J. The hierarchical structure and mechanics of plant materials. *J. R. Soc. Interface* **2012**, *9*, 2749–2766. [CrossRef] [PubMed]
34. Sperry, J.S. Evolution of Water Transport and Xylem Structure. *Int. J. Plant Sci.* **2003**, *164*, S115–S127. [CrossRef]
35. Ahmed, S.A.; Chun, S.K.; Miller, R.B.; Chong, S.H.; Kim, A.J. Liquid penetration in different cells of two hardwood species. *J. Wood Sci.* **2011**, *57*, 179–188. [CrossRef]
36. Gaitán-Alvarez, J.; Berrocal, A.; Mantanis, G.I.; Moya, R.; Araya, F. Acetylation of tropical hardwood species from forest plantations in Costa Rica: An FTIR spectroscopic analysis. *J. Wood Sci.* **2020**, *66*, 49. [CrossRef]
37. *ASTM D1102-84*; Standard Test Method for Ash in Wood. ASTM International: West Conshohocken, PA, USA, 2013; pp. 1–2.
38. *ASTM D6357-19*;Standard test method for Determination of Trace Elements in Coal, Coke, and Combustion Residues from Coal Utilization Processes by Inductively Coupled Plasma Atomic Emission Spectrometry, Inductively Coupled Plasma Mass Spectrometry. ASTM International: West Conshohocken, PA, USA, 2019.
39. Gao, X.; Dong, Y.; Wang, K.; Chen, Z.; Yan, Y.; Li, J.; Zhang, S. Improving dimensional and thermal stability of poplar wood via aluminum-based sol-gel and furfurylation combination treatment. *BioResources* **2017**, *12*, 3277–3288. [CrossRef]
40. Gao, H.L.; Wu, G.Y.; Guan, H.T.; Zhang, G.L. In situ preparation and magnetic properties of Fe_3O_4/wood composite. *Mater. Technol.* **2012**, *27*, 101–103. [CrossRef]
41. Hamaya, T.; Kono, T.; Aono, R.; Nishimoto, K. Research on the properties of magnetic wood. I. Preparation of magnetic wood by means of enzyme dependent reaction. *Wood Preserv.* **1996**, *22*, 287–293. [CrossRef]
42. Lin, C.-C.; Ho, J.-M. Structural analysis and catalytic activity of Fe_3O_4 nanoparticles prepared by a facile co-precipitation method in a rotating packed bed. *Ceram. Int.* **2014**, *40*, 10275–10282. [CrossRef]
43. Yang, L.; Lou, Z.; Han, X.; Liu, J.; Wang, Z.; Zhang, Y.; Wu, X.; Yuan, C.; Li, Y. Fabrication of a novel magnetic reconstituted bamboo with mildew resistance properties. *Mater. Today Commun.* **2020**, *23*, 101086. [CrossRef]
44. Garskaite, E.; Stoll, S.L.; Forsberg, F.; Lycksam, H.; Stankeviciute, Z.; Kareiva, A.; Quintana, A.; Jensen, C.J.; Liu, K.; Sandberg, D. The Accessibility of the cell wall in scots pine (*Pinus sylvestris* L.) sapwood to colloidal Fe_3O_4 Nanoparticles. *ACS Omega* **2021**, *6*, 21719–21729. [CrossRef] [PubMed]
45. Barauna, E.E.P.; Lima, J.T.; Monteiro, T.C.; dos Santos, V.B.; dos Santos, J.H. Permeability of Parkia gigantocarpa as affected by wood anatomy. *BioResources* **2021**, *16*, 4924–4933. [CrossRef]
46. França, F.J.; Shmulsky, R.; Ratcliff, T.; Farber, B.; Senalik, C.A.; Ross, R.; Seale, R.D. Interrelationships of specific gravity, stiffness, and strength of yellow pine across five decades. *BioResources* **2021**, *16*, 3815–3826. [CrossRef]

47. Mankar, A.R.; Pandey, A.; Modak, A.; Pant, K.K. Pretreatment of lignocellulosic biomass: A review on recent advances. *Bioresour. Technol.* **2021**, *334*, 125235. [CrossRef] [PubMed]
48. Merk, V.; Chanana, M.; Gierlinger, N.; Hirt, A.M.; Burgert, I. Hybrid wood materials with magnetic anisotropy dictated by the hierarchical cell structure. *ACS Appl. Mater. Interfaces* **2014**, *6*, 9760–9767. [CrossRef]
49. Segmehl, J.S.; Laromaine, A.; Keplinger, T.; May-Masnou, A.; Burgert, I.; Roig, A. Magnetic wood by in situ synthesis of iron oxide nanoparticles via a microwave-assisted route. *J. Mater. Chem. C* **2018**, *6*, 3395–3402. [CrossRef]
50. Lou, Z.; Zhang, Y.; Zhou, M.; Han, H.; Cai, J.; Yang, L.; Yuan, C.; Li, Y. Synthesis of magnetic wood fiber board and corresponding multi-layer magnetic composite board, with electromagnetic wave absorbing properties. *Nanomaterials* **2018**, *8*, 441. [CrossRef]
51. Lou, Z.; Wang, W.; Yuan, C.; Zhang, Y.; Li, Y.; Yang, L. Fabrication of Fe/C composites as effective electromagnetic wave absorber by carbonization of pre-magnetized natural wood fibers. *J. Bioresour. Bioprod.* **2019**, *4*, 43–50. [CrossRef]
52. Fabián-Plesníková, I.; Sáenz-Romero, C.; Cruz-De-León, J.; Martínez-Trujillo, M.; Sánchez-Vargas, N.M.; Terrazas, T. Heritability and characteristics of resin ducts in Pinus oocarpa stems in Michoacán, Mexico. *IAWA J.* **2021**, *42*, 258–278. [CrossRef]
53. Leggate, W.; Redman, A.; Wood, J.; Bailleres, H.; Lee, D.J. Radial permeability of the hybrid pine (Pinus elliottii × Pinus caribaea) in Australia. *BioResources* **2019**, *14*, 4358–4372. [CrossRef]
54. Li, J.; Chen, C.; Zhu, J.Y.; Ragauskas, A.J.; Hu, L. In situ wood delignification toward sustainable applications. *Acc. Mater. Res.* **2021**, *2*, 606–620. [CrossRef]
55. Kojima, E.; Yamasaki, M.; Imaeda, K.; Lee, C.G.; Sugimoto, T.; Sasaki, Y. XRD investigation of mechanical properties of cellulose microfibrils in S1 and S3 layers of thermally modified wood under tensile loading. *Wood Sci. Technol.* **2021**, *55*, 955–969. [CrossRef]
56. Li, C.; Weng, Q.; Chen, J.-B.; Li, M.; Zhou, C.; Chen, S.; Zhou, W.; Guo, D.; Lu, C.; Chen, J.-C.; et al. Genetic parameters for growth and wood mechanical properties in Eucalyptus cloeziana F. Muell. *New For.* **2017**, *48*, 33–49. [CrossRef]
57. Lou, Z.; Yuan, C.; Zhang, Y.; Li, Y.; Cai, J.; Yang, L.; Wang, W.; Han, H.; Zou, J. Synthesis of porous carbon matrix with inlaid Fe3C/Fe3O4 micro-particles as an effective electromagnetic wave absorber from natural wood shavings. *J. Alloys Compd.* **2019**, *775*, 800–809. [CrossRef]
58. Kania, A.; Berent, K.; Mazur, T.; Sikora, M. 3D printed composites with uniform distribution of Fe_3O_4 nanoparticles and magnetic shape anisotropy. *Addit. Manuf.* **2021**, *46*, 102149. [CrossRef]
59. Echeverría, J.C.; Moriones, P.; Garrido, J.J.; Ugarte, M.D.; Cervera, L.; Garaio, E.; Gómez-Polo, C.; Pérez-Landazábal, J.I. Steering the synthesis of Fe_3O_4 nanoparticles under sonication by using a fractional factorial design. *Mater. Chem. Phys.* **2021**, *270*, 124760. [CrossRef]
60. Barabaszová, K.Č.; Holešová, S.; Hundáková, M.; Mohyla, V. Mechanically treated vermiculite particles in PCL/vermiculite thin films. *Mater. Today Proc.* **2022**, *52*, 239–247. [CrossRef]
61. Nguyen, M.D.; Tran, H.V.; Xu, S.; Lee, T.R. Fe_3O_4 Nanoparticles: Structures, synthesis, magnetic properties, surface functionalization, and emerging applications. *Appl. Sci.* **2021**, *11*, 11301. [CrossRef]

5. Artículo 2: Magnetic and physical-mechanical properties of wood particleboards composite (MWPC) fabricated with Fe_3O_4 nanoparticle and three plantation wood.

MAGNETIC AND PHYSICAL-MECHANICAL PROPERTIES OF WOOD PARTICLEBOARDS COMPOSITE FABRICATED WITH FE_3O_4 NANOPARTICLES AND THREE PLANTATION WOODS

*R. Moya**†
Professor
E-mail: rmoya@itcr.ac.cr

J. Gaitán-Alvarez
Research Scientist
E-mail: jgaitan@itcr.ac.cr

A. Berrocal
Professor
Escuela de Ingeniería Forestal
Instituto Tecnológico de Costa Rica
Apartado 159-7050, Cartago, Costa Rica
E-mail: aberrocal@itcr.ac.cr

K. J. Merazzo
Researcher
BCMaterials, Basque Center for Materials, Applications and Nanostructures
UPV/EHU Science Park
48940 Leioa, Spain
Escuela de Física
Universidad de Costa Rica
San Pedro 11501-2060, Costa Rica
Materials Science and Engineering Research Center (CICIMA)
Universidad de Costa Rica
San Pedro, Costa Rica
and
Instituto Tecnológico de Costa Rica
Escuela de Física
Apartado 159-7050, Cartago, Costa Rica
E-mail: karlamerazzo@gmail.com

(Received February 2023)

Abstract. This study has the main objective to synthesize in situs Fe_3O_4 nanoparticles (NPs) in fiber particles of three tropical wood (*Pinus oocarpa*, *Vochysia guatemalensis*, and *Vochysia ferruginea*) using two different solutions of Fe^{3+} and Fe^{2+} in an aqueous ammonia solution. The magnetic properties were measured by determining fiber particles' Fe_3O_4 magnetization parameters (coercivity, remanence, and saturation magnetization). The Fourier transform IR and X-ray diffraction spectra were also obtained. After the magnetic wood particleboard (MWPC) was fabricated with 100% magnetic particles (MWPC-100) and a superficial layer magnetized with fiber (MWPC-layer), their physical, mechanics, and magnetic properties were compared. The results showed that Fe_3O_4 NPs content was similar in two Vochyseas species but higher than *Pinus oocarpa*. Ash content was similar in the three species. It was difficult to demonstrate the presence of Fe_3O_4 NPs in the FT-IR spectrum. The diameter of NPs varied from 51 to 68 nm and the saturation magnetization parameters were low, but these values were higher in *Pinus oocarpa*. MWPC showed that the use of NPs decreases the density of *Pinus oocarpa* but increases the density of the Vochyseas

* Corresponding author
† SWST member

Wood and Fiber Science, 55(3), 2023, pp. 211-227
https://doi.org/10.22382/wfs-2023-19

species. Swelling and moisture absorption increased in the MWPC-100 of *Pinus oocarpa* and *Vochysia guatemalensis* but decreased in *Vochysia guatemalensis* composite. The internal bond decreased in MWPC-100, but not in the MWPC layer. Hardness increased in the MWPC layer in *Pinus oocarpa*, but not in MWPC-100, and this property increased in MWPC-100 and the MWPC layer fabricated with *Vochysia ferruginea* and *Vochysia guatemalensis*.

Keywords: Wood composites, wood-based magnetic composites, magnetic properties, tropical wood, wood modification, applied magnetics.

INTRODUCTION

The increasing use of electronic and wireless devices in people's daily lives, such as mobile phones, wireless networks, and home robots, are increasingly generating electromagnetic waves, affecting health in an unprecedented way (Oka et al 2012; Lou et al 2018a). Due to this situation, there is a need to reduce the source of unwanted radiation or reduce its impact on the surrounding area (Oka et al 2012). Several recent works of research have been carried out on the development of materials that are lightweight, which have low thicknesses with the ability to reduce or block electromagnetic waves (Lou et al 2018b; Lv et al 2018).

The combination of magnetic materials with lightweight dielectric materials has been studied, taking advantage of the synergistic effect between the two components (Liu et al 2012; Zheng et al 2014). Among these materials, modified wood has been studied as a material that blocks magnetic waves, which is a renewable and naturally degradable material, highly attractive as a biologically based composite material (Oka et al 2007, 2009; Rahayu et al 2022). The Oka group (Oka et al 2002), more than two decades ago, experimented with wood as a material that blocks electromagnetic waves by proposing the impregnation of magnetic powder inside the wood (Oka et al 2002, 2004a).

Nowadays, three different methods of fabrication of magnetic wood composites have been studied: impregnation of nanoparticles (NPs) of iron in combination with different solvents (Oka et al 2009), powder-type made of magnetic and wood materials, mixed with resins and then pressed under temperature (Oka et al 2007) and wood coatings with magnetic substances (Oka et al 2004b). Among the different methods studied, the impregnation of pretreated wood in a mixed solution with ferrite NPs as Fe_3O_4 (Gan et al 2016), $CoFe_2O_4$ (Gan et al 2017a), and $MnFe_2O_4$ (Wang et al 2017) are the methods that stand out. This synthesis of the magnetic material within the wood occurs by in situ coprecipitation of the ferrite NPs through a chemical reaction of two sources of Fe^{3+} and Fe^{2+} in an aqueous solution, followed by impregnation with an ammonia solution, all this under a vacuum-pressure process (Dong et al 2016; Lou et al 2018a; Mashkour and Ranjbar 2018).

However, wood can come in different forms, from solid wood, through veneers, to particles, and each form will have a different performance/efficiency in the impregnation of Fe^{3+} and Fe^{2+} sources in solution. For shielding or deviating direct magnetic fields, the magnetic susceptibility is the magnetic property that defines the efficiency of the material, and it can be calculated or obtained by the hysteresis loop. When recounting the different ways in which wood has been investigated, the wood solid shape has had the greatest interest and has been investigated in different species, such as *Scots pine* (Garskaite et al 2021), *Populus tormentosa* (Dong et al 2015), fir woods (Gao et al 2012), *Picea abies*, *Fagus sylvatica* (Oka et al 2004a; Dong et al 2015), and poplar wood (Gan et al 2017a). In wood shavings, poplar wood (Mashkour and Ranjbar 2018) and *Populus deltoides* (Mashkour and Ranjbar 2018) have been investigated. Sawdust was magnetized in fir wood and cedar wood (Oka et al 2004a; Lou et al 2019b) and wood in the shade of flours or veneer was tested in two species of Populus (Mashkour and Ranjbar 2018; Lou et al 2019b). The wood fiber shape, flour or veneer, was poorly investigated, although *Populus* spp. and cedar wood reported magnetic properties (Trey et al 2014; Dong et al 2015).

The shape of the wood will determine the degree of penetration of the solution in the liquid state (Bolton and Humphrey 1994). Therefore, a solution from a ferrous source, for the in situ formation of NPs, will also depend on the shape of the wood. For example, in the case of solid wood the penetration depends on the permeability of the wood, in the case of veneer the permeability is less important, since, in general, the thicknesses are not greater than 3 mm; and in the case of shaped wood particle, the thickness is small and the dimensions are big enough to have a greater contact surface between the wood and the iron solutions (Bolton and Humphrey 1994). Thus, it is necessary to investigate different forms of wood for different species.

Another important aspect of the technique of magnetizing the wood in situ, in addition to the shape of the wood, is the species; this method has been applied to different species, such as the genus *Populus*, *Picea abies*, poplar and fir woods, *Scots pine*, *Fagus sylvatica*, and cedar sapwood (Oka et al 2004a; Gao et al 2012; Dong et al 2015; Gan et al 2017a; Mashkour and Ranjbar 2018; Lou et al 2019b; Garskaite et al 2021). These studies have been limited to species of temperate climate.

Recently, Moya et al (2022) carried out the first investigations in tropical woods, applying the in-situ method with good results of coercivity (Hc), retentivity (Mr), and saturation magnetization (Ms) in two different species. They concluded that the use of the method of in situ synthesis of the magnetic material within the wood is appropriate. However, the amount of NPs added is not adequate to achieve high values of Hc, Mr, and Ms. Several authors point out the weaknesses of this method, which can be applied to the results obtained in tropical woods. Lou et al (2019b) and Trey et al (2014) pointed out that the dipolar forces between the impregnated particles easily add to each other forming conglomerates, affecting the uniformity of the particle deposition in different parts of the magnetic wood. Also, Lou et al (2019b) and Trey et al (2014) argued that indeed the magnetic particles mixed with polymers and wood in large quantities lead to brittle compounds, a situation that restricts the adequate application of the particles in the wood in situs.

Other studies (Oka et al 2007; Lou et al 2018b) have described the in situ method as the one that uses immersion impregnation of solid wood or veneer although without the vacuum pressure. Therefore, the impregnation is superficial. Oka et al (2007) noted that low values of Hc, Mr, and Ms in solid wood or veneer are due to the superficial impregnation as it is not possible to control the shape and size of the surface. The process is not feasible and the magnetic particles cannot be deposited properly. Another cause of low values of magnetization parameters is that the surface of the wood is rich in hydroxyl groups, which are electronegative in aqueous solutions, so they are not attractive for assembling layers of NPs on the surface (Tang and Fu 2020). Rao et al (2016) and Renneckar and Zhou (2009), demonstrated that impregnation of wood superficially through the union of polyelectrolytes. However, despite these important advances, the manufacture of magnetic fiber boards by chemical surface coprecipitation, together with the investigation of the properties of magnetic field-blocking of the wood, is limited (Bolton and Humphrey 1994; Dong et al 2015; Lou et al 2018a).

Magnetizing the particles of wood has the advantage of, as we have indicated, a greater contact area (Bolton and Humphrey 1994). Therefore this would be one more option to increase the magnetic properties of tropical woods.

On the other hand, reforestation programs for wood production have been implemented with fast-growing hardwoods using a wide variety of species (Tenorio et al 2016). Recently different methods to improve wood properties such as dimensional stability, MC, biodeterioration, and durability, have been investigated, among which mineralization, acetylation, furfurylation, and densification modification have been achieved (Gaitán-Alvarez et al 2020a, 2021; Moya et al 2020). In addition, in situ magnetized wood has been previously studied in tropical woods with good results in Hc, Mr, and Ms values. However, the amount of NPs added is not adequate to achieve higher

values of these magnetic values (Moya et al 2022).

Therefore, to produce tropical wood species with adequate magnetic properties, this work elaborates magnetic wood particleboards composite (MWPC) with NPs synthesized in situ with $FeCl_3 \cdot 6H_2O$, $FeCl_2 \cdot 4H_2O$, as a source of Fe^{3+} and Fe^{2+}, using the wood of three different tropical species from fast-growth plantations in Costa Rica: *Pinus oocarpa*, *Vochysia ferruginea*, and *Vochysia guatemalensis*. The characterization consists of obtaining the physical properties (density, thickness, swelling, and water absorption), mechanical properties (internal bond and hardness), chemical properties (Fourier transform IR [FTIR] and X-ray diffraction [XRD]), and magnetic properties (vibrating sample magnetometry [VSM]) of wood fiber particles and wood boards.

MATERIALS AND METHODS

Experimental Materials

The reagents used were iron (III) hexahydrate ($FeCl_3 \cdot 6H_2O$) ≥98%; iron (II) chloride tetrahydrate ($FeCl_2 \cdot 4H_2O$) ≥98%; ammonium hydroxide solution at 30%; and absolute ethyl alcohol and toluene.

Sapwood particles of *Pinus oocarpa*, *Vochysia ferruginea*, and *Vochysia guatemalensis* extracted from trees from fast-growing forest plantations in Costa Rica, which have shown good permeability of liquids (Gaitán-Alvarez et al 2020a), were used. These species have shown excellent absorption of different substances by different treatments that have been used to improve their wood properties, such as dimensional stability and resistance to biodeterioration and fire (Gaitán-Alvarez et al 2020a, 2020b; Moya et al 2020). Likewise, the solid wood of these three species has shown acceptable magnetic properties when they were copolymerized in situs with NPs of Fe_3O_4 using the two solutions of Fe^{3+} and Fe^{2+}.

Preparation Wood Particles

For the three species, all logs were first chipped and then milled in a Nogueira DPM-2 blade-hammer mill using a sieve with 5 mm diameter holes. The particles were dried to an MC of approximately 8%. Then, the particles were screened and two sizes were selected to fabricate the composites: 1) particles between 4.9 and 3.0 mm were called large particles and 2) particles between 2.9 and 1.5 mm were called small particles.

In-situ Precipitation

The *in situs* precipitation of NPs Fe_3O_4 was carried out according to Dong et al's (2016) methods was carried out. Firstly, the wood particles were pretreated: 2 kg of each particle size were placed in 20 L (l) of distilled water and heated for 2 h (h), to extract the largest amount of water-soluble extractives. This process was repeated approximately 10 times until the water turned clear. The particles were then dried to constant MC in an oven at 105°C for 24 h. Then, the dried wood particles were placed with a solvent mixture of alcohol/toluene (1:2, V/V) overnight to remove the wood extractive compounds, such as gums, tropolones, fats and fatty acids, and to improve the surface affinity for the iron salts. After this time, the alcohol was allowed to evaporate and then the two groups of particles were dried at 4% MC in an oven. Next, a mixture solution of $FeCl_3 \cdot 6H_2O$ and $FeCl_2 \cdot 4H_2O$ (molar ratio of Fe^{3+}: Fe^{2+} = 2:1) was prepared and dissolved in distilled water to form the iron precursor solution with a concentration of 0.45 mol L^{-1} ferric chloride. The pretreated wood particles were impregnated in the mixture for 12 h, at atmospheric pressure. The particles were filtrated and washed several times with distilled water to remove the residual iron salts on the surface. Then, the particles were dried at 65°C for 12 h and were again impregnated in a 25% ammonia solution for 12 h. Again, the wood particles were filtrated and washed several times with distilled water until reaching neutral pH, and then, the particles were dried at 65°C for 24 h to reach 4% of MC.

Characterization of the Wood Particles

The Fe_3O4 NPs content formed and the ash content was determined for each species and each

treatment (untreated and treated). Three samples were taken with a size of 420 µm to 250 µm (40 and 60 mesh, respectively). The Fe_3O_4 NPs content was measured by direct aspiration in an atomic absorption spectrometer (AAnalyst 800, SpectraLab Scientific Inc, CA), following the ASTM D6357-19 standard (ASTM 2021). Then, the amount of Fe_3O_4 in the wood was calculated by Eq (1). The ash content was determined according to ASTM-D1102-84 (ASTM 2013).

$$Fe_3O_4\left(\frac{\text{mg}}{\text{kg wood}}\right) = \frac{\text{Ash content}_{\text{sample}}(\%)}{100} \times \frac{Fe_3O_4 \text{ content}_{\text{sample}}(\text{mg})}{1_{\text{ash}}(\text{g})} \times \frac{1000_{\text{ash}}(\text{g})}{1_{\text{ash}}(\text{kg})}, \quad (1)$$

where Ash content sample: ash percentage obtained in the laboratory.

FTIR spectroscopy. For each species, three different samples were obtained, for both treated and untreated-sample particles, with a size of 420 µm to 250 µm (40 and 60 mesh, respectively) and dried at 0% of MC (MC). FTIR spectroscopy scanning was performed on the samples using a Nicolet 380 FTIR spectrometer (Thermo Scientific, Mundelein, IL) with a single reflecting cell (equipped with a diamond crystal). The equipment was configured to perform readings accumulating 32 scans with a resolution of 1 cm^{-1}, with a background correction before each measurement. The FTIR spectra obtained were processed with Spotlight 1.5.1, HyperView 3.2, and Spectrum 6.2.0 software developed by Perkin Elmer Inc. (Waltham, MA). The main vibrations where the greatest changes in the wood occurred were identified according to Dong et al (2016), Gao et al (2017), and Gan et al (2017a): the peak in 1251 cm^{-1} was related to C–O stretching vibration, the peak at 1505 cm^{-1} was attributed to the methylene and methyl groups in the saturated hydrocarbons, the peak at 1601 cm^{-1} to C=C aromatic skeletal vibrations of lignin components, the peak at 1739 cm^{-1} was assigned to the C=O stretching in nonconjugated ketones and ester groups, the peak at 2901 cm^{-1} corresponded to $-CH_3$ asymmetric and the peak at 3340 cm^{-1} the absorption band assigned to the O-H stretching vibration of hydroxyl groups.

X-ray diffraction. The XRD spectrum was performed on the treated and untreated particles of the three species. The XRD spectrum was obtained on a PANanalytical Empyrcan Series 2 diffractometer (Malvern Panalytical Ltd, Malvern, United Kingdom) (Cu-Kα, 6° - 40°20), in conjunction with the PANalytical High Score Plus software. The particles were placed in a neoprene rectangle that was placed on a glass plate for measurement. The apparatus parameters were set as follows: Cu-Ka radiation with a graphite monochromator, voltage 40 kV, electric current 40 mA, and 2 h scan range from 5° to 90° with a scanning speed of 2° min^{-1}. The average diameter of crystalline Fe_3O_4 NPs (D) in magnetic wood was evaluated based on its XRD pattern using the Scherrer Eq (2) (Lin and Ho 2014).

$$D = \frac{K\lambda}{(\beta \cos\theta)}, \quad (2)$$

where K is the X-ray wavelength (0.15418 nm), λ is the Scherrer constant (0.89), β is the peak full width at half maximum (FWHM), and θ is the Bragg diffraction angle.

Vibrating sample magnetometry. Three samples of the treated and untreated particles of the studied species were used. Three hundred microgram of particles were pelleted to a cylindrical shape of 5 mm diameter and 5 mm length. Then, the magnetic hysteresis loops (magnetization vs applied magnetic field) were determined at room temperature using a MicroSense EZ7 VSM, in an external magnetic field from −20 to 20 kOe in 2 Oe and 10 Oe steps at a low magnetic field, and in 100 and 500 Oe steps at higher fields, and an average time of 100 ms (Fig 1[a]). The Ms, Hc, and remanence (Mr) were extracted from the hysteresis loops. To evaluate the stability of the magnetic property in the acid environment, acid resistance tests were conducted by immersing the specimens

Figure 1. Vibrating sample magnetometer and location of composite sample (a), metal rack utilized (b), and press application during heating in the particleboards fabrication (c).

in 4% hydrochloric acid solution for 7 d. Then, the magnetic property was evaluated by VSM.

Preparation of MWPC

Three treatments of MWPC were fabricated with 12 mm thickness of the three species: 1) particleboards with untreated wood particles, 2) particleboards with 100% magnetic wood particles (MWPC-100), and 3) particleboards with two layers, one layer of 10 mm thickness with particles untreated and an external layer of 2 mm thickness with magnetic wood particles or treated (MWPC-layer). For the construction of MWPC, a small metal rack was built to make the specimens (Fig 1[b]), according to the methodology used by Moya-Roque et al (2014): 21 specimens for treatment were fabricated, for a total of 63 specimens per species. The fabrication of specimens was circular, with dimensions of 53 mm in diameter and 12 mm in thickness. The rack consisted of a 5 cm diameter metal pipe, 7 cm long with a plug at each end introduced at a 2.9 cm depth as blocks, leaving a 12 mm gap in the middle that corresponds to the thickness of the test specimen. The particleboards specimen was fabricated at a density of approximately 0.70 g cm^{-3} and was made up of 90% coarse chips (4.9 to 3.0 mm) and 10% thin chips (2.9 to 1.5 mm). The particles were uniformly mixed and glued with urea formaldehyde in 10% proportion (weight/weight). Once the mixture was made, the rack was carefully filled and pressed until they filled up the 12 mm gap in the middle with the help of a manual press (Fig 1[c]), after which the semipressed tubes were transferred to a heat press for hot pressing. Using a pressure of 35 MPa at a temperature of 120°C for 30 min. Lastly, the samples were left for a 24 h room-temperature-conditioning period.

Physical Properties

The following physical properties of MWPC specimens were determined: density, thickness swelling,

and water and moisture absorption. The density was measured in all the specimens made in the three species; this was obtained by measuring volume and weight (weight/volume). To determine the thickness swelling and moisture absorption, five MWPC specimens in each treatment were conditioned and weighed at 12% EMC, and then conditioned for 3-4 wk at 18% EMC. After conditioning, the samples were weighed and measured again. This procedure was based on the ASTM D4933-99 norm (ASTM 1999) but modified to the conditions in Costa Rica, where environmental moisture conditions are around 18%. The thickness swelling was calculated using Eq 3. Moisture absorption was determined through Eq 4 by obtaining the percentage weight gain from 12% to 18% of MC with respect to dry weight. The difference between both moisture measurements (12% and 18%) represented the sample moisture absorption (Eq 5).

$$\text{Swelling(mm)} = (\text{g})\frac{\text{measurement 12\% (mm)} - \text{measurement 18\% (mm)}}{\text{measurement 12\% (mm)}} \times 100 \quad (3)$$

$$\text{Moisture content}_{MC} = \frac{\text{Weight}_{MC}(\text{g}) - \text{Weight}_{\text{oven-dried}}(\text{g})}{\text{Weight}_{\text{oven-dried}}(\text{g})} \times 100 \quad (4)$$

$$\text{Moisture absorption} = \text{Moisture content}_{18\%} - \text{Moisture content}_{12\%} \quad (5)$$

For water absorption, another five MWPC specimens for each species/treatment previously weighed were immersed in water for 24 h. After this period, the samples were again weighed, and weight gain or water absorption was determined following Eq 5, according to ASTM D4446-13 (ASTM 1985).

Mechanical Properties

Mechanical properties tested were Janka hardness and internal bond. Janka hardness was determined for eight MWPC specimens per treatment in each species, according to ASTM D143-14 (ASTM 1999). The internal bond test was performed in accordance with the ASTM D1037-12 (ASTM 1999) standard, using another eight specimens per treatment in each species. All mechanical tests were performed on a Tinius Olsen H10KT universal testing machine.

Statistical Analysis

First, the normality and homogeneity of the data and the elimination of strange data or "outliers" of the variables evaluated were checked. Then a descriptive analysis was made, determining the average, standard deviation, and coefficient of variation for each variable studied. Then, analysis of variance was applied to determine the differences in the three treatments, where this represents the independent variable of the model and the measured variables as the dependent variables. Tukey's test was used to determine the statistical significance of the difference between the means of the variables.

RESULTS AND DISCUSSION

Fe_3O_4 and Ash Content

The Fe_3O_4 content of MWPC varied between 176.26 and 466.307 mg kg^{-1}. The composites fabricated with three species were statistically different from untreated wood. The two Vochysias species have similar Fe_3O_4 content (Fig 2[a]), but *Pinus oocarpa* has the statistically lowest values of the three species. Ash values varied between 0.26% and 2.76% for untreated wood and between 3.28% and 4.86% for MWPC, with statistical differences observed in all species between untreated and MWPC (Fig 2[b]).

The retention of Fe_3O_4 NPs, measured by Fe_3O_4 content in ash, was variable in the three different tropical species. This variability is attributed to the fact that the species present different permeability to the flow of liquids within the wood (Thomas 1976). Moya et al (2022) explained that the anatomical structures of the three species used are different and that the species *Vochysia guatemalensis* and *Vochysia ferruginea* have anatomical elements that are more appropriate for fluid

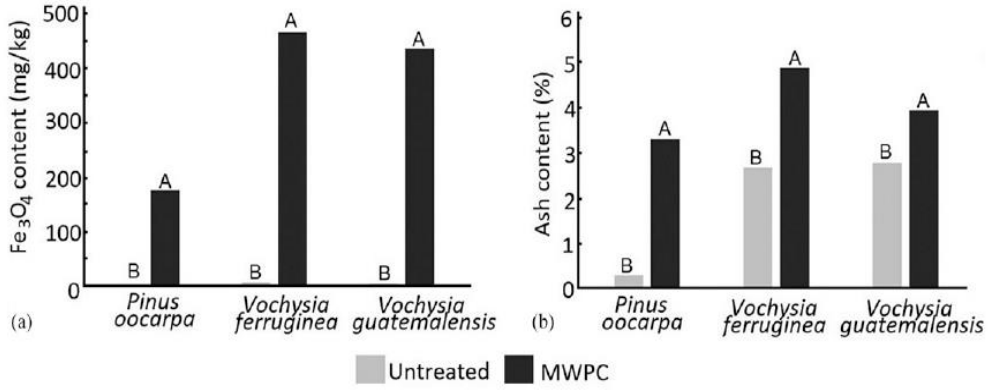

Figure 2. Fe_3O_4 (a) and Ash (b) content of magnetic wood particleboards composite (MWPC) of three tropical species from fast-growth plantations in Costa Rica. Note: Uppercase letters mean statistical differences between treatments at 95% significance.

flow. Thus, these two species achieve greater precipitation of the Fe_3O_4 NPs compared with *Pinus oocarpa* wood.

On the other hand, regarding the Fe_3O_4 content comparison of the three species with solid wood using the same in situ synthesis systems (Moya et al 2022), it was observed that the Fe_3O_4 content in *Pinus oocarpa* average was 817.19 mg kg^{-1}, it ranged from 1600 to 4298 mg kg^{-1} in *Vochysia ferruginea* and the average is 1907 mg kg^{-1} in *Vochysia guatemalensis* and the ash content values were from 3.5% to 4.11% for *Pinus oocarpa*, between 9.47% and 10.40% for *Vochysia ferruginea*, and between 6.51% and 7.85% for *Vochysia guatemalensis* in solid wood (Moya et al 2022). These value ranges of Fe_3O_4 and ash content in solid wood are higher than the values obtained when the wood was magnetized in fiber shape (Fig 2[b]). Therefore, although the formation of NPs was evident, it was lower than when it came to magnetizing solid wood.

The shape of the wood (solid or particle wood) will determine the degree of penetration of the solution in the liquid state (Bolton and Humphrey 1994). Therefore, a ferrous source solution, for the in situ formation of NPs, will also depend on the shape of the wood. In solid wood, the penetration depends on the permeability of the wood; in the case of wood in particle shape, the thickness was small and there was a greater contact surface between the wood and the iron solutions (Bolton and Humphrey 1994). However, regardless of the shape of the wood to be magnetized, it is important to apply pressure during the process. In the case of the solid wood of these species, Moya et al (2022) concluded that the use of the method of synthesis of the magnetic material in situ within the wood was appropriate. However, in the case of the fiber shape, there was no application of pressure, so the ferrous solution was only superficial, and therefore, there was less formation of Fe_3O_4 NPs in relation to the solid wood, in which pressure was applied in the copolymerization process of the Fe_3O_4 content.

Chemical Composition: FTIR

Figure 3 shows only the FT-IR spectrum from 500 to 1800 cm^{-1} (Fig 3[a-c]) and not the band from 1900 to 3500 cm^{-1}; this region represents the absorption bands assigned to the O-H stretching vibration of hydroxyl groups (3340 cm^{-1}) and the bands at 2901 correspond to -CH_3 asymmetric (Gan et al 2017b). The band from 500 to 1800 cm^{-1} corresponds to the organic region of the wood and the presence of Fe_3O_4 formation (Garskaite et al 2021). In the case of the organic region, changes in the structure of cellulose, hemicellulose, and lignin are evident and to a different degree in each of the species (Fig 3). In the

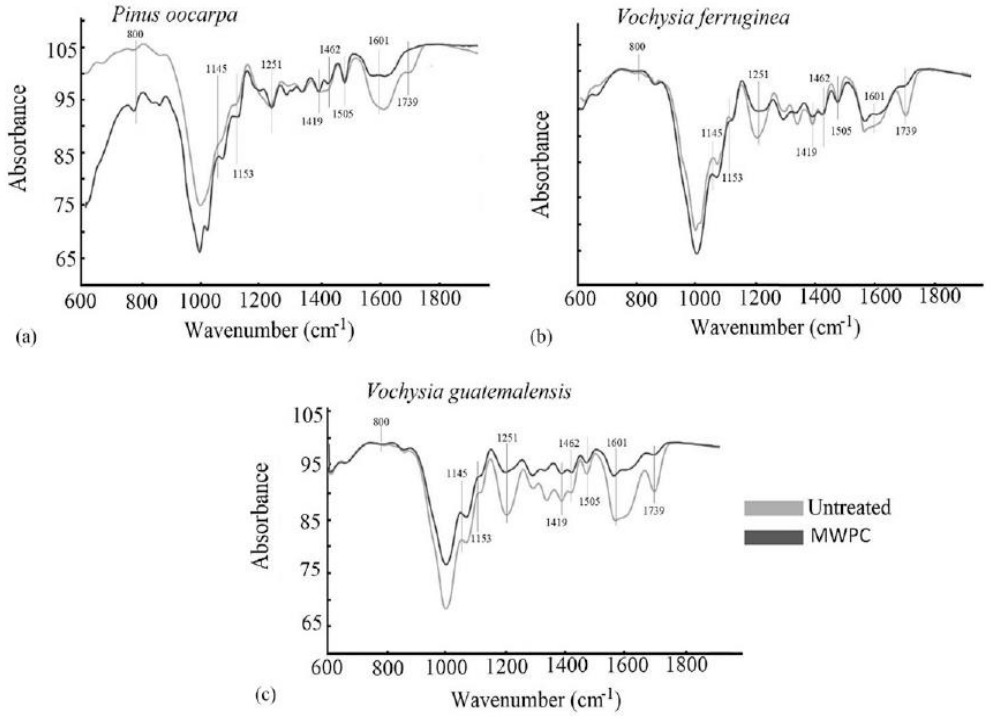

Figure 3. Fourier transform IR spectrum of magnetic wood particleboards composite (MWPC) of three tropical species (a-c) from fast-growth plantations in Costa Rica. a) Pinus oocarpa b) Vochysia ferruginea c) Vochysia guatemalensis. Note: Superscript letters mean statistical differences between treatments at 95% significance.

region of 500-800 cm^{-1}, the presence of Fe_3O_4 in MWPC of different degrees in each of the species is also evidenced.

The wavelengths associated with the cellulose: 896 cm^{-1} show a heterophase carbon, and an increase in *Pinus oocarpa* (Fig 3[a]), but in both Vochyseas did not change (Fig 3[b] and [c]), the vibrations at 1054 cm^{-1} associated with C-H/C-O cellulose and 1090 associated with C-H/C-O cellulose (Lou et al 2018b) changed in the Vochyseas species (Fig 3[b] and [c]), but not in *Pinus oocarpa* (Fig 3[a]). While the vibration at 1145 cm^{-1} signal, stretching vibration of C-O in glucose of cellulose (Gao et al 2012), was similar in untreated and treated wood. Thus, the previous results indicate that there was a modification of cellulose in *Vochysia guatemalensis* and *Vochysia ferruginea* due to the magnetization, and *Pinus oocarpa* was less affected.

In the case of vibrations of the hemicellulose, the vibration at 1379 cm^{-1} is associated with C-H bending cellulose and hemicellulose (Yang et al 2020); these decreased only in the Vochyseas species, but not in *Pinus oocarpa*. The vibrations at 1601 and 1739 cm^{-1}, associated with the C=O stretching vibration absorption peak of hemicellulose (Yang et al 2020), decreased with the presence of magnetic particles in the three species and are associated with hemicellulose degradation (Gao et al 2012; Dong et al 2016; Gan et al 2017a, 2017b; Wang et al 2019; Garskaite et al 2021). Finally, the vibrations associated with lignin: 1601 cm^{-1}, which is associated with C=C aromatic skeletal vibrations (Garskaite et al 2021), and 1462 cm^{-1}, to an aromatic C=C stretching of aromatic rings of lignin, increased in the vochyseas (Fig 3[b] and [c]), but not in *Pinus oocarpa* (Fig 3[a]), 1505 cm^{-1} associated with lignin, did not show significant changes, peak at 1419 cm^{-1}

associated with C-H bonds of lignin, decreased in all three species and 1251 cm^{-1} associated with the ester linkage of carboxylic groups of the ferrulie and p-coumaric acids of lignin (Lou et al 2019a) decreased in the vochyseas, but not in *Pinus oocarpa* (Fig 3[a]). Again, according to the results of the signals associated with hemicellulose and lignin, it is observed that the two species of Vochyseas (*Vochysia guatemalensis* and *Vochysia ferruginea*) showed greater degradation than *Pinus oocarpa*.

The formation of Fe_3O_4 in the wood samples is evident in the bands from minor to 800 cm^{-1}, specifically bands around 561 and 667 cm^{-1}. However, with the FTIR spectrum, it is difficult to demonstrate the formation of Fe_3O_4, since they overlap with other signals, so, it is better to use techniques that measure the wavelength between 650 and 450 cm^{-1} (Lou et al 2019a, 2019b). Despite this drawback, a signal at 800 cm^{-1} obtained—corresponding to tetrahedral sites of the crystal lattice, which is due to the oxidation of Fe^{2+} and Fe^{3+} splits (Garskaite et al 2021)—increased mainly in the wood of *Vochysia ferruginea* and *Vochysia guatemalensis* (Fig 3[b] and [c]). In *Pinus oocarpa*, the peak is less evident (Fig 3[a]), thus confirming the low measurement of Fe_3O_4 content (Fig 2[a]) and the lesser formation in relation to the other two species of wood.

Crystalline Structure: XRD

The crystalline structures of untreated and treated specimens were characterized by XRD (Fig 4[a-c]). Untreated wood of the three species shows a typical diffraction angle at 20° due to cellulose (Cave and Walker 1994), which are 15.8°, 22.2°, and 34.6°

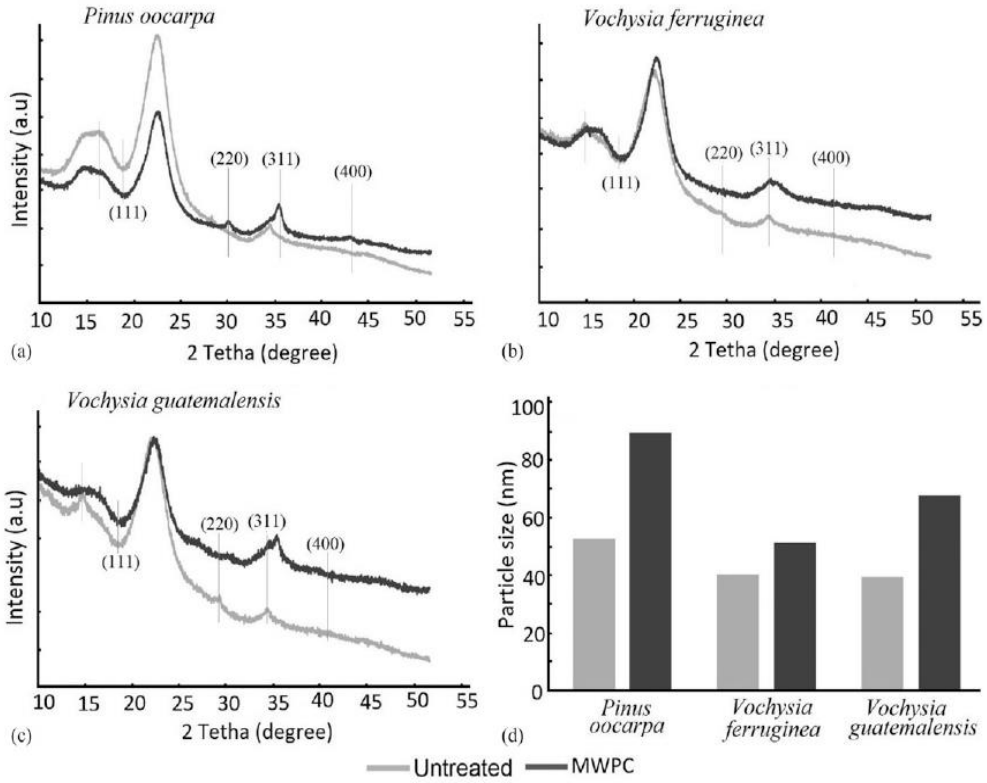

Figure 4. X-ray diffraction of magnetic wood particleboards composite (MWPC) (a-c) and particle size of Fe_3O_4 of three tropical species (d) from fast-growth plantations in Costa Rica.

corresponding to the planes (101), (102), and (400), respectively. But in samples with magnetized wood particles, two additional peaks are observed (at 15.8° and 22.2°), which belong to the cellulose and show that there were lightly weakened bonds of the cellulose. According to Dong et al (2016), these changes indicate that a part of the crystalline structure of the wood was damaged, confirming that the ammonia treatment affected the wood structure.

In addition, it was observed that diffraction angles at 20°, 30°, 35°, and 44° were more pronounced in the magnetic wood (Fig 4[a-c]). In the case of *Pinus oocarpa*, the peak was less intense at 30° and 35° representing (220) and (311), respectively (Fig 4[a]), which corresponds to the cubic phase with the space of $Fd\bar{3}m$ (Lou et al 2019a). In the magnetized *Vochysia ferruginea* and *Vochysia guatemalensis*, the peaks are placed at 35° (311) (Fig 4[b] and [c]). In the case of the *Pinus oocarpa*, the strongest diffraction peak is seen at 34° (311), in *Vochysia ferruginea*, the strongest peaks are at 30° and 35° and in *Vochysia guatemalensis*, the strongest peaks are at 30°, 35°, and 44°. These differences in patterns and particle size (determined using the Scherrer Eq 2) (Lin and Ho 2014) show that the amount of Fe_3O_4 NPs deposited was different in each of the species. The largest size was obtained in *Pinus oocarpa*, followed by *Vochysia guatemalensis* and the least size was obtained in *Vochysia ferruginea* (Fig 4[d]), which correspond to 89.58, 67.80, and 51.39, respectively. The particle sizes in *Pinus oocarpa* were in agreement with the values found by Mashkour and Ranjbar (2018). The values of *Vochyceas* species were slightly higher than those reported by Lou et al (2018b) and Gao et al (2012).

Magnetic Properties

Figure 5(a)-(c) shows the hysteresis curves of the untreated and magnetic wood particles. Representative magnetic properties, Hc, Mr, and Ms were extracted from these hysteresis curves, while the percentage of magnetic NPs present in the samples was calculated with the Ms of the magnetic NPs present in the samples; these values are presented in Table 1. In the case of untreated wood, the hysteresis curves show negligible Ms (Fig 5), which is the expected behavior of wood (Kojima et al 2009).

On the other hand, the magnetized material, in all species, exhibited a clear hysteresis loop corresponding to ferromagnetic behavior (Fig 5), but large differences between species were found. For example, Ms was lowest in *Vochysia guatemalensis* (Fig 5[c]) and highest in *Pinus oocarpa* (Fig 5[a]), while *Vochysia ferruginea* had intermediate values (Fig 5[b]).

It has been observed that there is significant variation in the precipitation of Fe_3O_4 NPs between species, proving their different absorption capacity of NPs (Fig 2[a]). As indicated above, this variability is attributed to the permeability of the wood or the flow of fluids in it (Lin and Ho 2014), which varies depending on the anatomical elements present in the wood samples (Moya et al 2022).

An important aspect to highlight, regarding the values of Hc, Mr, and Ms of the species using fiber in this work, is that they presented lower values than when they are treated with solid wood (Moya et al 2022) or previous studies with other species (Dong et al 2016; Gan et al 2016). Although these latest studies have used other precipitation methods for Fe_3O_4 NPs, these low values may be associated with the low permeability of wood to the flow of liquid substances in the species studied (Gaitán-Alvarez et al 2020a, 2020b). However, an appropriate immersion time in ammonia had positive effects on the magnetic properties of wood (Lou et al 2018b; Moya et al 2022), which could increase the magnetic properties of wood when they are treated in the form of particles.

If we compare these values of Ms (Table 2) with the NP content of Fe_3O_4 (Fig 2[a]), the highest value of Ms in *Pinus oocarpa* (Table 2) contrasts with the lowest contents of Fe_3O_4), while the Ms values of *Vochysia guatemalensis* and *Vochysia ferruginea* are low, but with high values of Fe_3O_4 content (Fig 2[a]). This inconsistent behavior across species could be because there are inhomogeneities

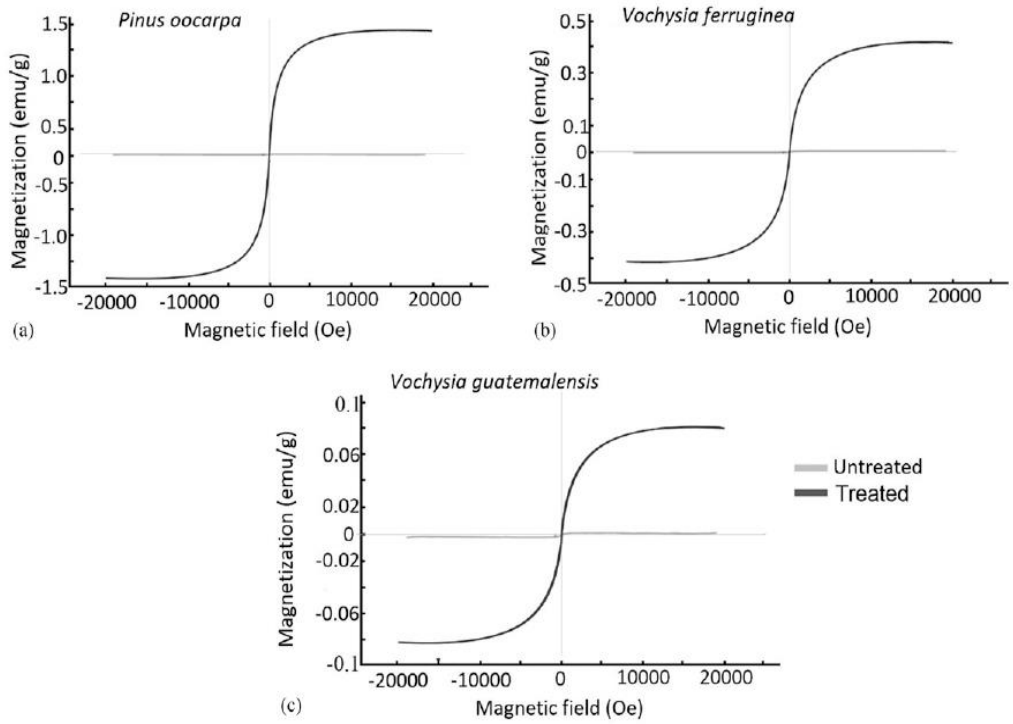

Figure 5. Magnetic hysteresis curves of three magnetic wood particleboards composite of tropical species (a-c) from fast growth plantations in Costa Rica.

in the dispersion of NPs along the samples (Lou et al 2019a), and since these measurements are made locally, ie, in different areas of the same sample, the values might change from one place to another, resulting in small differences in the magnetic values. This can be verified by the values that have been obtained in the three different samples of the same wood, where it can be seen that they have different amounts of NP.

In general, the values of Hc and Ms are low (Table 2), which indicates the magnetically soft properties of the wood, compared with the results obtained previously by Moya et al (2022), which reported the highest values of Ms in *Vochysia ferruginea* and *Vochysia guatemalensis*, and similar values in *Pinus oocarpa*.

Regarding the process, Gan et al (2017a) indicated that alkaline immersion is more invasive of the structural components of wood than other magnetization methods. So, in the case of these species, the immersion time did not significantly alter the magnetic properties of the materials,

Table 1. The Hc, Mr, Ms, and the experimental percentage of three MWPC of tropical species from fast growth plantations in Costa Rica.

Species	Hc (Oe)	Mr (emu g g^{-1})	Ms (emu g^{-1})	% experimental
Pinus oocarpa	11.94	0.02	1.39	9.04
Vochysia ferruginea	14.12	0.00	0.32	2.09
Vochysia guatemalensis	21.85	0.00	0.06	0.41

Hc, coercivity; Mr, retentivity; Ms, saturation magnetization; MWPC, magnetic wood particleboards composite.

Table 2. Physical properties of three MWPC of tropical species from fast growth plantations in Costa Rica.

Species	Treatment	Density (g cm^{-3})	Thickness swelling (mm)	Moisture absorption (%)	Water absorption (%)
Pinus oocarpa	WPC	0.73 (1.62)^{AB}	5.80 (6.19)^{B}	4.90 (2.34)^{A}	41.11 (4.42)^{A}
	MWPC-layer	0.75 (2.20)^{A}	6.84 (26.18)^{AB}	4.84 (1.38)^{A}	37.07 (1.68)^{B}
	MWPC-100	0.74 (4.64)^{B}	8.60 (22.88)^{A}	4.25 (4.21)^{B}	29.21 (16.06)^{C}
Vochysia ferruginea	WPC	0.72 (2.18)^{B}	8.78 (11.57)^{A}	5.35 (1.98)^{A}	45.60 (9.25)^{B}
	MWPC-layer	0.74 (1.88)^{A}	10.14 (36.11)^{A}	4.33 (5.30)^{A}	42.26 (7.71)^{B}
	MWPC-100	0.73 (1.49)^{A}	6.77 (19.79)^{A}	4.39 (0.83)^{A}	52.07 (8.57)^{A}
Vochysia guatemalensis	WPC	0.73 (2.01)^{A}	10.96 (36.18)^{A}	5.31 (1.09)^{A}	37.24 (13.03)^{AB}
	MWPC-layer	0.74 (2.08)^{A}	5.83 (22.09)^{B}	4.83 (1.89)^{B}	42.46 (7.56)^{B}
	MWPC-100	0.73 (1.97)^{A}	5.39 (24.12)^{B}	4.39 (1.53)^{C}	33.00 (16.91)^{A}

Superscript letters mean statistical differences between treatments at 95% significance. And number in parentheses the coefficient of variation of the data.
MWPC, magnetic wood particleboards composite.

wood composites, although the immersion itself could affect the adhesion of the magnetic NPs in the samples.

Physical and Mechanical Properties

The results of the physical properties of the different particleboards (WPC, MWPC-100, and MWPC layers) are presented in Table 2. These results show that in *Pinus oocarpa* the density is higher in the MWPC layer and MWPC-100. The same situation was presented by the particleboards of *Vochysia ferruginea*, in which the density in MWPC-100 and the MWPC layers are higher. While in *Vochysia ferruginea*, there were no differences in density (Table 2). In the case of swelling in thickness, *Pinus oocarpa* particleboards with magnetic particles presented greater swelling. On the contrary, the *Vochysia guatemalensis* boards decreased the swelling values with magnetization and, in the case of *Vochysia ferruginea*, there were no differences (Table 2).

In the case of moisture absorption, this value decreased statistically with the magnetization of the *Pinus oocarpa* particleboard material from MWPC-100. This same effect is observed in *Vochysia guatemalensis*, where the lowest value of moisture absorption was presented in the MWPC-100 and the highest in MPC. For the *Vochysia ferruginea* particleboards, there were no differences between the different treatments (Table 2). For the capability of water absorption, in the case of the *Pinus oocarpa*, MWPC shows a higher absorption, while MWPC-100 shows a lower absorption. In *Vochysia ferruginea*, the MWPC-100 treatment shows higher values. Finally, in *Vochysia guatemalensis*, the highest percentage of water absorption occurs in the MWPC layer (Table 2).

The slight differences between the densities of the WPC in the three types of treatments and, in all the species studied, may be related to the fact that the pressing process was very similar (temperature, time, and pressure) for all the particleboards under the same conditions. On the other hand, the swelling of the thickness did not present a clear trend in the three species, but a high variation in the results was observed. As for the MC, it is observed that there was a decreasing trend in the values with respect to the control, which is due to the chemical synthesis of the Fe_3O_4 NPs in the material since the amorphous fractions in the cellulose decreases the access to moisture and water absorption (Mashkour and Ranjbar 2018). The same situation occurs in the water absorption, especially in *Pinus oocarpa* where in MWPC-layer and MWPC-100, a decrease is observed compared with WPC (Table 2), meaning that in this species the synthesis of Fe_3O_4 was carried out correctly. On the other hand, the increase of the water absorption in MWPC-layer and MWPC-100 in *Vochysia ferruginea* and the *Vochysia guatemalensis* with respect to WPC (Table 2) is attributed to the fact that during the magnetic treatment, the acidic condition of the ferric and ferrous chloride solution, and the subsequent basic

Table 3. Mechanical properties of three MWPC of tropical species from fast growth plantations in Costa Rica.

Species	Treatment	Internal bond (MPa)	Hardness (N)
Pinus oocarpa	WPC	0.70 (21.61)^{A}	8.60 (6.97)^{B}
	MWPC-layer	0.65 (38.53)^{A}	11.37 (3.48)^{A}
	MWPC-100	0.57 (47.65)^{A}	6.99 (11.08)^{C}
Vochysia ferruginea	WPC	0.64 (26.08)^{A}	9.70 (11.08)^{B}
	MWPC-layer	0.67 (24.79)^{A}	10.82 (11.97)^{AB}
	MWPC-100	0.17 (49.90)^{B}	11.30 (11.35)^{A}
Vochysia guatemalensis	WPC	0.50 (24.93)^{A}	12.85 (21.74)^{B}
	MWPC-layer	0.39 (53.71)^{AB}	15.96 (20.24)^{AB}
	MWPC-100	0.26 (30.75)^{B}	17.51 (16.06)^{B}

Superscript letters mean statistical differences between treatments at 95% significance. And number in parentheses the coefficient of variation of the data.
MWPC, magnetic wood particleboards composite.

condition of the aqueous ammonia solution lead to a partial decomposition and collapse of the wood components (Dong et al 2016), which damages the wood and contributes to water absorption.

Regarding the mechanical properties, it was observed that the internal bond decreased in the MWPC (Table 3). In *Pinus oocarpa*, there was no statistical difference in the property of internal bond, while in *Vochysia ferruginea* and *Vochysia guatemalensis*, the value decreased significantly in MWPC-100, but in both the species the MWPC layer treatment did not present differences with WPC (Table 3). Regarding the hardness in *Pinus oocarpa*, it increased significantly in the MWPC layer but decreased in MWPC-100. In *Vochysia ferruginea* and *Vochysia guatemalensis*, the hardness value increased in MWPC-100 and the MWPC layer (Table 3).

When comparing the results of internal bonds with other works, in *Pinus oocarpa*, the values are between the range obtained by Santos et al (2021), where it presents internal bond values between 0.42 and 0.66 MPa. In the case of *Vochysias*, the values obtained are compared with those obtained by Rigg-Aguilar et al (2019), which reported internal bond values between 0.14 and 0.589 MPa. On the other hand, the decrease in this property with magnetism can be attributed to the collapse of the wood components with the treatment (Lou et al 2019a). A collapse in the bonds of cellulose and lignin results in there being no effective interaction between the hydroxyl groups of the cellulose and the urea-formaldehyde adhesive (Sheng Han et al 2006) used in the elaboration of the WPC (Figure 6). Regarding the hardness, it was possible to observe that this property improves slightly with magnetism, especially

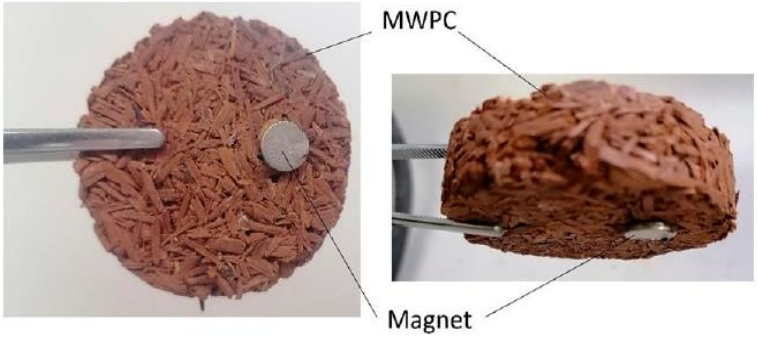

Figure 6. A magnetized sample of magnetic wood particleboards composite (MWPC) for *Pinus oocarpa*, attracted by a magnet.

in the Vochyseas (Table 3). This can be attributed to the Fe_3O_4 NPs, as they create a higher resistance on the surface of the MWPC (Martins et al 2021), which makes the material more resistant to mechanical stress on the surface.

CONCLUSION

The use of wood composites with fiber magnetized with Fe_3O_4 NPs and synthesized in situs by means of an in-situ impregnation of Fe^{3+} and Fe^{2+} and immersed in ammonia in three tropical species (*Pinus oocarpa*, *Vochysia ferruginea*, and *Vochysia guatemalensis*) presented low values of Hc, Mr, and Ms compared with solid wood of this species or other species, which is attributed to the low permeability and penetration of solutions in the species. The least precipitation occurred in *Pinus oocarpa*, but it presented better magnetic properties and, on the contrary, the species with less magnetic properties were *Vochysia guatemalensis* and *Vochysia ferruginea*. Despite the little effect on MWPC, there was evidence of changes in the chemical components of the wood, a decrease in density, an increase in swelling and moisture absorption, and a few changes in the mechanical properties of the wood because immersion in ammonia produces changes in the chemical components of wood. In general, the in-situs precipitation by immersion limits the synthesis of the NPs within the wood, to this added the size of the wood fiber, which makes the impregnated surface smaller, therefore the magnetic data were reduced.

ACKNOWLEDGMENTS

The authors thank to Vicerrectoría de Investigación y extensión of the Instituto Tecnológico de Costa Rica for the finantial support to develop the proyect.

REFERENCES

ASTM (1985) Standard test method for anti-swelling effectiveness of water-repellent formulations and differential swelling of untreated wood when exposed to liquid water environments. Annu B ASTM 4:702-706. doi: 10.1520/D4446-08R12.when.

ASTM (1999) Standard guide for moisture conditioning of wood and wood-based materials. Current i:1-8. doi: 10.1520/D4933-99R10.2.

ASTM (2013) Standard test method for ash in wood. Annu B ASTM Stand 410:1-2.

ASTM (2021) Test methods for determination of trace elements in coal, coke, & combustion residues from coal utilization processes by inductively coupled plasma atomic emission, inductively coupled plasma mass, & graphite furnace atomic absorption spec. Annu B ASTM Stand 5:406–410.

Bolton AJ, Humphrey PE (1994) The permeability of wood-based composite materials: Part 1. A review of the literature and some unpublished work. Holzforschung 48: 95-100. doi: 10.1515/HFSG.1994.48.S1.95/HTML.

Cave I, Walker J (1994) Stiffness of wood in fast-grown plantation softwoods: The influence of microfibril angle. Forest Prod J 44:43-48.

Dong Y, Yan Y, Zhang S, Li S, Wang J (2015) Flammability and physical–mechanical properties assessment of wood treated with furfuryl alcohol and nano-SiO_2. Eur J Wood Wood Prod 73:457-464. doi: 10.1007/s00107-015-0896-y.

Dong Y, Yan Y, Zhang Y, Li J (2016) Combined treatment for conversion of fast-growing poplar wood to magnetic wood with high dimensional stability. Springer 50:503-517. doi: 10.1007/s00226-015-0789-6.

Gaitán-Alvarez J, Berrocal A, Mantanis GI, Moya R, Araya F (2020a) Acetylation of tropical hardwood species from forest plantations in Costa Rica: An FTIR spectroscopic analysis. J Wood Sci 66:1–49. doi: 10.1186/s10086-020-01898-9.

Gaitán-Alvarez J, Moya R, Berrocal A, Araya F (2020b) In-situ mineralization of calcium carbonate of tropical hardwood species from fast-grown plantations in Costa Rica. Carbonates Evaporites 29:09184-9144.

Gaitán-Alvarez J, Moya R, Mantanis GI, Berrocal A (2021) Furfurylation of tropical wood species with and without silver nanoparticles: Part I: Analysis with confocal laser scanning microscopy and FTIR spectroscopy. Wood Mater Sci Eng 17:410-419. doi: 10.1080/17480272.2021.1886166.

Gan W, Gao L, Liu Y, Zhang Y, Li J (2016) The magnetic, mechanical, thermal properties and Uv resistance of $CoFe_2O_4/SiO_2$-coated film on wood. J Wood Chem Technol 36:94-104. doi: 10.1080/02773813.2015.1074247.

Gan W, Gao L, Xiao S, Zhang S, Zhan W, Li J (2017a) Transparent magnetic wood composites based on immobilizing Fe_3O_4 nanoparticles into a delignified wood template. J Mater Sci 52:3321-3329. doi: 10.1007/s10853-016-0619-8.

Gan W, Liu Y, Gao L, Zhan X, Li J (2017b) Magnetic property, thermal stability, UV-resistance, and moisture absorption behavior of magnetic wood composites. Wiley Online Libr 38:1646-1654. doi: 10.1002/pc.23733.

Gao HL, Wu GY, Guan HT, Zhang GL (2012) In situ preparation and magnetic properties of Fe_3O_4/wood composite. Mater Technol 27:101-103. doi: 10.1179/175355511X13240279339806.

Gao X, Dong Y, Wang K, Chen Z, Yan Y, Li J, Zhang S (2017) Improving dimensional and thermal stability of

poplar wood via aluminum-based sol-gel and furfurylation combination treatment. BioResources 12 2:3277-3288. doi: 10.15376/biores.12.2.3277-3288.

Garskaite E, Stoll SL, Forsberg F, Lycksam H, Stankeviciute Z, Kareiva A, Quintana A, Jensen CJ, Liu K, Sandberg D (2021) The accessibility of the cell wall in scots pine (*Pinus sylvestris* L.) sapwood to colloidal Fe_3O_4 nanoparticles. ACS Omega 6:21719-21729. doi: 10.1021/acsomega.1c03204.

Kojima M, Yamamoto H, Marsoem SN, Okuyama T, Yoshida M, Nakai T, Yamashita S, Saegusa K, Matsune K, Nakamura K, Inoue Y, Arizono T (2009) Effects of the lateral growth rate on wood quality of *Gmelina arborea* from 3.5-, 7- and 12-year-old plantations. Ann Sci 66: 507. doi: 10.1051/forest/2009031.

Lin C-C, Ho J-M (2014) Structural analysis and catalytic activity of Fe_3O_4 nanoparticles prepared by a facile co-precipitation method in a rotating packed bed. Ceram Int 40:10275-10282. doi: 10.1016/j.ceramint.2014.02.119.

Liu J, Che R, Chen H, Zhang F, Xia F, Wu Q, Wang M (2012) Microwave absorption enhancement of multifunctional composite microspheres with spinel Fe_3O_4 cores and anatase TiO_2 shells. Small 8:1214-1221. doi: 10.1002/smll.201102245.

Lou Z, Han H, Zhou M, Han M, Cai J, Huang C, Sun Z (2018a) Synthesis of magnetic wood with excellent and tunable electromagnetic wave-absorbing properties by a facile vacuum/pressure impregnation method. ACS Sustain Chem Eng 6:1000-1008. doi: 10.1021/acssuschemeng.7b03332.

Lou Z, Wang W, Yuan C, Zhang Y, Li Y, Yang L (2019a) Fabrication of Fe/C composites as effective electromagnetic wave absorber by carbonization of pre-magnetized natural wood fibers. J Bioresour Bioprod 4:43-50. doi: 10.21967/jbb.v4i1.185.

Lou Z, Yuan C, Zhang Y, Li Y, Cai J, Yang L, Zou J (2019b) Synthesis of porous carbon matrix with inlaid Fe_3C/Fe_3O_4 micro-particles as an effective electromagnetic wave absorber from natural wood shavings. J Alloys Compd 775:800-809. doi: 10.1016/j.jallcom.2018.10.213.

Lou Z, Zhang Y, Zhou M, Han M, Cai J, Yang L, Li Y (2018b) Synthesis of magnetic wood fiber board and corresponding multi-layer magnetic composite board, with electromagnetic wave absorbing properties. Nanomaterials 8(6):441. doi: 10.3390/nano8060441.

Lv H, Yang Z, Wang PL, Ji PL, Song J, Zheng L, Xu ZJ (2018) A voltage-boosting strategy enabling a low-frequency, flexible electromagnetic wave absorption device. Adv Mater 30:1706343. doi: 10.1002/adma.201706343.

Martins RSF, Gonçalves FG, Segundinho PGdA, Lelis PG, Paes JB, Lopez YM, Oliveira RG (2021) Investigation of agro-industrial lignocellulosic wastes in fabrication of particleboard for construction use. J Build Eng 43:102903. doi: 10.1016/j.jobe.2021.102903.

Mashkour M, Ranjbar Y (2018) Superparamagnetic Fe_3O_4 wood flour/polypropylene nanocomposites: Physical and mechanical properties. Ind Crops Prod 111:47-54. doi: 10.1016/j.indcrop.2017.09.068.

Moya R, Gaitán-Alvarez J, Berrocal A, Araya F (2020) Effect of $CaCO_3$ in the wood properties of tropical hardwood species from fast-grown plantation in Costa Rica. BioResources 15:4802-4822.

Moya R, Gaitán-Alvarez J, Berrocal A, Merazzo KJ (2022) In *Situ Synthe*sis of Fe_3O_4 nanoparticles and wood composite properties of three tropical species. Materials (Basel) 15:3394. doi: 10.3390/ma15093394.

Moya-Roque R, Camacho D, Soto-Fallas R, Mata-Segreda J (2014) Internal bond strength of particle boards manufactured from a mixture of *Gmelina arborea*, *Tectona grandis* and *Cupressus lusitanica* with the fruit of *Elaeis guineensis*, leaves of *Ananas comosus* and tetra pak packages. Rev For Mesoam Kurú 12:36. doi: 10.18845/rfmk.v12i28.2098.

Oka H, Hamano H, Chiba S (2004a) Experimental study on actuation functions of coating-type magnetic wood. J Magn Magn Mater 272:E1693-E1694.

Oka H, Hojo A, Osada H, Namizaki Y, Taniuchi H (2004b) Manufacturing methods and magnetic characteristics of magnetic wood. J Magn Magn Mater 272:2332-2334.

Oka H, Kataoka Y, Osada H, Aruga Y, Izumida F (2007) Experimental study on electromagnetic wave absorbing control of coating-type magnetic wood using a grooving process. J Magn Magn Mater 310:e1028-e1029. doi: 10.1016/j.jmmm.2006.11.073.

Oka H, Narita K, Osada H, Seki K (2002) Experimental results on indoor electromagnetic wave absorber using magnetic wood. J Appl Physics 91:7008-7010. doi: 10.1063/1.1448796.

Oka H, Tanaka K, Osada H, Kubota K, Dawson FP (2009) Study of electromagnetic wave absorption characteristics and component parameters of laminated-type magnetic wood with stainless steel and ferrite powder for use as building materials. J Appl Phys 105:07E701. doi: 10.1063/1.3056403.

Oka H, Terui M, Osada H, Sekino N, Namizaki Y, Oka H, Dawson FP (2012) Electromagnetic wave absorption characteristics adjustment method of recycled powder-type magnetic wood for use as a building material. IEEE Trans Magn 48:3498-3500. doi: 10.1109/TMAG.2012.2196026.

Rahayu I, Prihatini E, Ismail R, Darmawan W, Karlinasari L, Laksono GD (2022) Fast-growing magnetic wood synthesis by an in-situ method. Polymers (Basel) 14: 2137. doi: 10.3390/polym14112137.

Rao X, Liu Y, Fu Y, Liu Y, Yu H (2016) Formation and properties of polyelectrolytes/TiO_2 composite coating on wood surfaces through layer-by-layer assembly method. Holzforschung 70:361-367. doi: 10.1515/hf-2015-0047.

Renneckar S, Zhou Y (2009) Nanoscale coatings on wood: Polyelectrolyte adsorption and layer-by-layer assembled film formation. ACS Appl Mater Interfaces 1:559-566. doi: 10.1021/am800119q.

Rigg-Aguilar P, Moya R, Vega-Baudrit J, Navarro-Mora A, Gaitán-Alvarez J (2019) European pallets fabricated with composite wood blocks from tropical species reinforced with nanocrystalline cellulose: Effects on the properties of blocks and static flexure of the pallet. BioResources 14(2):3651-3667. doi: 10.15376/biores.14.2.3651-3667.

Santos J, Pereira J, Ferreira N, Paiva N, Ferra J, Magalhaes FD, Carvalho LH (2021) Valorisation of non-timber by-products from maritime pine (*Pinus pinaster*, Ait) for particleboard production. Ind Crops Prod 168:113581. doi: 10.1016/j.indcrop.2021.113581.

Sheng Han Y, Hadiko G, Fuji M, Takahashi M (2006) Crystallization and transformation of vaterite at controlled pH. J Cryst Growth 289:269-274. doi: 10.1016/j.jcrysgro.2005.11.011.

Tang T, Fu Y (2020) Formation of chitosan/sodium phytate/nano-Fe_3O_4 magnetic coatings on wood surfaces via layer-by-layer self-assembly. Coatings 10:51. doi: 10.3390/coatings10010051.

Tenorio C, Moya R, Salas C, Berrocal A (2016) Evaluation of wood properties from six native species of forest plantations in Costa Rica. Bosque (Valdivia) 37:71-84. doi: 10.4067/S0717-92002016000100008.

Thomas RJ (1976) Anatomical features affecting liquid penetrability in three hardwood species. Wood Fiber Sci 4:256-263.

Trey S, Olsson RT, Ström V, Berglund L, Johansson M (2014) Controlled deposition of magnetic particles within the 3-D template of wood: Making use of the natural hierarchical structure of wood. RSC Adv 4:35678-35685. doi: 10.1039/c4ra04715j.

Wang H, Yao Q, Wang C, Ma Z, Sun Q, Fan B, Chen Y (2017) Hydrothermal synthesis of nanooctahedra mnfe2o4 onto the wood surface with soft magnetism, fire resistance and electromagnetic wave absorption. Nanomaterials (Basel) 7:118. doi: 10.3390/nano7060118.

Wang L, Li N, Zhao T, Li B, Ji Y (2019) Magnetic properties of $FeNi_3$ nanoparticle modified *Pinus radiata* wood nanocomposites. Polymers (Basel) 11:421. doi: 10.3390/polym11030421.

Yang L, Lou Z, Han X, Liu J, Wang Z, Zhang Y, Li Y (2020) Fabrication of a novel magnetic reconstituted bamboo with mildew resistance properties. Mater Today Commun 23:101086. doi: 10.1016/j.mtcomm.2020.101086.

Zheng J, Lv H, Lin X, Ji G, Li X, Du Y (2014) Enhanced microwave electromagnetic properties of Fe3O4/graphene nanosheet composites. J Alloys Compd 589:174-181. doi: 10.1016/j.jallcom.2013.11.114.

6. Artículo 3: Efecto del método de impregnación de partículas magnéticas en chapas de madera de tres especies cultivadas en plantaciones de rápido crecimiento en Costa Rica

Resumen

En este estudio se planteó el objetivo de sintetizar nanopartículas de Fe_3O_4 en chapas de madera de tres especies tropicales (*Gmelina arborea*, *Vochysia ferruginea* y *Pinus oocarpa*,) por medio de una impregnación in-situ de Fe^{3+} y $Fe^{2+,}$ seguido de una impregnación con una solución de amoniaco. También se evaluó el efecto de la impregnación por medio de un método vació-presión, para compararlo con el de inmersión. Para determinar la efectividad se evaluó el contenido de cenizas, contenido de Fe_3O_4, observaciones en el SEM, espectro FTIR, difracción de rayos X y propiedades magnéticas por medio de un magnetómetro de muestra vibrante (VSM). Los resultados mostraron que el método de impregnación sí tuvo efecto en la síntesis de las nanopartículas, en este caso la impregnación a vació-presión fue la que presentó la mayor cantidad de Fe_3O_4 en las chapas. De la misma forma, al usar la impregnación vació-presión se evidenció mayor señal de ferrita en los análisis SEM y XDR. Mientras que, en el análisis de propiedades magnéticas fue claro que la curva de histéresis de la madera presentó un comportamiento ferromagnético en la síntesis por medio del método vacío- presión, mientras que por el método de inmersión el cambio fue de leve a nulo. A su vez también, se observó que la especie que logró mayor magnetización fue *Vochysia ferruginea*.

Palabras clave: chapas de madera, propiedades magnéticas, madera tropical, modificación de la madera, magnetismo aplicado.

Abstract

The objective of this paper was to synthesize Fe_3O_4 nanoparticles in wood veneers of three tropical species (*Gmelina arborea*, *Vochysia ferruginea* and *Pinus oocarpa*) by in-situ impregnation of Fe3+ and Fe2+, followed by impregnation with an ammonia solution. The effect of impregnation was also evaluated by means of a vacuum-pressure method, to compare it with that of immersion. To determine the effectiveness of each treatment, ash content, Fe_3O4 content, SEM observations, FTIR spectra, X-ray diffraction and magnetic properties were evaluated by means of a vibrating sample magnetometer (VSM). The results showed that the impregnation method did influence the synthesis of the nanoparticles, in this case the vacuum-pressure impregnation was the one that presented the highest amount of Fe_3O_4 in the sheets. Likewise, when using vacuum-pressure impregnation, a higher ferrite

signal was evidenced in the SEM and XDR analysis. Meanwhile, in the analysis of magnetic properties it was clear that the hysteresis curve of the wood presented a ferromagnetic behavior in the synthesis by means of the vacuum-pressure method, while by the immersion method the change was from slight to null. It was also observed that the species that achieved the greatest magnetization was *Vochysia ferruginea*.

Key words: wood veneers, magnetic properties, tropical wood, wood modification, applied magnetism.

1. Introducción

El uso cada vez mayor de dispositivos electrónicos e inalámbricos en la vida diaria de las personas, como teléfonos móviles, redes inalámbricas y robots domésticos, generan cada vez más ondas electromagnéticas que afectan la salud de una manera sin precedentes (Oka et al. 2012; Lou et al. 2018). Debido a esta situación, existe la necesidad de reducir la fuente de radiación no deseada o reducir su impacto en el área circundante (Oka et al. 2012). Investigaciones recientes se han llevado a cabo en el desarrollo de materiales ligeros, de bajo espesor y con capacidad de reducir o bloquear las ondas electromagnéticas (Lou et al. 2018; Lv et al. 2018).

En este ámbito se ha estudiado la combinación de materiales magnéticos con materiales dieléctricos ligeros, aprovechando el efecto sinérgico entre ambos componentes (Zheng et al.; Liu et al. 2012) Entre estos materiales, se ha estudiado la madera modificada como material bloqueador de ondas magnéticas, que es un material renovable y naturalmente degradable, altamente atractivo como material compuesto de base biológica (Oka et al. 2007; Ahmed et al. 2018) El grupo Oka (Oka et al. 2002), hace más de 2 décadas, experimentó con la madera como material bloqueador de ondas electromagnéticas, proponiendo la impregnación de polvo magnético en el interior de la madera (Oka et al. 2002, 2004a).

En la actualidad, se han estudiado tres métodos diferentes de fabricación de compuestos magnéticos de madera: impregnación de nanopartículas de hierro en combinación con diferentes solventes (Oka et al. 2009), tipo polvo hecho de materiales magnéticos y de madera, mezclado con resinas y luego prensado bajo temperatura (Oka et al. 2007), y revestimientos de madera con sustancias magnéticas (Oka et al. 2004b). Entre los diferentes métodos estudiados, la impregnación de madera pretratada en solución mixta con nanopartículas de ferrita (NPs) como Fe_3O_4 (Gan et al. 2016), $CoFe_2O_4$ (Gan et al. 2017a) y $MnFe_2O_4$ (Wang et al. 2017) son los métodos que se destacan. En esta síntesis del material magnético dentro de la madera ocurre por coprecipitación in situ de las NPs de ferrita a través de una reacción química de dos fuentes de Fe^{3+} y Fe^{2+} en una solución

acuosa, seguida de impregnación con una solución de amoníaco, todo esto bajo vacío. -proceso de presión (Dong et al. 2016a; Lou et al. 2018; Mashkour and Ranjbar 2018).

Recientemente, Moya et al. (Moya et al. 2022) han realizado las primeras investigaciones en maderas tropicales, aplicando el método in-situ con buenos resultados de coercitividad (Hc), retentividad (Mr) y magnetización de saturación (Ms) en dos especies diferentes. Sus conclusiones fueron que el uso del método de síntesis in-situ del material magnético dentro de la madera es apropiado, sin embargo, la cantidad de NP añadida no es adecuada para lograr valores altos de Hc, Mr y Ms. Varios autores señalan las debilidades de este método, que puede ser aplicado a los resultados obtenidos en maderas tropicales.

Al respecto, Lou et al. (Lou et al. 2019a) y Trey et al. (Trey et al. 2014), señalan que las fuerzas dipolares entre las partículas impregnadas se suman fácilmente formando conglomerados, afectando la uniformidad de la deposición de partículas en diferentes partes de la madera magnética. También Lou et al. (Lou et al. 2019b)y Trey et al. (Trey et al. 2014), mencionan que efectivamente las partículas magnéticas mezcladas con polímeros y madera en grandes cantidades conducen a compuestos quebradizos, situación que restringe la adecuada aplicación de las partículas magnéticas en la madera in-situ.

Otro punto importante a parte del método de impregnación es la presentación de los productos de madera a impregnar, porque se ha utilizado desde madera sólida, pasando por chapas, hasta partículas de madera, lo cual provoca que cada forma presente un desempeño/eficiencia diferente en la impregnación con fuentes de Fe^{3+} y Fe^{2+} en solución.

La forma de la madera determinará el grado de penetración de la solución en estado líquido (Bolton and Humphrey 1994), por lo tanto, una solución de fuente ferrosa, para la formación in situ de NPs, también dependerá de la forma de la madera. Por ejemplo, en el caso de la madera solida la penetración depende de la permeabilidad de la madera, en el caso de la chapa la permeabilidad es menos importante, ya que por lo general los espesores no superan los 3 mm; y en el caso de la partícula de madera conformada, el espesor es pequeño y las dimensiones lo suficientemente grandes como para tener una mayor superficie de contacto entre la madera y las soluciones de hierro (Bolton and Humphrey 1994). Por lo tanto, es necesario conocer el mejor método de impregnación para cada tipo de madera.

Comúnmente los estudios (Oka et al. 2007; Lou et al. 2018) han descrito varios métodos de impregnación como el in-situ por inmersión de una madera maciza o chapa aunque sin la presión del vacío, por lo que la impregnación es superficial. Sin embargo, Oka et al. (Oka et al. 2007),señala que en este método se registran valores bajos de propiedades magnéticas coercitividad (Hc), retentividad (Mr) y magnetización de saturación (Ms) en madera sólida y contrachapada, ya que no es posible controlar la forma y tamaño de la superficie, por lo que el proceso no es factible, y las partículas magnéticas no se pueden

depositar correctamente. Asimismo, otras causas de valores bajos de los parámetros de magnetización es que la superficie de la madera es rica en grupos hidroxilo, los cuales son electronegativos en soluciones acuosas, por lo que no son atractivos para ensamblar capas de nanopartículas en la superficie (Tang and Fu 2020). Un buen método que fue demostrado por Rao et al. (Rao et al. 2016) y Renneckar y Zhou (Renneckar and Zhou 2009), es la impregnación de la madera superficialmente mediante la unión de polielectrolitos. Sin embargo, a pesar de estos importantes avances, la fabricación de tableros de fibra magnética por coprecipitación química superficial, junto con la investigación de las propiedades de bloqueo de campo magnético de la madera, es limitada (Bolton and Humphrey 1994; Dong et al. 2015; Lou et al. 2018).

Es por esto por lo que el presente estudio tiene como objetivo principal evaluar la síntesis de partículas de madera magnética en chapas de madera tres especies de rápido crecimiento de Costa Rica: *Pinus oocarpa, Vochysia ferruginea y Gmelina arborea*, por medio de una impregnación in-situ de $FeCl_3 \cdot 6H_2O$, $FeCl_2 \cdot 4H_2O$ y amoniaco, evaluando dos métodos diferentes de impregnación (inmersión y por vació-presión). La evaluación del grado de síntesis de las nanopartículas de hierro dentro de la madera se llevará a cabo por medio de absorción de Fe^{+3}, microscopía electrónica de barrido (SEM), espectroscopía infrarroja con transformada de Fourier (FTIR), difracción de rayos X (XDR) y magnetometría de muestra vibrante (VSM).

2. Materiales y métodos

2.1. Materiales

Los reactivos utilizados fueron cloruro de hierro (III) hexahidratado ($FeCl_3 \cdot 6H_2O$) ≥ 98% pureza de la marca comercial Sigma-Aldrich (USA) (https://www.sigmaaldrich.com/webapp/wcs/stores/servlet/OrderCenterView?storeId=11001) ; cloruro de hierro (II) tetrahidratado ($FeCl_2 \cdot 4H_2O$) ≥ 98% pureza de la marca comercial Sigma-Aldrich (USA) (https://www.sigmaaldrich.com/webapp/wcs/stores/servlet/OrderCenterView?storeId=11001) ; solución de hidróxido de amonio al 30% de pureza de la marca comercial LABQUIMAR (San Jose, Costa Rica) (http://www.labquimar.com/); alcohol etílico absoluto de la marca comercial J.T. Baker (Madrid, España) (https://www.fishersci.es/es/es/brands/IPF8MGDA/jt-baker.html); y tolueno de la marca comercial J.T. Baker (Madrid, España) (https://www.fishersci.es/es/es/brands/IPF8MGDA/jt-baker.html), todos distribuidos por Industrial Casjim Costa Rica.

En cuanto a la madera utiliza, se usó chapa de albura de *G. arborea*, *V. ferruginea* y *P. oocarpa*, provenientes de plantaciones forestales de rápido crecimiento en Costa Rica, las cuales han sido estudiadas y comprobadas que presentan buena permeabilidad (Gaitán-Álvarez et al. 2020), y también se ha probado su excelente absorción de diferentes sustancias para el tratamiento en la mejora de las propiedades de la madera (Gaitán-Álvarez et al. 2020; Moya et al. 2020a; Gaitán-Alvarez et al. 2020).

2.2. Preparación de las chapas

Se seleccionaron trozas de las 3 especies con diámetros >25 cm y unos 2,6 m de largo, las cuales fueron rebobinadas en un torno industrial, para obtener chapas de aproximadamente 3 mm. Una vez obtenidas las chapas estas fueron coladas en un horno solar hasta llegar a peso constante el contenido medio de humedad (MC) de las chapas secas varió de 6 a 8%. De cada especie se seleccionó 15 chapas de aproximadamente 5 x 5 cm.

2.3. Precipitación in situ

Una vez obtenidas las 15 chapas por especie se procedió a realizar la precipitación in situ, de estas las 15 chapas, cinco fueron seleccionadas para testigo o sin tratamiento, cinco para ser tratadas con el método de in-situ por inmersión y cinco por el método in-situ a vacío-presión.

Primeramente, las 10 chapas utilizadas en los tratamientos fueron pretratadas, lo que consistió en lavarlas en agua destilada caliente varias veces hasta que el agua saliera clara. Luego de esto se secaron para obtener el peso seco y fueron sumergidas en una solución de alcohol/tolueno (1:2, V/V) toda la noche para eliminar los extractivos de la madera, tales como gomas, tropolonas, grasas y ácidos grasos y así mejorar la afinidad superficial por las sales de hierro, después de esto fueron nuevamente secadas en horno a 104 °C hasta un contenido de humedad del 4%. La solución de hierros consistió en la mezcla de $FeCl_3 \cdot 6H_2O$ y $FeCl_2 \cdot 4H_2O$ a una concentración de radio molar de Fe^{3+}:Fe^{2+} = 2:1, la cual se disolvió en agua destilada para formar las soluciones precursoras de hierro con una concentración de 0.45 mol/L de cloruro de hierro. Luego de pretratadas, las cinco chapas seleccionadas para ser tratadas por el método de inmersión se impregnaron en la mezcla da sales de hierro durante 12 horas, a presión atmosférica. Después de filtrar y lavar varias veces con agua destilada para eliminar las sales de hierro residuales en la superficie, las muestras se secaron en estufa a 65 °C durante 12 h. Posteriormente, las muestras secas se impregnaron nuevamente en una solución de amoníaco al 25% durante otras 12 h. Luego se volvieron a lavar varias veces con agua destilada hasta alcanzar un pH neutro, los especímenes fueron secados en estufa a 65°C por 24 finalmente.

En el caso de las cinco chapas impregnadas con el método a vació-presión, primero se colocaron en un reactor y se aplicó vacío absoluto por 30 minutos, una vez completado el tiempo se introdujo la disolución de los hierros y se aplicó presión a por 2 horas. Una vez completado el tiempo estas fueron extraídas del reactor y se filtraron y lavaron varias veces con agua destilada para eliminar las sales de hierro residuales en la superficie, las muestras se secaron en estufa a 65 °C durante 12 h. Posteriormente, las muestras secas se impregnaron nuevamente en una solución de amoníaco al 25% durante otras 12 h. Luego se volvieron a lavar varias veces con agua destilada hasta alcanzar un pH neutro, los especímenes fueron secados en estufa a 65 °C por 24 finalmente.

2.4. Caracterización de las chapas de madera

Las chapas de madera tratadas fueron caracterizadas para comprobar la efectividad del proceso de impregnación. Primeramente, se determinó el porcentaje de cenizas y la cantidad de hierro formado en las muestras tratadas. De cada especie en los dos tratamientos y no tratadas fueron tomadas tres muestras y molidas a un tamaño de 420 µm a 250 µm (40 y 60 mesh, respectivamente) y se determinó el porcentaje de cenizas según la norma ASTM-D1102-84 (ASTM 2013). Una vez obtenidos el contenido de cenizas estas se utilizaron para determinar la cantidad de Fe_3O_4 en las muestras por medio del procedimiento de determinación de metales por aspiración directa realizado en un espectrómetro de absorción atómica marca AAnalyst 800, según la norma APHA-AWWWA-WEF, una vez obtenido el valor de hierro de la muestra testeada se calculó la cantidad de Fe_3O_4 en la madera siguiendo la ecuación (1).

$$Fe_3O_4\left(\frac{mg}{kg\ wood}\right) = \frac{Ash\ content_{sample}(\%)}{100} x \frac{Fe_3O_4\ content_{\ sample}(mg)}{1_{\ ash}(g)} x \frac{1000_{\ ash}\ (g)}{1_{\ ash}(kg)} \quad (1)$$

Donde:

Muestra del contenido de ceniza: porcentaje de ceniza obtenido en el laboratorio.

***Microscopía electrónica de barrido (FE-SEM)*:** De cada especie en los diferentes tratamientos y madera sin tratar se prepararon muestras de 5 mm de ancho x 3 mm de espesor x 5 mm de largo. La microscopia electrónica de barrido (SEM) se realizó en un equipo de marca Table Microscope TM 3000 sin película de oro o carbono que cubriera la muestra, se utilizó una distancia de trabajo (WD)= 3.8 a 5.8 mm; con 7.5 kv de voltaje y 400 aumentos. Se observó en los diferentes elementos anatómicos la formación de la magnetita y la parte del elemento anatómico donde se depositó el hierro.

Espectroscopía infrarroja con transformada de Fourier (FTIR): De cada especie en los dos tratamientos y muestras sin tratar fueron tomadas tres muestras y molidas a un

tamaño de 420 µm a 250 µm (40 y 60 mesh, respectivamente). El material molido fue secado al 0% de MC. A las muestras se les realizó el barrido de espectroscopia infrarroja de transformada de Fournier (FTIR), utilizando un espectrómetro Nicolet 380 FTIR (Thermo Scientific, Mundelein, Illinois, USA) con una célula reflectante única (equipada con un cristal de diamante). El equipo se configuró para realizar lecturas acumulando 32 exploraciones con una resolución de 1 cm^{-1}, con una corrección de fondo antes de cada medición. Los espectros FTIR obtenidos se procesaron con el software Spotlight 1.5.1, HyperView 3.2 y Spectrum 6.2.0 desarrollados por Perkin Elmer. Inc (Waltham, Massachusetts, USA).

Se identificaron las principales vibraciones donde se produjeron los mayores cambios en la madera, que estuvieron presentes en el pico 1251 cm^{-1} relacionado con la vibración de tensión del enlace C-O, 1505 cm^{-1} componentes de la pared celular de la lignina, 1601 cm^{-1} componentes de la pared celular de la celulosa, 1739 cm-1 asignado a la vibración de tensión de enlace C=O en cetonas no conjugadas y grupos éster, 2901 cm^{-1} corresponden a la vibración de tensión del grupo funcional -CH_3 asimétrico, 3340 cm^{-1} a la banda de absorción asignada a la vibración de tensión O-H de grupos hidroxilo.(Dong et al. 2016b;Gao et al. 2017; Gan et al. 2017a).

Difracción de rayos X (XDR): La difracción de rayos X (XRD) se realizó en cada especie estudiada en madera sin tratar y en la de los dos los tratamientos, en un difractómetro PANanalytical Empyrcan Series 2 (Cu-Kα, 6° - 40° 20). En conjunto con el software PANalytical High Score Plus. Se utilizó aserrín de las muestras tratadas y no tratadas y fue colocado en un rectángulo de neopreno colocado sobre una placa de vidrio para su medición. Los parámetros del aparato fueron fijados de la siguiente forma: radiación Cu-Ka con un monocromador de grafito, 40 kV de voltaje, 40 mA de corriente eléctrica, 2 horas de rango de escaneo de 5° a 90° con una velocidad de escaneo de 2°/min. El diámetro promedio de nanopartículas cristalinas de Fe_3O_4 *(D)* en la madera magnética fue evaluado en base a sus patrones difracción de rayos X usando la ecuación de Scherrer (2) (Lin and Ho 2014).

$$D = \frac{K\lambda}{(\beta cos\theta)} \qquad (2)$$

Donde: λ es la longitud de onda de los rayos X (0.15418 nm), *K* es la constante de Scherrer (0.89), β es el ancho máximo del pico a la mitad máxima (FWHM), and Θ es el ángulo de difracción de Bragg.

Magnometría de muestra vibrante (VSM): Los bucles de histéresis magnética (magnetización frente a campo magnético aplicado) de las probetas de madera con los diferentes tratamientos se determinaron a temperatura ambiente utilizando un

magnetómetro de muestra vibrante (VSM) MicroSense EZ7, en un campo magnético externo de -20 a 20 kOe en pasos de 2 Oe y 10 Oe a campo magnético bajo, y en pasos de 100 y 500 Oe a campos más altos; y un tiempo medio de 100 ms. La saturación de magnetización de (Ms), la coercitividad (Hc) y la remanencia (Mr) se extrajeron de los bucles de histéresis. Para evaluar la estabilidad de la propiedad magnética en el medio ácido, se realizaron pruebas de resistencia a los ácidos sumergiendo las muestras en una solución de ácido clorhídrico al 4% durante 7 días. A continuación, se evaluó la propiedad magnética mediante VSM. Las dimensiones de las probetas para los ensayos magnéticos fueron de 3 x 3 x 7 mm.

3. Resultados y discusión

3.1. Caracterización de las chapas de madera

En la Tabla 1 se observa los porcentajes de cenizas y el contenido de hierros de las muestras (Tabla 1). *Vochysia ferruginea* fue la especie con mayor contenido de cenizas en todos sus tratamientos, a su vez se observa que los menores contenidos de cenizas lo obtienen los testigos en las tres especies excepto en *G. arborea* que se da en el tratamiento magnético. En las tres especies estudiadas el tratamiento magnético-presión fue el que presentó el mayor porcentaje de cenizas (Tabla 1).

Tabla 1. Contenido de cenizas (a) y Fe_3O_4 (b) de chapas de madera magnética de tres especies tropicales provenientes de plantaciones de rápido crecimiento en Costa Rica.

Especie	Tratamiento	Cenizas (%)	Fe_3O_4 (mg/kg)
Gmelina arborea	Testigo	1.17 (4.99)^{A}	17.07 (8.82)^{A}
	Magnético	0.93 (6.86)^{A}	8.33 (56.60)^{A}
	Magnético-presión	4.96 (6.86)^{B}	418.67 (14.94)^{B}
Vochysia ferruginea	Testigo	2.65 (0.74)^{A}	0.19 (95.66)^{A}
	Magnético	2.69 (1.17)^{A}	0.03 (12.50)^{A}
	Magnético-presión	8.82 (0.39)^{B}	834.00 (8.79)^{B}
Pinus oocarpa	Testigo	0.26 (3.59)^{A}	0.15 (98.85)^{A}
	Magnético	2.08 (6.95)^{B}	3.27 (15.71)^{A}
	Magnético -presión	5.48 (1.90)^{C}	234.33 (31.34)^{B}

Nota: números entre paréntesis significan coeficiente de variación.

En cuanto al contenido de Fe_3O_4 en *G. arborea* y *V. ferruginea* el tratamiento magnético (sin presión) fue el que presentó el menor valor, mientras que el mayor en las tres especies se dio en el magnético a presión (Tabla 1), a su vez *V. ferruginea* fue la especie que presentó el mayor valor con 384 mg/kg, seguida de *G. arborea* con 418 mg/kg y por último

P. oocarpa con 234 mg/kg (Tabla 1), presentándose diferencias estadísticas entre ellos.

Estos resultados de aumento en el contenido de cenizas concuerdan con los llevados a cabo por otros autores en otras especies (Gao et al. 2012, Dong, Yan, Zhang, Zhang, and Li 2016, Mashkour and Ranjbar 2018, Yang et al. 2020), lo cual es atribuido a un aumento del material inorgánico en la madera producto del depósito in situ del hierro. De la misma forma se observa que el mayor aumento se da en el tratamiento magnético-presión, dando a entender que fue con el que se logró obtener mayor precipitación de Fe_3O_4 (Tabla 1).

3.2. Microscopia electronica de barrido (FE-SEM)

Las imágenes SEM de la Figura 1 a-c, muestra la presencia de la formación de magnetita en la superficie de las chapas de madera impregnadas a presión, se observa como la mayor cantidad de material queda depositado alrededor de las cavidades de la madera o los vasos (Figure 1 a-c). De la misma forma *V. ferruginea* es la que contiene visualmente mayor material magnético (Figure 1b).

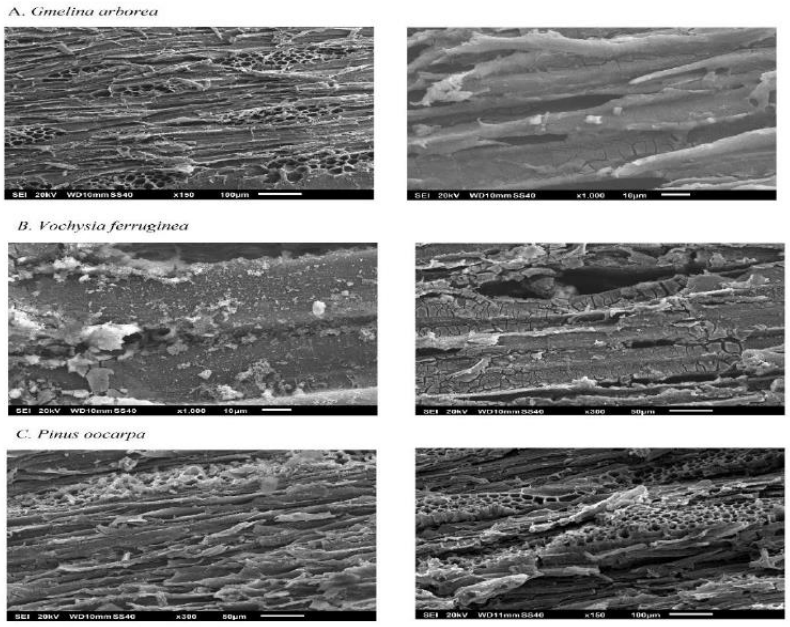

Figura 1. Imágenes SEM de chapas de madera magnética de tres especies tropicales (a-c) provenientes de plantaciones de rápido crecimiento en Costa Rica.

El principal elemento anatómico que promueve el flujo de fluidos en maderas latifoliadas son los vasos (Thomas 1976); por lo tanto, es de esperar una mayor formación in situ de nanopartículas de Fe_3O_4 en esta región, después de los vasos, los radios son el

siguiente elemento anatómico que permite el flujo de líquido en el interior de la madera, particularmente en la conducción radial (Moya et al. 2020b). Esto explica la formación de nanopartículas de Fe_3O_4 en esas estructuras anatómicas también. En el caso de las fibras en las especies latifoliadas, estas constituyen características anatómicas del árbol para el soporte estructural, no se utilizan para transportar líquidos (Thomas 1976). Al observar la ubicación específica de nanopartículas de Fe_3O_4 en cada una de las especies, se tiene que estas están depositadas mayormente alrededor de los vasos y en menor medida en las fibras de la madera (Figura 1 a-c).

3.3. Espectroscopía infrarroja con transformada de Fourier (FTIR)

Los espectros infrarrojos presentados en la Figura 2 reflejan los cambios en la composición química del material después de la magnetización. El debilitamiento de la señal en 1739 cm^{-1}, pertenecen al pico de absorción de vibración de la tensión del enlace C=O de la hemicelulosa (Yang et al. 2020), que tendió a disminuir con la magnetización en las tres especies, este debilitamiento concuerda con los estudios de Gao et al. (Gao et al. 2012; Gan et al. 2017a), Dong, Yan, Zhang, Zhang y Li (Dong et al. 2016a), Gan, Liu, et al. (Gan et al. 2017b), Wang, et al. (Wang et al. 2010)(2019), Lou, Yuan, et al. (Lou et al. 2019b), Yang et al. (Yang et al. 2020) y Garskaite et al. (Garskaite et al. 2021), quienes indican que el debilitamiento se atribuye a la degradación de la hemicelulosa. La modificación de la estructura de la celulosa no se vio afectada significativamente, la señal de 1145 cm^{-1}, la vibración de tensión del enlace C-O en la glucosa de la celulosa (Gao et al. 2012), fue similar en la madera tratada y sin tratar. Mientras tanto, la señal de lignina, el mayor debilitamiento ocurrió en la banda de 1601 cm^{-1} (C-C vibraciones esqueléticas aromáticas, Garskaite et al. 2021) y 1251 cm-1 (el enlace éster de los grupos carboxílicos, (Lou et al. 2018) en las tres especies de madera.

La formación de Fe_3O_4 en las muestras de madera, en las bandas de menores a 800 cm^{-1} y alrededor de 561 y 667 cm^{-1} con el FT-IR, evidencia una mayor formación de Fe_3O_4, especialmente en el tratamiento magnético-presión, esta señal a 800 cm^{-1}, corresponde a los sitios tetraédricos de la red cristalina, que se debe a la oxidación de las divisiones de Fe^{2+} y Fe^{3+}(Garskaite et al. 2021), la cual es más prenunciada principalmente en la madera de *G. arborea* seguida por *V. ferruginea* (Figure 2b-c). En la madera de *P. oocarpa* se evidencia poco este pico (Figure 2a), confirmando así la baja medición del contenido de Fe_3O_4 (Figure 2a).

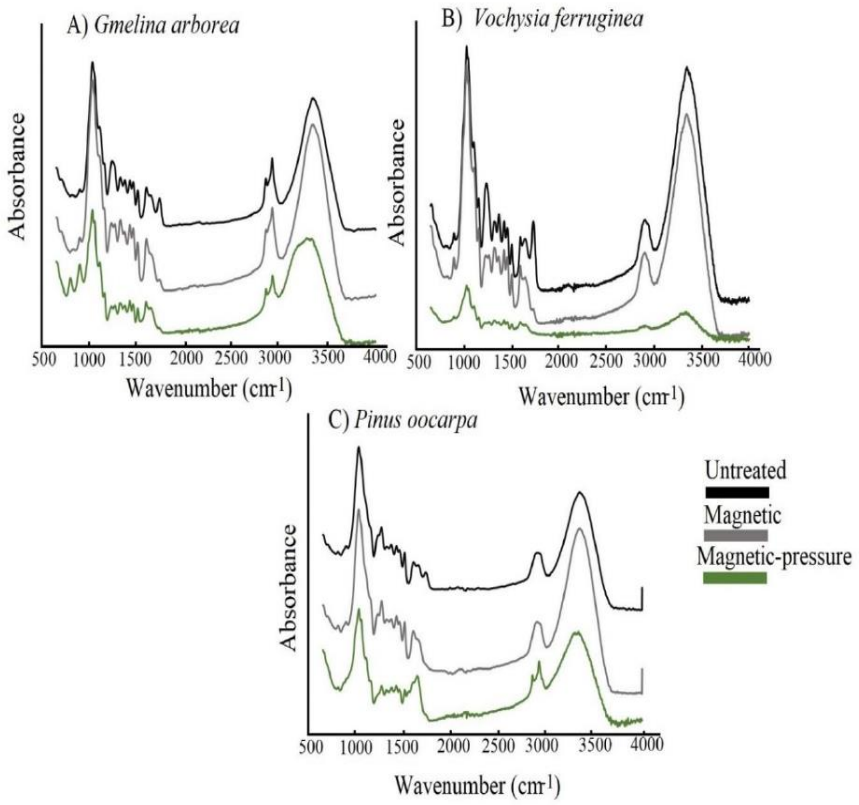

Figura 2. Espectro FTIR de chapas de madera magnética de tres especies tropicales (a-c) de plantaciones de rápido crecimiento en Costa Rica.

3.4. Difracción de rayos X (XDR)

Las estructuras cristalinas de las muestras no tratadas y tratadas se caracterizaron mediante XRD (Figura 3a-c). En los espectros se logra observar como en las muestras tratadas existen unos picos más pronunciados en comparación con las no tratadas, los cuales se pueden observan en el ángulo a 30° y 35°, de la misma forma en el tratamiento magnético-presión es donde se logra observar una mayor intensidad de los picos (Figure 3 a-c). Con respecto al tamaño de partícula se observó un aumento del tamaño con los tratamientos magnéticos (Figure 3d), en especial en *G. arborea* en el tratamiento magnético- presión seguido de *P. oocarpa* y por último *V. ferruginea* (Figure 3d).

Además de los cambios anteriores, la madera magnetizada presentó fuertes picos de difracción a 2θ: a 19°, 30°, 35° y 44° que corresponden a los planos (111), (220), (311) y (400) de magnetita respectivamente (JCPDS número 19-0629) (Figura 3a-b), que corresponde a la fase cúbica con el espacio de $Fd3\bar{m}$ (Lou et al. 2019b).

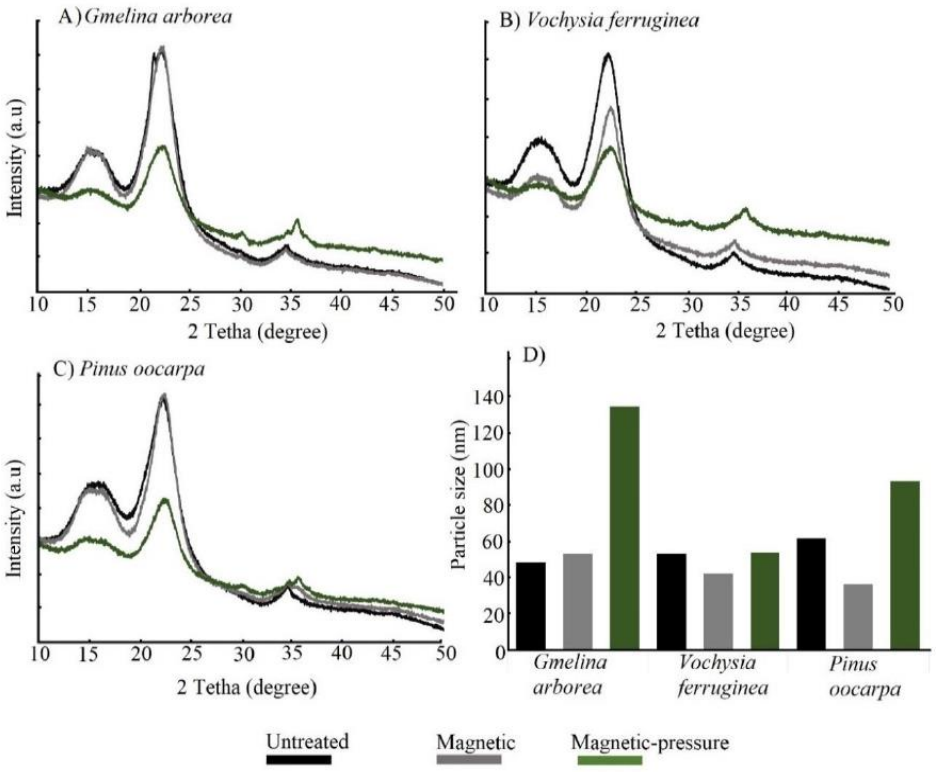

Figura 3. Difracción XDR de chapas de madera magnética de tres especies tropicales (a-c) de plantaciones de rápido crecimiento en Costa Rica.

En *G. arborea* la difracción más fuerte se está registrando en el pico a 34° (311), especialmente en el tratamiento a presión (Figura 3a). *En V. ferruginea* los más fuertes se ven en 35° mayormente en el tratamiento a presión (Figura 3b). Mientras que en *P. oocarpa* las difracciones más fuertes se están viendo en 30°, 35° y 44° y también especialmente en el tratamiento a presión (Figura 3c). Estás diferencias en los patrones y la determinación del tamaño de las partículas usando la ecuación de Scherrer (4) (Lin and Ho 2014), muestra que el depósito de Fe_3O_4 nanopartículas fue diferente en cada una de las especies, el mayor tamaño se obtuvo en *G. arborea,* seguido de *P. oocarpa* y el menor en *V. ferruginea* (Cuadro 2). Los tamaños de partículas coincidieron con los valores encontrados por Mashkour y Ranjbar (Mashkour and Ranjbar 2018) y Lou, Han, et al. (Lou et al. 2018) y Gao et al. (Gao et al. 2012), en el tratamiento a presión.

3.5. Magnometría de muestra vibrante (VSM)

La figura 4a-c muestra las curvas de histéresis de la madera sin tratar y la madera magnética con los procesos de impregnación. Las curvas de histéresis de la madera sin

tratar en tres especies se aproximaron a una línea recta cercana a cero (Figura 4), se determinaron todos los parámetros, la coercitividad (Hc), la retentividad (Mr), la magnetización de saturación (Ms), el porcentaje experimental de madera magnética y las curvas mostraron valores cero (Tabla 2), indicando la propiedad no magnética de la madera.

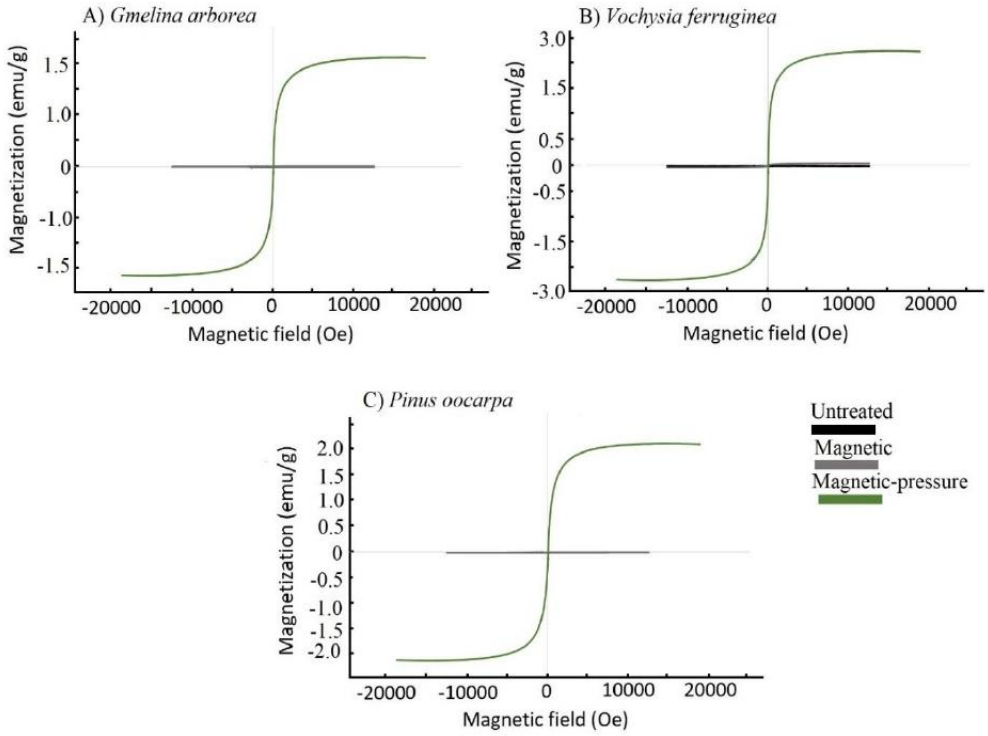

Figura 4. Curvas de histéresis magnética de chapas de madera magnética de tres especies tropicales (a-c) de plantaciones de rápido crecimiento en Costa Rica.

Por otro lado, las chapas de madera magnéticas de todos los especímenes exhibieron un claro comportamiento histerético y un comportamiento ferromagnético, especialmente en el tratamiento magnético-presión (Figura 4). A pesar de esto se observaron diferencias entre especies, la magnetización de saturación fue la más baja (de 1,0 a 1,5 emu) en *G. arborea* (Figura 4a) y la más alta en *V. ferruginea* (Figura 5c), indicando con estos resultados que la especie *V. ferruginea* es la más magnetizada. Este comportamiento se confirma al observar los valores de los parámetros de magnetismo (Hc, Mr, Ms) que son bajos en *G. arborea* y altos en *V. ferruginea* (Tabla 2). Esto para el tratamiento magnético- presión ya que, en el tratamiento magnético, las especies tratadas no se presentan diferencias significativas con respecto a los testigos (Figura 4 y Tabla 2).

Tabla 2. Coercitividad (Hc), retentividad (Mr), saturación de magnetización (Ms) y porcentaje experimental de chapas de madera magnética de tres especies tropicales (a-c) de plantaciones de rápido crecimiento en Costa Rica.

Especie	Tratamiento	Masa (mg)	Hc Oe	Mr (emu/g)	Ms (emu/g)	Porcentaje experimental
Gmelina arborea	Testigo	0.16				
	Magnético	0.14	17.20	0.00	0.01	0.04
	Magnético – presión	127.40	2.14	0.01	1.05	6.82
Vochysia ferruginea	Testigo	0.16				0.00
	Magnético	0.16	17.64	0.00	0.04	0.27
	Magnético – presión	160.87	4.21	0.04	2.10	13.68
Pinus oocarpa	Testigo	0.35			0.00	0.00
	Magnético	0.22	9.33	0.00	0.01	0.09
	Magnético – presión	149.63	5.34	0.02	1.20	7.78

4. Conclusiones

La síntesis de nanopartículas de Fe_3O_4 en las chpapas de madera de tres especies tropicales (*Gmelina arborea*, *Vochysia ferruginea* y *Pinus oocarpa*) por medio de una impregnación in-situ Fe^{3+} y Fe^{2+} y la inmersión en amoniaco fue posible en las tres especies, sin embargo, el método de impregnación tuvo un efecto significativo en la síntesis de las nanopartículas, en este caso la impregnación a vació-presión fue la que presentó la mayor cantidad de Fe_3O_4 depositada en la madera. De la misma forma, al usar la impregnación con el método vació-presión se evidenció mayor señal de ferrita en los análisis SEM y XDR. Y en el análisis de magnetismo fue claro que la curva de histéresis de la madera presentó un comportamiento ferromagnético en la síntesis por medio de vacío- presión, mientras que por el método de inmersión el cambio fue catalogado de leve a nulo. Dando a entender que el mejor método de impregnación es el vació-presión ya que se logra que las nanopartículas ingresen con éxito a la estructura anatómica de la madera. Así mismo, la especie que logró mayor nivel de magnetización fue *Vochysia ferruginea*.

5. Referencias

Ahmed A, Abu Bakar MS, Azad AK, et al (2018) Intermediate pyrolysis of Acacia cincinnata and Acacia holosericea species for bio-oil and biochar production. Energy Convers Manag 176:393–408. https://doi.org/10.1016/j.enconman.2018.09.041

ASTM (2013) Standard test method for ash in wood. Annu B ASTM Stand Vol 410 1–2

Bolton AJ, Humphrey PE (1994) The permeability of wood-based composite materials: Part 1. A review of the literature and some unpublished work. Holzforschung 48:95–100. https://doi.org/10.1515/HFSG.1994.48.S1.95/HTML

Dong Y, Yan Y, Zhang S, et al (2015) Flammability and physical–mechanical properties assessment of wood treated with furfuryl alcohol and nano-SiO2. Eur J Wood Wood Prod 73:457–464. https://doi.org/10.1007/s00107-015-0896-y

Dong Y, Yan Y, Zhang Y, et al (2016a) Combined treatment for conversion of fast-growing poplar wood to magnetic wood with high dimensional stability. Springer 50:503–517. https://doi.org/10.1007/s00226-015-0789-6

Dong Y, Yan Y, Zhang Y, et al (2016b) Combined treatment for conversion of fast-growing poplar wood to magnetic wood with high dimensional stability. Wood Sci Technol 50:503–517. https://doi.org/10.1007/s00226-015-0789-6

Gaitán-Alvarez J, Berrocal A, Mantanis GI, et al (2020) Acetylation of tropical hardwood species from forest plantations in Costa Rica: an FTIR spectroscopic analysis. J Wood Sci 66:49. https://doi.org/10.1186/s10086-020-01898-9

Gaitán-Álvarez J, Moya R, Berrocal A, Araya F (2020) In-situ mineralization of calcium carbonate of tropical hardwood species from fast-grown plantations in Costa Rica. Carbonates and Evaporites submited:

Gan W, Gao L, Liu Y, et al (2016) The Magnetic, Mechanical, Thermal Properties and Uv Resistance of CoFe 2 O 4 /SiO 2 -Coated Film on Wood. J Wood Chem Technol 36:94–104. https://doi.org/10.1080/02773813.2015.1074247

Gan W, Gao L, Xiao S, et al (2017a) Transparent magnetic wood composites based on immobilizing Fe3O4 nanoparticles into a delignified wood template. J Mater Sci 52:3321–3329. https://doi.org/10.1007/s10853-016-0619-8

Gan W, Liu Y, Gao L, et al (2017b) Magnetic property, thermal stability, UV-resistance, and moisture absorption behavior of magnetic wood composites. Wiley Online Libr 38:1646–1654. https://doi.org/10.1002/pc.23733

Gao HL, Wu GY, Guan HT, Zhang GL (2012) In situ preparation and magnetic properties of Fe 3 O 4 /wood composite. Mater Technol 27:101–103. https://doi.org/10.1179/175355511X13240279339806

Gao X, Dong Y, Wang K, et al (2017) Improving Dimensional and Thermal Stability of Poplar Wood via Aluminum-based Sol-Gel and Furfurylation Combination Treatment. BioResources 12:. https://doi.org/10.15376/biores.12.2.3277-3288

Garskaite E, Stoll SL, Forsberg F, et al (2021) The Accessibility of the Cell Wall in Scots Pine (Pinus sylvestris L.) Sapwood to Colloidal Fe 3 O 4 Nanoparticles. ACS Omega 6:21719–21729. https://doi.org/10.1021/acsomega.1c03204

Lin C-C, Ho J-M (2014) Structural analysis and catalytic activity of Fe3O4 nanoparticles prepared by a facile co-precipitation method in a rotating packed bed. Ceram Int 40:10275–10282. https://doi.org/10.1016/j.ceramint.2014.02.119

Liu J, Che R, Chen H, et al (2012) Microwave Absorption Enhancement of Multifunctional Composite Microspheres with Spinel Fe3O4 Cores and Anatase TiO2 Shells. Small 8:1214–1221. https://doi.org/10.1002/smll.201102245

Lou Z, Wang W, Yuan C, et al (2019a) Fabrication of Fe/C Composites as Effective Electromagnetic Wave Absorber by Carbonization of Pre-magnetized Natural Wood Fibers. J Bioresour Bioprod 4:43–50. https://doi.org/10.21967/jbb.v4i1.185

Lou Z, Yuan C, Zhang Y, et al (2019b) Synthesis of porous carbon matrix with inlaid Fe3C/Fe3O4 micro-particles as an effective electromagnetic wave absorber from natural wood shavings. J Alloys Compd 775:800–809. https://doi.org/10.1016/j.jallcom.2018.10.213

Lou Z, Zhang Y, Zhou M, et al (2018) Synthesis of magnetic wood fiber board and corresponding multi-layer magnetic composite board, with electromagnetic wave absorbing properties. Nanomaterials 8:. https://doi.org/10.3390/nano8060441

Lv H, Yang Z, Wang PL, et al (2018) A Voltage-Boosting Strategy Enabling a Low-Frequency, Flexible Electromagnetic Wave Absorption Device. Adv Mater 30:1706343. https://doi.org/10.1002/adma.201706343

Mashkour M, Ranjbar Y (2018) Superparamagnetic Fe3O4@ wood flour/polypropylene nanocomposites: Physical and mechanical properties. Ind Crops Prod 111:47–54. https://doi.org/10.1016/j.indcrop.2017.09.068

Moya R, Gaitan-Alvarez J, Berrocal A, Araya F (2020) Effect of CaCO3 in the wood properties of tropical hardwood species from fast-grown plantation in Costa Rica. BioResources 15:4802–4822

Moya R, Gaitán-Álvarez J, Berrocal A, Merazzo KJ (2022) In Situ Synthesis of Fe3O4 Nanoparticles and Wood Composite Properties of Three Tropical Species. Materials (Basel) 15:3394. https://doi.org/10.3390/ma15093394

Oka H, Hamano H, Chiba S (2004a) Experimental study on actuation functions of coating-type magnetic wood. In: Journal of Magnetism and Magnetic Materials. pp E1693–E1694

Oka H, Hojo A, Osada H, et al (2004b) Manufacturing methods and magnetic characteristics of magnetic wood. In: Journal of Magnetism and Magnetic Materials. pp 2332–2334

Oka H, Kataoka Y, Osada H, et al (2007) Experimental study on electromagnetic wave absorbing control of coating-type magnetic wood using a grooving process. J Magn Magn Mater 310:e1028–e1029. https://doi.org/10.1016/j.jmmm.2006.11.073

Oka H, Narita K, Osada H, Seki K (2002) Experimental results on indoor electromagnetic wave absorber using magnetic wood. J Appl Phys 91:7008–7010. https://doi.org/10.1063/1.1448796

Oka H, Tanaka K, Osada H, et al (2009) Study of electromagnetic wave absorption

characteristics and component parameters of laminated-type magnetic wood with stainless steel and ferrite powder for use as building materials. J Appl Phys 105:07E701. https://doi.org/10.1063/1.3056403

Oka H, Terui M, Osada H, et al (2012) Electromagnetic wave absorption characteristics adjustment method of recycled powder-type magnetic wood for use as a building material. IEEE Trans Magn 48:3498–3500. https://doi.org/10.1109/TMAG.2012.2196026

Rao X, Liu Y, Fu Y, et al (2016) Formation and properties of polyelectrolytes/TiO2 composite coating on wood surfaces through layer-by-layer assembly method. Holzforschung 70:361–367. https://doi.org/10.1515/hf-2015-0047

Renneckar S, Zhou Y (2009) Nanoscale Coatings on Wood: Polyelectrolyte Adsorption and Layer-by-Layer Assembled Film Formation. ACS Appl Mater Interfaces 1:559–566. https://doi.org/10.1021/am800119q

Tang T, Fu Y (2020) Formation of Chitosan/Sodium Phytate/Nano-Fe3O4 Magnetic Coatings on Wood Surfaces via Layer-by-Layer Self-Assembly. Coatings 10:51. https://doi.org/10.3390/coatings10010051

Thomas RJ (1976) Anatomical features affecting liquid penetrability in three hardwood species. Wood fiber Sci 4:256–263

Trey S, Olsson RT, Ström V, et al (2014) Controlled deposition of magnetic particles within the 3-D template of wood: making use of the natural hierarchical structure of wood. RSC Adv 4:35678–35685. https://doi.org/10.1039/C4RA04715J

Wang Y, Moo YX, Chen C, et al (2010) Fast precipitation of uniform CaCO3 nanospheres and their transformation to hollow hydroxyapatite nanospheres. J Colloid Interface Sci 352:393–400. https://doi.org/10.1016/j.jcis.2010.08.060

Yang L, Lou Z, Han X, et al (2020) Fabrication of a novel magnetic reconstituted bamboo with mildew resistance properties. Mater Today Commun 23:101086. https://doi.org/10.1016/j.mtcomm.2020.101086

Zheng J, Lv H, Lin X, et al Enhanced microwave electromagnetic properties of Fe3O4/graphene nanosheet composites. Elsevier

7. Conclusiones

La madera de *Tectona grandis* no mostró características favorables para ser tratada con nanopartículas magnéticas de hierro, tanto en piezas sólidas, como en partículas de madera. Debido a la presencia de tílides en la madera el debobinado para obtener chapas, tampoco es un procedimiento factible de llevar a cabo en esta especie.

La síntesis de nanopartículas de Fe_3O_4 en las tres especies tropicales (*Pinus oocarpa, Vochysia ferruginea* y *Vochysia guatemalensis*), por medio de impregnación in situ de Fe^{3+} y Fe^{2+}, sí es posible.

Para la madera sólida de especies tropicales el tamaño de las nanopartículas fue menor a 20 nm y los valores de coercitividad (Hc), retentividad (Mr) y magnetización de saturación (Ms) fueron bajos en comparación con otras especies reportadas en la literatura, lo cual es atribuible a la baja permeabilidad de líquidos en estas especies, lo que no permite la precipitación de las nanopartículas

P. *oocarpa* fue la especie con más baja precipitación de nanopartículas y consecuentemente resultó en la más baja saturación de la magnetización en madera sólida, mientras que *V. guatemalensis* fue la que tuvo la más alta saturación de magnetización.

A pesar del poco efecto en las propiedades magnéticas, los cambios en las características de la madera sólida fueron evidentes, tal es el caso de la disminución en la densidad, cambios en la celulosa, hemicelulosa y lignina de la madera.

Otro aspecto contrario a otros tratamientos en otras especies fue que el tiempo de inmersión en amoniaco no tuvo efecto en las propiedades magnéticas o cambios en la estructura de la madera, al menos no ´cuando se trabajó con madera sólida.

El uso de compuestos de madera con partículas magnetizadas con nanopartículas de Fe_3O_4 sintetizada in situ, mediante una impregnación de Fe^{3+} y Fe^{2+} y posterior inmersión en amoníaco para tres especies tropicales (*P*. *oocarpa*, *V*. *ferruginea* y *V*. *guatemalensis*), presentó valores bajos coercitividad (Hc), retentividad (Mr) y magnetización de saturación (Ms), comparado con madera sólida de estas u otras especies, lo que es atribuido a la baja permeabilidad y penetración de soluciones en estas especies, al utilizarse un método de impregnación sin presión.

Para las partículas de madera la menor precipitación ocurrió en *P. oocarpa*, sin embrago, fue la especie que presentó mejores propiedades magnéticas en comparación con *V. guatemalensis* y *V. ferruginea*.

A pesar del reducido efecto de madera magnética en tableros de partículas (MWPC), hubo evidencia de cambios en los componentes químicos de la madera, una disminución en la densidad, un incremento en el hinchamiento y mayor absorción de humedad, así como también ligeros cambios en las propiedades mecánicas de la madera, debido a las

modificaciones en los componentes químicos de la madera que se producen al sumergirla en amoniaco.

La síntesis de nanopartículas de Fe_3O_4 en las chpapas de madera de tres especies tropicales (*Gmelina arborea*, *Vochysia ferruginea* y *Pinus oocarpa*) por medio de una impregnación in-situ Fe^{3+} y Fe^{2+} y la inmersión en amoniaco fue posible para las tres especies, sin embargo, el método de impregnación tuvo un efecto significativo en la síntesis de las nanopartículas, en este caso la impregnación a vació-presión fue la que presentó la mayor cantidad de Fe_3O_4 depositada en la madera.

De la misma forma, al usar la impregnación con el método vació-presión se evidenció mayor señal de ferrita en los análisis SEM y XDR. Y en el análisis de magnetismo fue claro que la curva de histéresis de la madera presentó un comportamiento ferromagnético en la síntesis por medio de vacío- presión, mientras que por el método de inmersión el cambio fue catalogado de leve a nulo. Dando a entender que el mejor método de impregnación es el vació-presión ya que se logra que las nanopartículas ingresen con éxito a la estructura anatómica de la madera.

Así mismo, la especie que logró mayor nivel de magnetización fue *Vochysia ferruginea*.

8. Referencias

Ali, M.Z.; Javaid, A. (2017) Mechanical and rheological characterization of efficient and economical structural wood-plastic composite of wood and PVC. J. Chem. Soc. Pak., 39, 183–189.

Butta, M., Ripka, P., Janosek, M., & Pribil, M. (2015). Electroplated FeNi ring cores for fluxgates with field induced radial anisotropy. Journal of Applied Physics, 117(17), 17A722.

Dong Y, Yan Y, Zhang Y, et al (2016a) Combined treatment for conversion of fast-growing poplar wood to magnetic wood with high dimensional stability. Springer 50:503–517. https://doi.org/10.1007/s00226-015-0789-6

Gaitán-Alvarez J, Berrocal A, Mantanis GI, et al (2020) Acetylation of tropical hardwood species from forest plantations in Costa Rica: an FTIR spectroscopic analysis. J Wood Sci 66:49. https://doi.org/10.1186/s10086-020-01898-9.

Gaitán-Álvarez J, Moya R, Berrocal A, Araya F (2020) In-situ mineralization of calcium carbonate of tropical hardwood species from fast-grown plantations in Costa Rica. Carbonates and Evaporites submited.

Gan W, Gao L, Liu Y, et al (2016) The Magnetic, Mechanical, Thermal Properties and Uv Resistance of CoFe 2 O 4 /SiO 2 -Coated Film on Wood. J Wood Chem Technol 36:94–104. https://doi.org/10.1080/02773813.2015.1074247

Gan W, Gao L, Xiao S, et al (2017) Transparent magnetic wood composites based on immobilizing Fe3O4 nanoparticles into a delignified wood template. J Mater Sci 52:3321–3329. https://doi.org/10.1007/s10853-016-0619-8.

Gao, H. L., Wu, G. Y., Guan, H. T., & Zhang, G. L. (2012). In situ preparation and magnetic properties of Fe 3 O 4 /wood composite. *Materials Technology*, *27*(1), 101–103. https://doi.org/10.1179/175355511X13240279339806.

Kojima M, Yamamoto H, Marsoem SN, et al (2009) Effects of the lateral growth rate on wood quality of Gmelina arborea from 3.5-, 7- and 12-year-old plantations. Ann For Sci 66:507–507. https://doi.org/10.1051/forest/2009031

Liu CLC, Kuchma O, Krutovsky K V. (2018) Mixed-species versus monocultures in plantation forestry: Development, benefits, ecosystem services and perspectives for the future. Glob. Ecol. Conserv. 15.

Liu, J.; Declercq, N.F. (2017) Acoustic Wood anomaly in transmitted diffraction field. J. Appl. Phys, 121, 114902.

Lou Z, Zhang Y, Zhou M, et al (2018) Synthesis of magnetic wood fiber board and corresponding multi-layer magnetic composite board, with electromagnetic wave absorbing properties. Nanomaterials 8:. https://doi.org/10.3390/nano8060441.

Lykidis, C.; Bak, M.; Mantanis, G.; Németh, R. (2016) Biological resistance of pine wood treated with nano-sized zinc oxide and zinc borate against brown-rot fungi. Eur. J. Wood Prod., 74, 909–911.

Mashkour M, Ranjbar Y (2018) Superparamagnetic Fe_3O_4@ wood flour/polypropylene nanocomposites: Physical and mechanical properties. Ind Crops Prod 111:47–54. https://doi.org/10.1016/j.indcrop.2017.09.068

Merk, V.; Chanana, M.; Gierlinger, N.; Hirt, A.M.; Burgert, I. (2014) Hybrid wood materials with magnetic anisotropy dictated by the hierarchical cell structure. ACS Appl. Mater. Interfaces, 6, 9760–9767.

Moya R, Gaitan-Alvarez J, Berrocal A, Araya F (2020) Effect of CaCO3 in the wood properties of tropical hardwood species from fast-grown plantation in Costa Rica. BioResources 15:4802–4822.

Oka H, Kataoka Y, Osada H, et al (2007) Experimental study on electromagnetic wave absorbing control of coating-type magnetic wood using a grooving process. J Magn Magn Mater 310:e1028–e1029. https://doi.org/10.1016/j.jmmm.2006.11.073

Oka H, Tanaka K, Osada H, et al (2009) Study of electromagnetic wave absorption characteristics and component parameters of laminated-type magnetic wood with stainless steel and ferrite powder for use as building materials. J Appl Phys.

Segmehl J S, Laromaine A, et al (2018) Magnetic wood by in situ synthesis of iron oxide nanoparticles via a microwave-assisted route. Journal of Materials. Chemistry C 6:3395-3402. **https://doi.org/10.1039/C7TC05849G**

Sohn, J.; Cha, S. (2018) Effect of Chemical modification on mechanical properties of wood-plastic composite injection-molded parts. Polymers, 10, 1391.

Tenorio C, Moya R, Salas C, Berrocal A (2016) Evaluation of wood properties from six native species of forest plantations in Costa Rica. Bosque (Valdivia) 37:71–84. https://doi.org/10.4067/S0717-92002016000100008

Wang, L., Li, N., Zhao, T., Li, B., & Ji, Y. (2019). Magnetic Properties of $FeNi_3$ Nanoparticle Modified Pinus radiata Wood Nanocomposites. Polymers, 11(3), 421. https://doi.org/10.3390/polym11030421

Wang H, Yao Q, Wang C, et al (2017) Hydrothermal Synthesis of Nanooctahedra MnFe2O4 onto the Wood Surface with Soft Magnetism, Fire Resistance and Electromagnetic Wave Absorption. Nanomaterials 7:118. https://doi.org/10.3390/nano7060118

9. Anexos

La investigadora Dra. Karla Jaimes Merazzo dentro de sus líneas de investigación en el BCMaterials, Basque Center for Materials, Applications and Nanostructures, UPV/EHU Science Park propuso que a raíz de los resultados promisorios, pero no concluyentes en lo que a madera magnética se refiere, se hicieran unas pruebas tanto en Costa Rica como en España de ver el comportamiento del ácido poliláctico (que ya han venido trabajando en este centro de investigación en España, combinado con nano partículas magnéticas y madera.

Para ello se realizó un ensayo donde se incorporaron nanopartículas de hierro y cobalto, madera, combinadas con ácido poliláctico (PLA), componentes que al combinarse en diferentes proporciones, permite crear una lámina compuesta que tiene diferentes aplicaciones como por ejemplo el desarrollo de filamentos para impresiones 3D, que al ser un biomaterial compuesto y con propiedades magnéticas, tendría el potencial de aplicarse en múltiples productos novedosos y de alto valor ingenieril y evaluar la capacidad de magnetismo en esta forma de incorporación de los materiales. A manera de ejemplo, para este apartado del informe, se presentan los resultad obtenidos al utilizar un 10% del material magnético y otro con un 60% de nanopartículas magnéticas.

El ácido poliláctico (PLA) es un polímero termoplástico producido a partir del ácido láctico que se ha utilizado principalmente en materiales biodegradables y como material de matriz compuesta. El PLA es un biomaterial destacado que se utiliza para sustituir a los polímeros tradicionales de base petroquímica en diversas aplicaciones, debido en gran medida a la preocupación por el medio ambiente (Llyas et al. 2022). Los materiales a partir de compuestos ecológicos han cobrado mayor protagonismo, a medida que ha crecido la conciencia ecológica, ya que tienen el potencial de ser más atractivos que los materiales compuestos convencionales basados en el petróleo, que son tóxicos y no biodegradables. Los compuestos a base de PLA con fibra natural se han utilizado ampliamente en diversas aplicaciones, desde el envasado hasta la medicina, debido a su biodegradabilidad, reciclabilidad, alta resistencia mecánica, baja toxicidad, buenas propiedades de barrera, procesamiento respetuoso con el medio ambiente y excelentes características (Llyas et al. 2022).

En la figura 1 se muestra la apariencia de dos polímeros conformados por PLA+madera+nanopartículas de cobalto o de hierro.

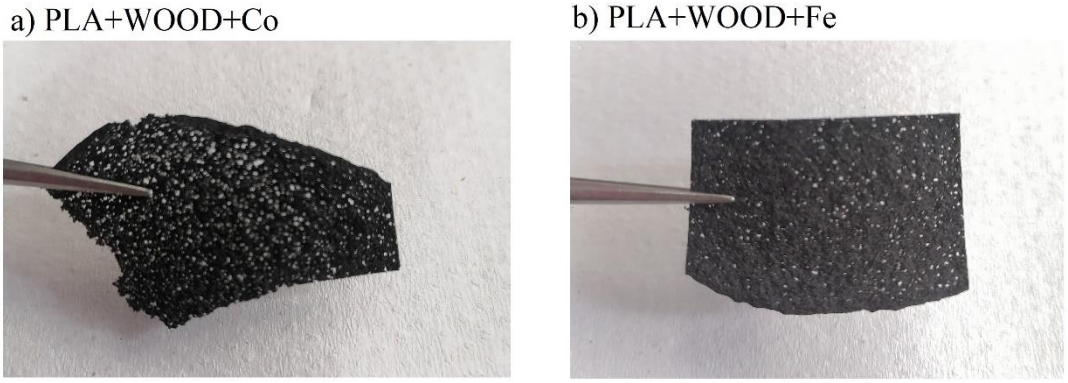

Figura 1. Imagen de biopolímero compuesto por PLA+madera+cobalto (a) y por PLA+madera+hierro.

En la figura 2 se muestra el espectro FTIR de nanopartículas de cobalto y de hierro y dos compuestos de PLA+madera con dos proporciones de las nanopartículas.

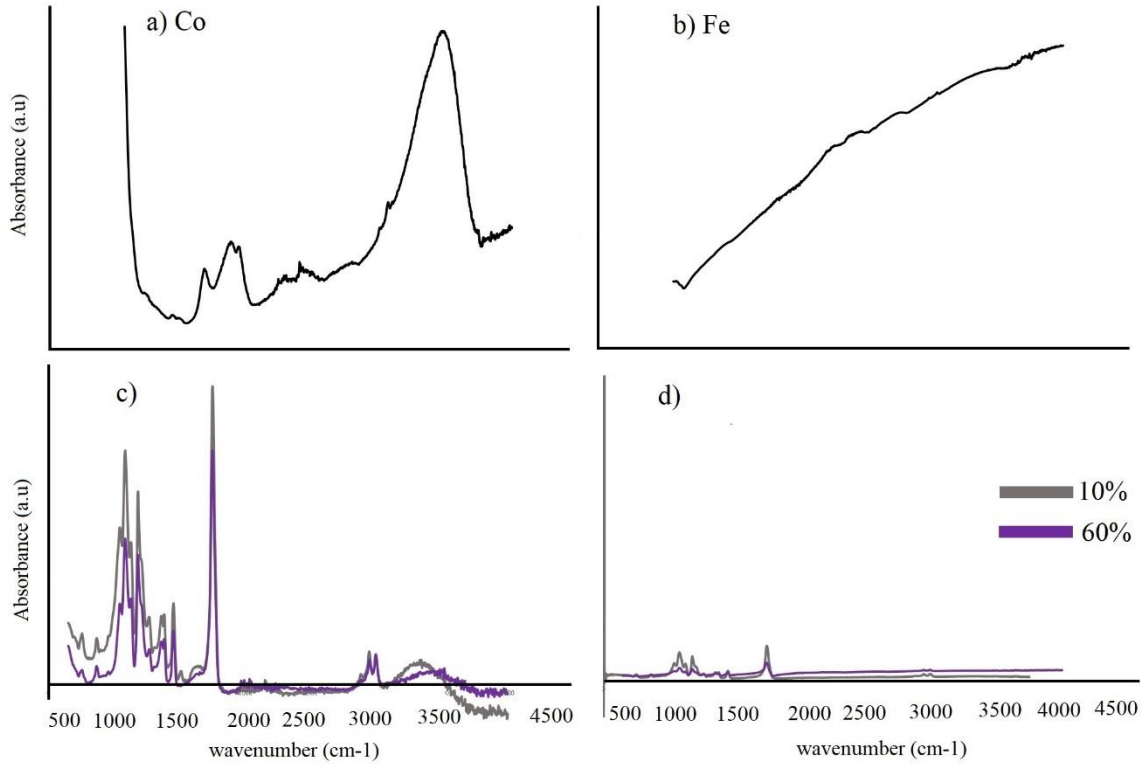

Figura 2. FTIR espectro de nanopartículas de cobalto (a), hierro (b), y dos compuestos de PLA+madera con dos proporciones de nanopartículas (c, d).

En las imágenes SEM (Figura 3) se observó una mejor incorporación de las nanopartículas en la proporción de 60% para ambos compuestos (Co y Fe) Figura 2 a-d. A la vez en el

mapeo elemental de la imagen SEM se observa como efectivamente al aumentar la proporción de nanopartículas las señales de los elementos Co y Fe aumentan Figura 3 a-d.

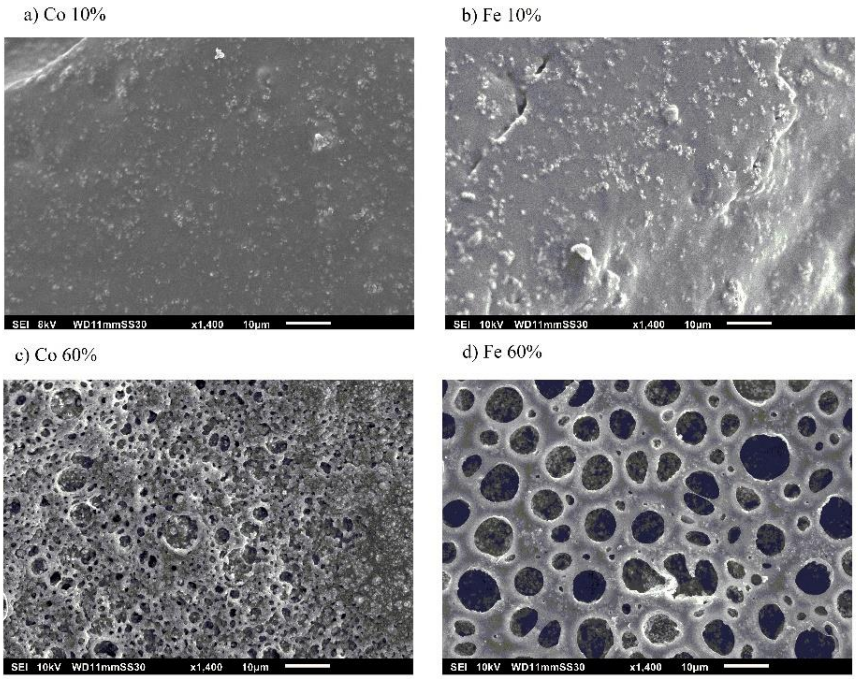

Figura 3: SEM de dos compuestos de PLA+madera con dos proporciones de nanopartículas diferentes.

En la figura 4 se muestra los mapeos elementales de compuestos de PLA+madera con dos proporciones de nanopartículas diferentes, mostrando la composición de cada uno.

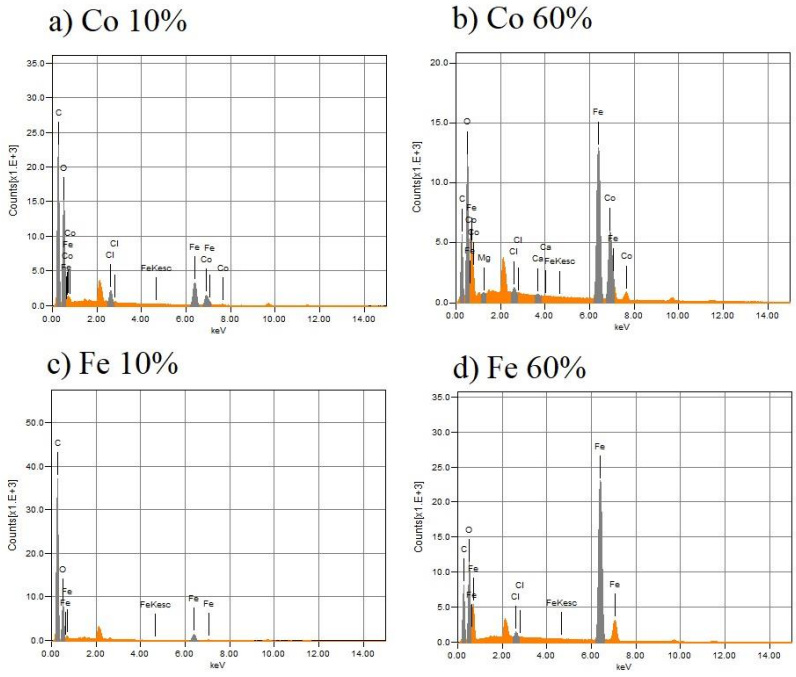

Figura 4. Mapeo elemental SEM en dos compuestos de PLA+madera con dos proporciones de nanopartículas diferentes.

En el análisis termogravimétrico se observa como el material compuesto con la proporción de 60% es más estable a la descomposición térmica con respecto al de 10% (Figura 5 a-d).

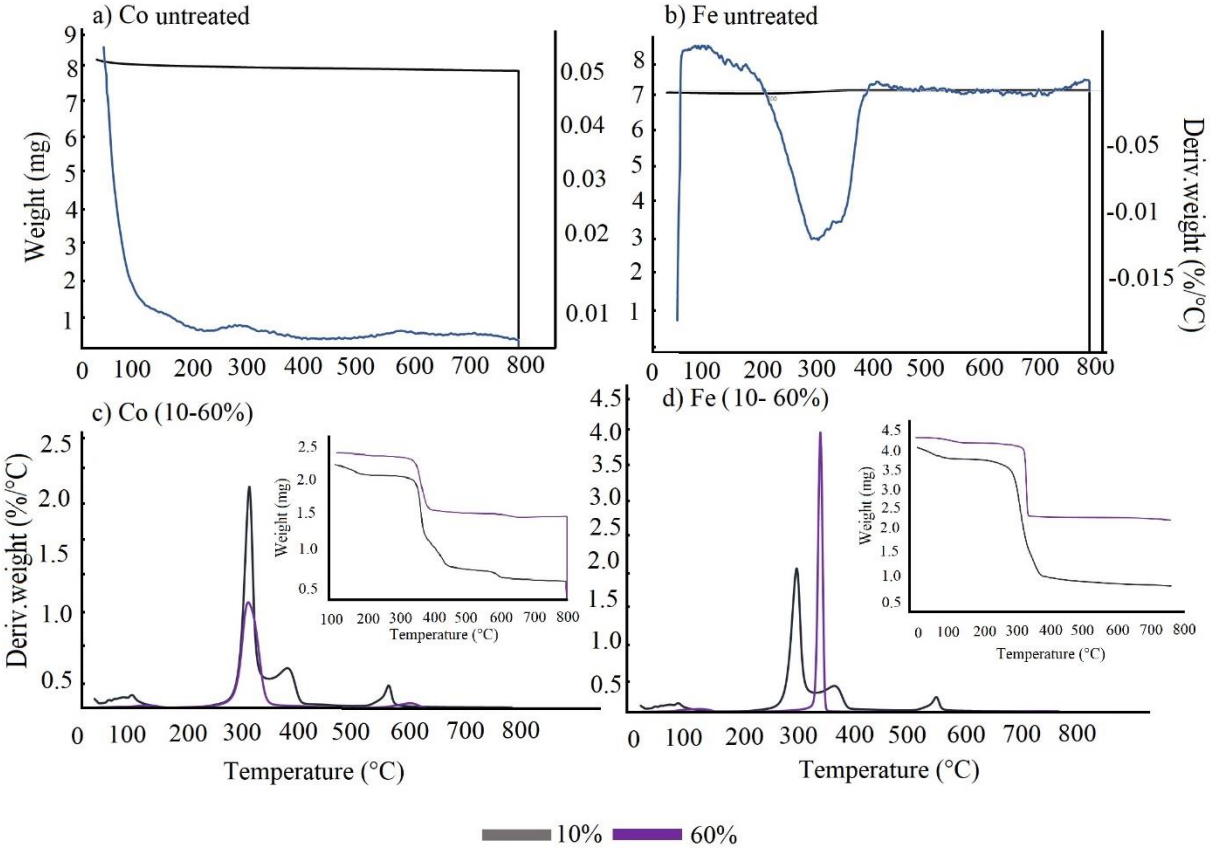

Figura 5. Análisis TGA y DTG, de nanopartículas de cobalto (a), hierro (b), y dos compuestos de PLA+madera con dos proporciones de nanopartículas (c, d).

De la misma forma en el análisis de la difracción de rayos-x se logró comprobar que el material compuesto con una proporción de 60%, cuenta con zonas de mayor cristalinidad que la partícula magnética sola y el compuesto PLA+madera+nanopartículas al 10% (Figura 6 a-b).

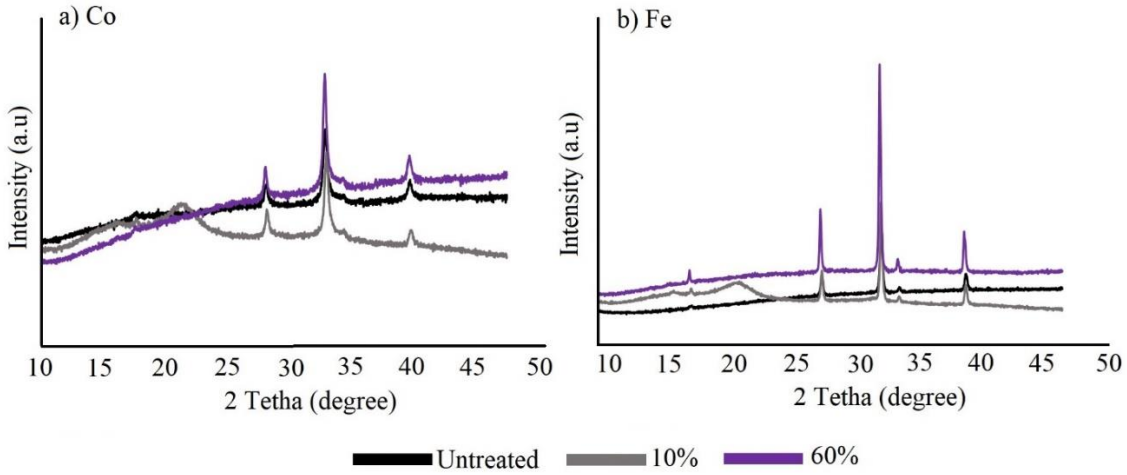

Figura 6. XDR espectro de nanopartículas dos compuestos de PLA+madera con dos proporciones de nanopartículas (c, d).

Tabla 1. Coercitividad (Hc), retentividad (Mr), magnetización de saturación (Ms) y porcentaje experimental de cobalto y de hierro, así como también de dos compuestos de PLA+madera con dos proporciones de nanopartículas

Material	Porcentaje	Mass (mg)	Hc (Oe)	Mr (emu/g)	Ms (emu/g)
Fe_3O_4	0	0,0	129,5	11,0	80,4
	10	10,1	147,7	1,2	8,1
	60	44,5	162,1	7,0	35,7
$CoFe_2O_4$	0	0,0	1944,3	24,5	52,0
	10	8,4	2336,3	2,5	4,4
	60	42,2	2420,8	12,9	21,9

En la figura 7 se muestran las curvas de histéresis magnética de los dos compuestos analizados

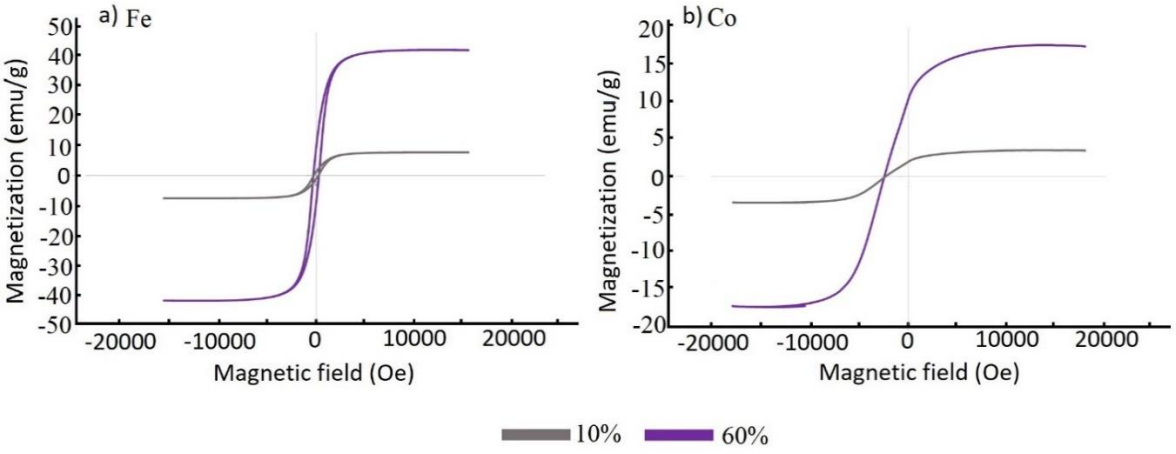

Figura 7. Curvas de histéresis magnética de dos compuestos de PLA+madera con dos proporciones de nanopartículas de hierro (a) y cobre (b).